UNCLASSIFIED
SECURITY CLASSIFICATION OF THIS PAGE

(2)

REPORT DOCUMENTATION PAGE

Form Approved OMB No. 0704-0188

1a. REPORT SECURITY CLASSIFICATION: UNCLASSIFIED	1b. RESTRICTIVE MARKINGS
2a. SECURITY CLASSIFICATION AUTHORITY	3. DISTRIBUTION/AVAILABILITY OF REPORT: APPROVED FOR PUBLIC RELEASE DISTRIBUTION IS UNLIMITED
2b. DECLASSIFICATION/DOWNGRADING SCHEDULE	
4. PERFORMING O	5. MONITORING ORGANIZATION REPORT NUMBER(S): AFOSR-TR-89-1225
6a. NAME OF PERI: UNIV OF MINNESOTA	7a. NAME OF MONITORING ORGANIZATION: AFOSR/NA
6c. ADDRESS (City, State, and ZIP Code): 125 MECHANICAL ENGINEERING MINNEAPOLIS, MN 55455	7b. ADDRESS (City, State, and ZIP Code): BUILDING 410 BOLLING AFB, DC 20332-6448
8a. NAME OF FUNDING/SPONSORING ORGANIZATION: AFOSR	8b. OFFICE SYMBOL (If applicable): NA
	9. PROCUREMENT INSTRUMENT IDENTIFICATION NUMBER: F49620-85-C-0049
8c. ADDRESS (City, State, and ZIP Code): BUILDING 410 BOLLING AFB, DC 20332-6448	10. SOURCE OF FUNDING NUMBERS

PROGRAM ELEMENT NO.	PROJECT NO.	TASK NO.	WORK UNIT ACCESSION NO.
61102F	2307	A4	

11. TITLE (Include Security Classification)
(U) STUDIES OF GAS TURBINE HEAT TRANSFER AIRFOIL SURFACES AND END-WALL COOLING EFFECTS

12. PERSONAL AUTHOR(S)
ECKERT, GOLDSTEIN, PATANKAR, SIMON

13a. TYPE OF REPORT	13b. TIME COVERED	14. DATE OF REPORT (Year, Month, Day)	15. PAGE COUNT
FINAL REPORT	FROM 1 Mar 86 TO 28 Feb 89	JULY 1989	88

16. SUPPLEMENTARY NOTATION

17. COSATI CODES			18. SUBJECT TERMS (Continue on reverse if necessary and identify by block number)
FIELD	GROUP	SUB-GROUP	TURBINES, HEAT TRANSFER, END-WALL COOLING

19. ABSTRACT (Continue on reverse if necessary and identify by block number)

The transfer of heat or mass has been used to detect characteristics of the flow which were not readily detectable by other means and computational models have been developed in conjunction to help discern physical aspects of the flow.

20. DISTRIBUTION/AVAILABILITY OF ABSTRACT	21. ABSTRACT SECURITY CLASSIFICATION
☐ UNCLASSIFIED/UNLIMITED ☒ SAME AS RPT. ☐ DTIC USERS	UNCLASSIFIED

22a. NAME OF RESPONSIBLE INDIVIDUAL	22b. TELEPHONE (Include Area Code)	22c. OFFICE SYMBOL
HENRY E. HELIN	202-767-0471	AFOSR/NA

DD Form 1473, JUN 86 — Previous editions are obsolete. — SECURITY CLASSIFICATION OF THIS PAGE

UNCLASSIFIED

Final Report

to

The Air Force Office of Scientific Research

Studies of Gas Turbine Heat Transfer Airfoil Surfaces and End-Wall Cooling Effects

AFOSR Grant No. F49620-85-C-0049
1 March 1986 - 28 February 1989

E. R. G. Eckert, R. J. Goldstein, S. V. Patankar and T. W. Simon
Co-Principal Investigators

July 1989

FOREWORD

The following report documents accomplishments made toward understanding the fluid flow and heat transfer processes in gas turbines. It covers the period of contract number F49620-85C-0049 which has now come to a close. Papers which present major findings from the Heat Transfer Laboratory on gas turbine heat transfer are listed in Appendix I. This list is restricted to papers published in the 1980s and papers which have been submitted for publication. Progress reports which have given the details of work in progress, for their respective periods, are listed in Appendix II. The main body of this submittal is a review of progress given with emphasis on the period since the most recent progress report, submitted in November, 1988.

INTRODUCTION

The following report documents work at the University of Minnesota Heat Transfer Laboratory, under AFOSR sponsorship on the topic of heat transfer from gas turbine airfoil and endwall surfaces. It reviews the work done under contract F49620-85C-0049 with emphasis on the period between November 1988 and the present. The research is divided into separate subtopics presented in the following order: turbine blade heat transfer, film cooling, flow around protruding cylinders, curved surface heat transfer, cascade fluid mechanics and numerical simulation of film cooling.

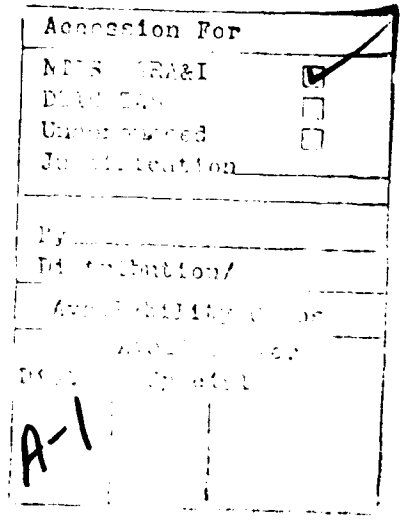

A - Turbine Blade Heat Transfer

Introduction and Objective

Understanding and prediction of the heat transfer in a turbine is dependent first on understanding the complex three dimensional flow that occurs around a blade. In a turbine passage there are complex (interacting) vortices, significant variation in surface curvature, flow separation, transition from laminar to turbulent flow and perhaps relaminarization, and the influence of high turbulence level in the free stream flow. Heat or mass transfer measurements, aside from providing the needed design information, can also tell us a great deal about the flow.

The transport of heat or mass has been used to detect characteristics of flow which were not readily detectable by other means. Modeling for computation of the flow and heat transfer, also, requires knowledge of the flow as well as transport data to check the validity of models and their accuracy.

To fulfill these needs a mass transfer technique which assures very accurate local mass transfer measurement has recently been developed and employed. The technique uses subliming naphthalene at ambient pressure and temperature together with a very precise system to measure the change in profile of the naphthalene surface. The method overcomes uncertainties associated with the conduction and radiation losses inherent in conventional heat transfer measurements and provides for very fine measurement grids; up to 2000 data points over an square inch area with great accuracy of the measured depth. Such resolution and accuracy enables one to detect the influence of minute variations of the flow, such as small separated regions and/or vortices, that could otherwise go unnoticed. It also indicates region of extreme mass (heat) transfer and points to the need of more refined numerical modeling.

Studies in Progress

Measurements in both two and three dimensional regions of the flow over the turbine blade, and over the endwall, are carried out. The two dimensional data are taken to test and qualify operation of the new measuring system designed and constructed to complement the sublimation technique. The system, which is controlled and operated by computer, is described by (Hain et al., 1989) in detail and is capable of scanning smoothly curved surfaces in a short time while measuring the sublimed depth of nearly 2000 points. The mass transfer coefficients (analogous to heat transfer coefficients) are calculated from the measured sublimed depth. These transport coefficients, presented on Figure A-1 and fully discused by(Chen and Goldstein, 1988), are in general agreement with the results of other investigators. These data show that the boundary layer on concave surface separates slightly downstream of the leading edge stagnation line (point

B on Fig. A-1). The separated boundary layer persists for a short distance downstream and then reattaches (point C on the figure). This is deduced from the drop in heat (mass) transfer coefficient followed by an increase to the reattachment point. Near the trailing edge, and at a short distance upstream of it where there is a point of inflection in the blade's surface curvature, the boundary layer detaches from the blade's surface to form a wake. This is also evidenced from a drop in mass (heat) transfer coefficient followed by a sharp rise to the trailing edge stagnation point, region D to E on Fig. A-1. This behavior of the flow, although anticipated, was not detected through the presure measurements taken earlier (shown as the blade surface velocity distribution on Fig. A-1). In a flow visualization study carried out afterward existence of separated region (detached boundary layer) and the vortex formed in it is verified. The near trailing edge separation, and its evolution into a vortex, also occurs on the convex side, region E to F on Fig. A-1. This is evidenced both from the mass transfer measurement and the visualization. The vortices formed at the trailing edge are counter rotating such that their common stream lines impinges on the trailing edge to make the trailing edge stagnation line. Some distance upstream of the trailing edge separation region, on the convex side, there appears to be a region of separated or retarded flow. This region, designated by G to H on the figure, is characterized by decreasing mass transfer followed by a sharp increase. It is also evidenced by the rundown of the visualizing paste under influence of gravity which has dominated the shearing force of the flow. It is not quite clear at this time whether the flow in this region has separated or changed velocity profile due to retardation. However, the separated flow reattaches, or the retarded flow recovers, farther downstream. On Fig. A-1, results of pressure measurements, mass transfer measurements, and visualization studies are compared. The comparison indicates that the mass transfer technique can effectively, and conveniently, be employed to get a basic understanding of the flow behavior in the neighborhood of a solid wall.

A sample of mass transfer measurements on the convex side and near the endwall are plotted on Fig. A-2. These results, presented in Chen and Goldstein (1989), show that the flow in this region is three dimensional. In this region, secondary flows in the form of multiple vortices originate near the leading edge and expand higher up and sometimes rise up into the passage as they move downstream. Very close to the endwall, $Z/C < 0.3$, mass transfer data indicate the existence of two counter rotating vortices. These vortices seem not to have been detected by some of the similar investigations available in literature. To give a better view of the effect of these vortices, a blown up plot of the mass transfer near the endwall is depicted on Fig. A-3. The relative maximum and minimum of mass transfer on this plot, respectively, belong to the points of attachment and detachment (also termed impingement and separation) of these vortices, to and from, the blade's suction side surface. This matter is substantiated and further explained in the next paragraphs.

Goldstein and Spores (1988) considered mass transfer from the endwall In this study effect of the forementioned vortices are also noticed, Fig. A-4. A cross plot of these contours and a schematic of the vortices are shown on Fig. A-5. On this figure, in addition to the vortices at the junction of endwall-suction side, a sketch of the vortices at

the leading edge and at the junction of endwall- pressure side is also shown. An attempt was made to verify the existence of the smaller vortices through pressure measurement and flow visualization. The results are presented on Figs. A-6 and A-7, respectively. The pressure contours show the existence of the vortices, but fail to show their detail as it is deduced from mass transfer data. Visualization results not only reveal the location of and the number of vortices, but also provide some indication of the direction of their rotation and movement. A close look at these figures, Fig. A-2 through Fig. A-7, and their comparison reveals that a complex system of vortices exist in the passage from which only the passage vortex is commonly acknowledged. Based on these observations, and those available in open literature, a system of vortices is conceived to fill the passage that is presented on Fig. A-8. As deduced from this schematic, besides the well known passage vortex there are a number of other vortices that their full detection and qualification requires further investigations.

Current Activities and Future Plans

Several studies are planned to be undertaken. One is a follow up on the visualization study. It is believed that there are a lot to be learned from visualization of flow about the nature, the number, and the movement of vortices in the passage bounded by turbine blades and the endwall. Consequently, smoke injection into the flow at predetermined locations and capturing of the results on high speed video tapes are being considered.

Mass transfer on the concave surface near the endwall must continue. Recalling that in most engines the aspect ratio (ratio of the height of blade to its cord) is about unity, it becomes clear that the passage height is mostly covered by three dimensional flow. Our study show that a height of the blade equal to about 75 % of it's cord from the endwall is affected by the presence of the endwall (Fig. A-2). Therefore, knowledge of the flow and heat transfer in that region is essential. Some mass transfer measurements on the concave wall in the three dimensional region were taken. But these measurements seemed doubtful because of occasional and slight detachment of the naphthalene cast from the blade surface during the test. That problem is now fixed and the measurement could commence and proceed.

It is planned to look into the effect of approaching flow turbulence on the vortices. The intensity, the number , and the size of vortices may be affected by the turbulence, subsequently, the mass transfer rate may change. Various turbulence levels of the approaching flow, encompassing the engine environment, will be applied. The disturbances will be generated in the mainstream ahead of the cascade employing cross bars or other means. A complete measurement of the turbulence intensity and qualification of flow will be accomplished. Then, for each case mass transfer measurements will be taken and the results will be compared to learn of the effect on mass transfer and the fluid flow near the surface in the three dimensional region.

Our measurements also show that the flow will separate wherever there is a change in the

surface curvature. Indeed, an early analysis has shown that flow fields around solid bodies are affected by the change in surface curvature. It would be of interest to investigate this notion further and determine the amount of change in curvature needed for separation or deformation of the velocity profile, its influence on the location where the deformation begins, and the distance downstream that it would persist.

B - Film Cooling

Introduction and Objective

To aid in understanding the complex flow and heat transfer with mass addition through film cooling holes on a turbine blade, we are first using a greatly simplified geometry in order to assess the relative importance of several of the most basic parameters. After this model has been thoroughly analyzed and is well understood, further complications can be added to assess their impact.

It is desired to understand the fundamental flow and heat transfer process of the film cooling of blades and vanes of gas turbines. The flow field in a gas turbine is extremely complicated, however, and resists any reasonably straightforward analysis. A first approximation to this extremely complicated situation would be film cooling over a flat plate, and over the past decades many variations of the flat-plate case have been studied, producing a base set of information to describe the flow including the jet-mainstream interaction and turbulent transport. Much work has also been done and is currently being done for film cooling in two-dimensional turbine cascades. Two "additional complications" are identified, the effect of streamwise curvature and the influence of the endwalls.

Since a turbine blade has varying curvature everywhere on its perimeter, however, and since the flow along a turbine blade may experience regions of transition, separation, relaminarization, etc., a turbine cascade is not well suited to isolating curvature effects. A wind tunnel with walls of constant though perhaps adjustable radius is better suited for such a study.

In light of this, a study was performed on film cooling in a constant curvature tunnel. Measurements of film cooling effectiveness for varying strengths of curvature for both a convex wall and a concave wall suggest that the normal and tangential components of momentum of the injected flow are extremely important parameters influencing the film cooling effectiveness on curved walls. The angle of injection defines the jets' ratio of normal to tangential momentum. Therefore, as a logical next step in understanding the general film cooling problem a study is now underway to quantify the influence of injection angle on the flow and film cooling effectiveness of curved surfaces.

The specific objectives of this current study are:

- To measure film cooling effectiveness along a convex and a concave wall (scaled to match the relative strength of curvature typical of a turbine blade moderately far downstream of the stagnation point) for injection angles of 15, 25, and 45 degrees; blowing rates of 0.25 to 2.50; and jet to freestream density ratios of unity and about two.
- To use both high-speed video and still photography in order to better understand the behavior of the film cooling jets. Specific points of interest include jet interaction

and the level of jet penetration into the mainflow.

- To analyze and provide correlations of the data which build directly upon the flat-plate analyses. The flow visualization should prove invaluable in this effort.

Studies in Progress

Film cooling investigation of curved surfaces have continued. Results of part of the investigation are presented in Karni and Goldstein (1989) and Schwarz and Goldstein (1989). Investigation with various angle of injection is underway. The first series of theses experiments are completed, yielding film cooling effectiveness data for concave-wall row-of-holes injection at streamwise angles of 15, 25, and 45 degrees, at a density ratio of 0.96 and blowing rates from 0.25 to 2.50. The results at high blowing rates are surprising, with both the steepest and shallowest injection angles outperforming the medium angle for X/D up to 20.

Figures B-1a thru B-1c summarize the measured dependence of film cooling effectiveness on injection angle and blowing rate. Since jets with lower injection angles have larger tangential components and smaller normal components of momentum, suggesting a mean jet trajectory closer to the wall, one might expect that film cooling effectiveness would monotonically increase as the injection angle is decreased. Whereas at low blowing rates (M=0.5 or higher, Fig. B-1a) the experiments show that injection angle is actually quite unimportant, at moderate blowing rates (M=1.0, Fig. B-1b) this explanation does appear validated.

However, a third regime is encountered at higher blowing rates (Fig. B-1c) where both steep and shallow angles outperform medium angles (for $X/D < 20$). The lowest angle of 15 degrees is indeed the best, and by far, but that 45-degree injection would outperform 25-degree injection is most unexpected.

Figures B-2a to B-2c reveal another interesting fact about injection at steep angles and high blowing rates. These plots include the effectiveness variations at centerline and midline ($z/3d = 0.5$) stations, thus providing a good measure of the spanwise uniformity of film cooling effectiveness.

At 15 degrees the centerline effectiveness is much higher than the midline effectiveness, implying a spanwise periodic variation with very high peaks in line with the holes. This seems expected. At 25 degrees the spanwise profiles are flat everywhere, suggesting either a thorough mixing of the jet with the freestream, or what is more likely in light of previous visualization for 35-degree injection, the paths of the jets are fluctuating rapidly enough to give time-mean uniform coverage after a short distance downstream. In Fig. B-2c the spanwise profiles for the 45-degree case are also essentially flat except near injection, where peaks are now found midway between the holes (this happens only for 45-degree injection, $M > 1.5$). An explanation of why 45-degree injection outperforms 25-degree injection at high blowing rates should take this fact into account.

Obviously, more intense interactions with the freestream would be associated with steeper injection angles; but the exact nature of these interactions is not obvious. Perhaps at 45 degrees a distinct kidney shape obtains (in a time-mean sense) whereas at lower angles the jets are better able to penetrate the flow undeformed or "cylindrically." Interactions among neighboring jets may also become significant at steep angles. Or, perhaps the jets are indeed violently broken apart over a very short distance. Flow visualization is planned and should provide an accurate picture of the situation.

Current Activities and Future plans

Measurements will now be taken on the convex wall for a density ratio of about one. Convex curvature introduces stabilizing effects to boundary layers, in sharp contrast to destabilizing concave curvature, so here the effects of injection angle are expected to be of a different nature. In fact, somewhat counterintuitive arguments abound which predict lower film cooling effectiveness for shallower injection angles on convex walls. These arguments will be tested.

Density ratio is one of the most important film cooling parameters, so density ratio effects will be measured by repeating each run at a density ratio of about two. Finally, flow visualization at the various injection angles will be performed to aid in the analysis and understanding of the data.

C - Flow Around Protruding Cylinders

Introduction and Objectives

Flow on the endwall and immediately ahead of the blade's leading edge is very complicated; it includes several interacting vortices and possibly a separation bubble. Mass transfer measurements, Fig. A-5, and flow visualization indicate this complexity. To obtain an insight into the fundamentals of formation of these vortices, their number and their behavior, flow around cylinders protruding perpendicularly from a flat plate is investigated. The first of the studies used a round cylinder and the naphthalene sublimation technique, Karni and Goldstein (1985). The results of this investigation show formation of a small vortex (V2), ahead of the cylinder, in addition to the commonly named horseshoe vortex (V1), Fig. C-1. Existence of the small vortex is not detected by some investigations employing other methods. The effect of this small vortex on the cylinder and on the endwall is a substantial increase in local heat transfer. This investigation is continued to include flow around square cylinder where effects of angle of attacks and non-circular cross-section could be examined.

Studies In Progress

Using naphthalene sublimation technique and flow visualization an investigation of the flow at the base of a square cylinder is initiated. Cylinder's axis is perpendicular to the endwall and angle of approaching flow, relative to the normal to cylinder's upstream side, could vary by rotating the cylinder. Mass transfer measurements on the cylinder's sides and on the endwall are taken. A typical distribution on the side of the cylinder normal to the flow is shown on Fig. C-2. The peaks of the transfer coefficient on this plot indicate the location where vortices have impinged (touched) on cylinder. The higher peak is due to the small (corner) vortex and the lower peak due to the horseshoe vortex.

On Figure C-3, contours of constant mass transfer on the sides of the cylinder is depicted, Goldstein and Yoo (1989). These contours show that the effects the three dimensional flow are sensed for some distance along the height of the cylinder, and that, on the front surface, the edges of the cylinder is exposed to an accelerating flow; variation of the transfer coefficient at a fixed height and its increase toward the edge. On the side surface, however, the low heat transfer following the upstream edge is indicative of separation of flow which attaches on the surface just upstream of the downstream edge.

Effect of the cylinder's orientation in the flow is shown on Fig. C-4. It is seen that angle of attack has its most pronounced effect on the side surface where flow first separates and then reattaches. Local effect of the angle of attack on mass transfer is currently under analysis.

Mass transfer from the endwall ahead of the cylinder is depicted on Fig. C-5. It is interesting to note that rising mass transfer due to acceleration of flow around the edge is

also felt on the endwall (Y/D=+0.5, -0.5), followed by a drop and a rise in mass transfer indicating, respectively, the locations of detachment and attachment of the vortex as it turns the corner. A contour plot of the endwall mass transfer at two different angle of attacks are shown on Figs. C-6 and C-7. These contours show that the change in orientation of cylinder would considerably change the flow pattern, in particular makes the vortex accelerate at one corner (the corner that first cuts into the flow, "leading corner") while decelerating at the other. This is also evident from visualization of flow on the endwall, Fig. C-8. It is striking that the compression of vortex as it turns the leading corner (due to acceleration) and its expansion upon deceleration around the other corner is also observed at the leading edge of a turbine blade. This similarity of the behavior and the underlying reasons of it is worth further investigation.

Current Activities and Future Plans

Measurements obtained with square cylinder is being analyzed and prepared for publication. Meanwhile, further studies are being planned to fully understand the reasons of similar pattern of vortex behavior as it turns a sharp leading edge (square cylinder) versus a round one (turbine blades). The effect of the surface curvature on the turning vortex is also of importance. This effect may be one of the factors that render the leg of the vortex which follows the convex surface of the blade to contract and eventually lift up from the endwall, while, the the leg which follows the concave side expands and disappears. It is intended to examine the role of the surface curvatures on contraction and expansion of a vortex as it turns a solid corner using mass transfer technique and the visualization methods.

D. RECOVERY OF A TURBULENT BOUNDARY LAYER FROM CURVATURE

INTRODUCTION OF PROGRAM AND OBJECTIVES

The purpose of this experiment is to document the processes by which the turbulent boundary layer recovers from sustained concave curvature. The study will be conducted in the presence of low and elevated free-stream turbulence intensity and with and without streamwise pressure gradients. To the best of the authors' knowledge this is the first time that the recovery from a sustained concave curvature will be experimentally documented. The results are expected to be valuable to turbulence modellers who have thus far failed to satisfactorily predict this process.

WORK COMPLETED TO DATE

Elevated Free-Stream Turbulence

A bi-plane grid of tubes with jet injection capabilities has been constructed to produce high levels of free-stream turbulence (shown in Fig. D-1). The bar size of the grid is 4.15 cm and the solidity ratio is 60%. A turbulence establishment chamber has also been constructed to allow the turbulence to develop before entering the test section. Although inhomogeneities were expected, due to the high solidity of the grid, none were generated. The streamwise turbulence intensity at various downstream locations is shown in Fig. D-2. The turbulence intensity is uniform to + 6% of its value and the mean velocity is uniform to + 2% at each location. The isotropy of the turbulence, measured with a cross-wire probe, is shown in Fig D-3.

The measurement of 3-D turbulence quantities such as the 3-D mean velocity and the complete Reynolds' stress tensor was the next topic studied. Two methods were considered. The first method was the use of an orthogonal, triple-wire probe. The signal processing using this type of sensor was studied and a simple technique to obtain accurate measurements was developed. This technique is described in the attached paper "Signal processing using the orthogonal probe equations", which has been submitted to TSI Flowlines. The second method was the use of a rotating slant-wire probe. The signal processing with this type of probe was also investigated. Since this method seemed

easier to implement it was the method initially pursued. This method has been successfully implemented. Results are shown in Fig D-3. Because the rotating slant-wire probe is somewhat awkward to use, the orthogonal triple-wire technique will be investigated further in search of a better method for our measurements in highly turbulent flows and flow with embedded vortical structure, as in the turbine end-wall flow.

Developing Section

a). Low and intermediate TI cases.

The transitional flow over the developing, bendable wall has been studied for two free-stream turbulence intensity (TI=0.32% and 1.79%) levels. Both cases were with this bendable wall in the flat-wall configuration. The flow, initially laminar, underwent natural transition, becoming fully turbulent by the test section end. Measurements of wall Stanton number, mean and rms velocity and temperature profiles, shear stress and turbulent heat flux profiles, and turbulent Prandtl number profiles have been made for both cases. These results are summarized in the attached paper by Kim, Simon and Kestoras (1989).

b). High TI case.

More recently, a case with a high free-stream turbulence level (TI=8.3% at the entrance of the test section) with the same tunnel configuration was studied. This case is more representative of the conditions encountered in gas turbine engines. The measurements were taken with the turbulence generating jet grid, described above, in place. The free-stream turbulence level was so high that it was difficult to distinguish between laminar and turbulent flow in the transition region by looking at the hot-wire traces. For this reason, no intermittency-based processing was performed. A plan view of the test facility is shown on Fig. D-4. A short summary of the results follows:

Free-stream Turbulence Intensity and Spectra. The power spectral density measured in the free-stream at Station 1 was clean, with no significant spikes. The high free-stream turbulence generated by the jet grid apparently overwhelms any tunnel unsteadiness and/or electronic noise.

The free-stream turbulence intensity at the tunnel centerline was found to be quite isotropic, and decays from 8.3% at Station 1 to 5.9% at Station 4. There was a significant variation in v' in the cross-stream direction, however, with v' changing by as much as 45% from just outside the boundary layer to the tunnel centerline. This is thought to be due to the particular jet-grid geometry used.

Stanton Number. The wall Stanton number variation is shown on Fig. D-5. The data is seen to deviate from the turbulent correlation for $Re_x<1x10^5$, indicating a short transition region, consistent with the intermittent hot-wire signal discussed above. The laminar region (if one exists) is too short to be measured.

In contrast to the data sets of Blair (1983) and Simonich and Bradshaw (1978), the increase in free-stream turbulence is not seen to augment the heat transfer. This may be due to the low Reynolds number, however, as suggested by Simonich and Bradshaw (1978). An energy balance, in which the energy added to the flow through the wall was equated to the energy carried by the flow, was within 3% for all stations.

Mean Velocity Profile. Profiles of mean velocity plotted in wall coordinates are shown on Fig. D-6. The profiles corresponding to stations 2, 3, and 4 are seen to agree very well with the log-linear law -- the log-linear region grew in y^+ distance with Re_x until station 3 then changed only slightly with streamwise distance. A notable feature of the profiles is the absence of a wake. This is due to the high free-stream turbulence level. The profile corresponding to station 1 appears to be transitional. As there was some difficulty in assigning an appropriate C_f value at this station, due to the absence of a log-linear region, this profile may not be the correct profile. Determining the local skin friction for this profile, using a momentum balance, was not possible since no data upstream of Station 1 was taken.

Velocity Fluctuation. Fluctuations of the streamwise velocity, turbulence intensity, are shown on Fig. D-7. The peak in the profile at Station 1 is relatively broad and is indicative of a transitional flow. The peaks for the profiles at stations 2, 3, and 4 are much sharper, with the peaks dropping monotonically with Re_x and in step with the drop in free-stream turbulence level.

Mean Temperature Profiles. Mean temperature profiles measured using a thermocouple probe, and normalized on wall coordinates, are shown on Fig. D-8. The profiles at stations 2, 3, and 4 all show log-linear regions that increase with Re_x for all stations. Unlike the corresponding velocity profiles, the temperature profiles are seen to continually evolve in the streamwise direction. The profiles do not show a wake

region. Turbulent Prandtl numbers deduced from the profiles were consistently near unity. The temperature profile at Station 1 does not seem to possess a log-linear region, consistent with the transitional nature of the flow at this station. This profile was obtained using the uncertain value of C_f, obtained from the mean velocity profile, however. Thus, it is not reliable.

Shear Stress Profiles. Profiles of u'v' are shown on Fig. D-9. The profile at Station 1 with it's broad peak is indicative of a transitional flow profile, while the profiles at station 2, 3, and 4 have a turbulent flow shape. The near-wall peak is seen to decrease with Re_x.

Turbulent Prandtl Number Measurements. Profiles of the turbulent Prandtl number (Pr_t) measured with a special triple-wire probe are presented on Fig. D-10. Pr_t values are greatly increased above unity for the early turbulent boundary layer (Stations 2 and 3), but are seen to decay to near unity by station 4. This suggests that the momentum boundary layer establishes itself more quickly than does the thermal boundary layer in the early turbulent flow, resulting in higher values of the eddy diffusivity of momentum relative to the eddy diffusivity of heat. This view is supported by the mean velocity and temperature profiles, where similar velocity profiles were seen at stations 3 and 4 while the temperature profiles were still evolving. There is no reason to expect the momentum and thermal boundary layers to develop at the same rate, since the boundary conditions are different. The momentum boundary layer sees a non-zero fluctuation (a non-zero u') in the free-stream whereas t' in the free-stream, the boundary condition on the temperature profile, must equal zero. It is postulated that having eddies present in the free-stream enables the momentum boundary layer to respond more quickly than if it had to grow by turbulent diffusion alone. Creating a temperature fluctuation in the free-stream (possibly by injecting heated air through the grid) may cause the thermal and momentum boundary layers to grow at comparable rates. Pr_t values are in the vicinity of unity by station 4, indicating that the momentum and thermal boundary layers have grown to comparable thicknesses.

Recovery Section

An intermediate composite wall has been built to join the existing recovery wall to the flexible (concave) wall (Fig. D-11). It consists of a plexiglass back wall, a layer

of lexan, a heater, a layer of tape and a layer of stainless steel. Fiberglass insulation is used to minimize the heat loss through the back wall.

The dimensions of the heater are carefully chosen so that its heating foils end where the foils of the flexible wall and the recovery wall begin. The heater is very thin (0.254 cm). A layer of liquid crystal (0.210 cm thick) covers the three walls. It is to be used for heat transfer visualization, but it also provides a hydrodynamically smooth surface.

Three thermocouples have been embedded in the intermediate wall to measure its streamwise temperature variation. Two additional thermocouples were embedded across the fiberglass insulation to determine the heat loss through the back wall.

The recovery wall has been connected to the flexible wall while the latter was still in the straight configuration (Fig. D-4). The objective was to qualify the wall.

The uniform heat flux requirement was met by designing and building the circuit shown in Fig. D-12. The heat flux over the four heaters produced by the circuit was found to be uniform within 4% over the entire range of operation. The heat flux values of the flexible and the recovery wall heaters are determined by measuring the voltages across the heaters and the precision resistor, R_{pr}. In the case of the intermediate wall heaters, however, an uncertainty analysis showed that using the $P=V^2/R$ formulation for the power dissipation is preferable, due to the high resistance value of the heaters. The switches shown in the circuit were included to allow separate heating of the flexible wall.

Stanton number measurements, as well as velocity and temperature profiles, were taken as part of the qualification of the wall. All measurements were taken at a negligible streamwise pressure gradient, at a high free-stream turbulence intensity (~8%). The latter was necessary to not impede the progress of the transition study. The test has indicated a problem with the data reduction of the recovery wall. This problem has been traced to an incorrect estimate of the thermal resistance of the composite wall. An experiment is now in progress to determine this more precisely.

Intermittency Circuit

An intermitteny circuit has been constructed (Fig. D-13), tested, qualified and is being used to take measurements in the transition region over a flat wall [Kim J., Simon T. W. and Kestoras M., 1989]. It will be used in the boundary layer recovery

study to document the characteristics of the turbulent wake. In the transition study, the output of the circuit was used to separate the turbulent flow from the laminar flow in the intermittent boundary layer region. In the recovery study, the intermittency circuit will be used to separate signals taken within the turbulent-like flow in the wake from signals taken within the free-stream flow entrained in the wake region.

This circuit takes advantage of the much larger time derivative of the turbulent signal as compared to the time derivative of the laminar signal: the hot-wire-anemometer signal is processed by a series of filters, differentiators and rectifiers (Fig. D-14). At the level detector, the signal is compared to an adjustable threshold value. If it is higher, the output signal of the level detector is high (turbulent), otherwise it is low (laminar).

It can be seen in Fig. D-14 that the intermittency measuring unit has two channels, the direct channel and the differentiated channel. The two channels are used to solve the problem of zero-crossing. This problem is explained in (Fig. D-15) where the time derivative of a turbulent signal is shown. When this signal is compared to a threshold value at the level detector, it is seen that at times the signal is higher than the threshold value, giving a high (turbulent) signal. However it is also seen that the signal unavoidably becomes smaller than the threshold as it crosses zero, the time axis. During this time the flow is falsely declared turbulent. This is the zero-crossing problem. To correct this problem the circuit uses the second derivative of the signal (differentiated channel). The differentiated signal (second derivative) retains the characteristics of the first-derivative with one important difference; it is zero when the first derivative has a maximum or minimum value. When the second-time derivative is compared with the threshold value, there will again be regions where the flow will falsely be declared laminar. However the time-regions during which the two channels are at fault do not coincide. An "OR" gate is then used to combine the two signals. Its output is high when either or both inputs are high, and it is low only when both inputs are low. The threshold values of the two level detectors are adjustable and should be tuned for each different flow situation. A tuning procedure that works well has been established.

Although most of the zero crossings were eliminated by using the two branches of the circuit, as explained above, some drop-outs still persisted. A filter was thus introduced to average the signal and thus eliminate all the drop-outs. An additional level detector was next used to clean the signal. Finally a summer was included to add the

output of the intermittency unit to the hot-wire anemometer signal. This allowed conditional sampling of the hot wire signal and the desired separation of the laminar from the turbulent contribution of the quantity being investigated.

NEAR TERM ACTIVITY

Elevated Free-Stream Turbulence

The work on the generation of high free-stream turbulence is complete. Future work may focus on, possibly, implementing the triple-wire technique.

Developing Section

Measurements are currently being made with the developing section in a concave curvature configuration with the high free-stream turbulence generating grid in place. The curvature parameter (ratio of boundary layer thickness to radius of curvature) at the end of the test section is $\delta/R=0.02$. Measurements should be completed by June, 1989.

Recovery Section

An experiment will be run to accurately determine the effective thermal resistance of the layers between the thermocouples and the wall surface for both the intermediate and the recovery wall. Then the data obtained from the qualification run on the recovery wall will be reprocessed with the updated data reduction program and a momentum and an energy balance will be performed.

Intermittency Circuit

The intermittency circuit will be further tested in various flows. The possibility of using u'v' as the quantity sent to the circuit, instead of u', will be examined. It is believed that this is a better signal for determining the intermittency of a flow [2]. The experience thus gained will be valuable when the circuit is used in the

wake of the recovering boundary layer where it is harder to distinguish turbulent-like flow from free-stream flow entrained by the boundary layer.

E. THE THREE-DIMENSIONAL FLOW AND HEAT TRANSFER IN A LARGE-SCALE, TWO HALF-BLADE CASCADE

OBJECTIVES

The losses in a turbine can broadly be divided into profile losses, secondary losses, and clearance losses. The so-called secondary losses include those due to the annular wall boundary layers and their interaction with the blade rows. The secondary flow within the cascade has very complicated features such as horseshoe vortices, passage vortices and three-dimensional separation and reattachment lines. They are not understood well and, since the losses amount to roughly half the total losses, the lack of knowledge about secondary flow effects makes accurate prediction of turbine performance difficult.

In this study, static and dynamic mechanisms in a three-dimensional flow which is encountered in an actual turbomachine are to be taken in a large-scale, two half-blade cascade section.

The complexity in the flow and the small scale of actual-size turbine blades prevents one from probing the flow field and measuring the effects of parameters in detail. Furthermore, turbine blades tend to have small aspect ratios so that the range which is influenced by the endwall cannot be ignored and the secondary flow becomes much more complicated. This large-scale test facility is therefore of value.

The purpose of this study is, first, to document the three-dimensional flow field in the end-wall region in detail by means of simulating the real flow in a simulated cascade constructed with two, large half-blade sections, one wall simulating the pressure surface and the other wall simulating the suction surface. The advantage of using two walls is that one can test in quite a large cascade that is easily accessible with probes, using a small wind tunnel. Also one can change the cascade geometry easily. Most of the investigators who studied the secondary flow effects used multi-blade cascades which are of much smaller scale and are not easily modified.

The second purpose of the study is to begin an investigation into flow control techniques in the end-wall region in order to devise means for reducing the damage on the blade surface due to the vortex structure. Examples may be fences or jet flows used to manipulate the vortices in the end-wall region.

This study would provide enhanced understanding of the flow for the design of turbomachines and for the development of analytical models. It also may yield some techniques for modifying the end-wall region flow.

Later, heat transfer and film cooling effectiveness values will be investigated in the simulated cascade test facility. The three-dimensional flow field is expected to result in complex convective heat transfer coefficient patterns on both the end-wall and airfoil surfaces. It is known that local peaks in heat transfer correlate with secondary flow patterns in the end-wall region.

PROGRESS TO DATE

The test section for this study has been constructed. The chord length of blade which is composed of plexiglass tubing and thin lexan sheet is 23.1 cm and the aspect ratio is 2.64. The incidence angle is 45.7° and the maximum Reynolds number based on the chord length and the nozzle exit velocity is 4.62×10^5.

The two half-blade test section, set up at the nozzle of the wind tunnel, is used to simulate the three-dimensional cascade flow (Fig. E-1a). Confirmation of the 3-D flow through the cascade passage has been made by visualizing the resultant flow field with various visualization techniques. Vorticity indicators and tuft grids were used to observe the behavior of the vorticies within the cascade passage, such as the horseshoe vortex, the passage vortex and the tiny corner vortices. The tuft grid is composed of fishing line constructed in a rectangular grid with yarn pieces connected, with loops, to the grid at each intersection. The yarn filaments point in the direction of the flow. This tuft grid shows the very enhanced motion of the passage vortex and the track of the pressure side leg of the horseshoe vortex within the passage and at the outlet (Fig. E-2).

Due to the pressure gradient, the center of the vortex shifts toward the suction wall near the mid-passage and then climbs the suction wall, becoming bigger as it proceeds downstream. The tiny and weak corner vortex, which is induced by the strong motion of the passage vortex, was not detected by the tuft grid. It was observed in the corner between the endwall and the suction wall by using a vorticity indicator, a small straight-vaned device that spins when inserted into a vortex. The vortex is also shown by the oil and lampblack visualization technique (Fig. E-3b).

Three-dimensional flow at the end-wall and on the blade surface

We conducted another flow visualization study using the oil and lampblack technique which shows the stagnation lines and separation lines on the surface (Fig. E-3). The most striking feature is the separation saddle point, which is the intersection point of the three-dimensional separation line and the reattachment line (stagnation streamline). It divides the entire endwall flow field into distinct regions of three-dimensional flow [Langston, L. S., Nice, M.L. and Hooper, R.M., 1977]. The dark region ahead of the left-hand leading edge in Fig. E-3b represents a stagnant separation bubble, the location and expansion of which depend on the end-wall boundary layer characteristics, the shape of the leading edge and the incidence angle [Sieverding, C. H., 1985]. The track of the suction side leg of the horseshoe vortex is shown near the junction between the endwall and the suction wall of the right-hand blade. The crossflow of the main stream through the passage is a result of the strong pressure gradient from the pressure side to suction side.

More interesting behavior of the passage vortex and the corner vortex formed at the junction of the endwall and the suction wall can be observed in Fig. E-3b, which is the visualization of the three-dimensional flow on the suction surface near the endwall. The figure shows the stagnation line on the leading edge and the lifting of the passage vortex along the suction wall as the vortex grows. There is a reattachment line on the blade surface near the endwall. Below that, a tiny corner vortex of the opposite sign exists.

Based upon the results of the flow visualization study, it is confirmed that this two half-blade cascade simulator displays the main characteristics of the cascade flow, such as the horseshoe vortices, the passage vortex, the saddle point, and the separation bubble region. This preliminary test shows that this facility simulates the three-dimensional flow observed in a true cascade. Since it was observed that the location of the saddle point determines the structure of the horseshoe vortex, which, in turn, has a large effect on the suction wall aerodynamics and heat transfer, more tests to investigate the location and characteristics of the saddle point and separation bubble are planned.

Current Study

Currently, the inflow condition is varied until the upstream region of a typical cascade passage flow, including saddle point, is replicated. This change is effected by moving the sidewalls which extend from the nozzle exit to the leading edges of the two blades. This, in turn, changes the amount of tunnel flow which passes through the cascade passage. The extreme case of these tests is the curved duct flow where the side wall extends all the way to the leading edge. Visualization of this case shows the crossflow, due to the pressure gradient, and the lifting of the passage vortex at the suction wall (Fig. E-3c). On the other hand, the pressure side leg of the horseshoe vortex becomes very weak and not representative of the cascade flow. A bendable sidewall with which the gap ahead of the leading edge can be adjusted was next built (Fig. E-1b). The different type of tuft grid (thinner yarn to minimize flow disturbance) was attached at the endwall to see the movement of the saddle point with the adjustment of the gap. It was observed that the saddle point moves toward the leading edge of the left-side blade, from the mid-passage, as the gap becomes more narrow. This study shows that this wall, with the adjustable gap, is useful for changing the inflow condition and, thus, replicating the upstream region of the cascade flow. The test section is considered satisfactory when the saddle point is at the same position as that in cascade flow, under the same flow conditions. Since the blade in this simulator has the same geometry as the blade used in the naphthalene study, we can qualify our flow by comparison with the results of that cascade, under similar conditions such as Re number based upon chord length and endwall boundary layer thickness.

FUTURE RESEARCH

When this test section has been satisfactorily qualified, it will be available for the study of the three-dimensional endwall flow with great opportunity for access and better resolution than previously made in multi-blade cascades.

The cascade flow shows various patterns which are qualitatively and even quantitatively correct. Dunham [1970] states that the magnitude of the secondary losses depends on the upstream endwall boundary layer thickness. Therefore, much attention

will be given to the endwall boundary layer and the region upstream of the leading edge. The boundary layer thickness will be measured and the effect of it on the endwall vortex structure will be investigated. A more sophisticated vorticity indicator, possibly with the photo-detector, would be useful for measuring the strength of a vortex.

The advantage of this simulator test section is that we can easily investigate the effects of the various upstream conditions on the turbine blade. For example, the effect of the vortices which have been formed at the combustor or upper step of the turbine as well as the vortices which are formed in or upstream of the cascade can be investigated by putting a vortex generator upstream of the blade in our simulator. The detrimental effects of the hot streaks from the combustor on the turbine blade also can be studied with ease.

The facility will eventually allow a study of ways to manipulate the cascade flow. The shape and appropriate position of fences which can change the track of the vorticies, thus reducing their damage on the blade surfaces, can be determined. Jets in the endwall region may also be tried as another flow control technique. When detailed measurements are called upon, continued development of triple-wire velocity probes or vorticity probes will be used.

F. NUMERICAL PREDICTION OF FILM COOLING ON ADIABATIC FLAT PLATE BY INJECTION THROUGH A SINGLE ROW OF HOLES

INTRODUCTION AND OBJECTIVES

High temperature of gases lead to significant increase in output and economy in gas turbine systems, but these high temperatures have detrimental effect on the surfaces exposed to the gases. Most widely used method to locally cool the exposed surface is the injection of a low temperature coolant through a rows of holes. Since, slot cooling (two-dimensional) is not practicable in most applications, film cooling through row(s) of holes is more practical and popular. The effectiveness of the three-dimensional film cooling is significantly lower than the slot injection cooling because the hot mainstream fluid can flow underneath the injected jet due to the secondary flow in the cross-stream direction. In spite of a large amount of experimental effort to study this complicated flow and heat transfer situation, it is still not a well-understood phenomenon. Many studies cite the effects of mainstream turbulence intensities, turbulence scales, blowing rates, injection hole geometries, mainflow and injection Reynolds numbers on the film cooling effectiveness on an adiabatic wall. Some experimental investigations have been reported the effects of the nature of injection viz. injection angle, injection Reynolds number, turbulence intensities and scales, and injection velocity profiles on the cooling effectiveness.

An attempt to study the injection film cooling through a row of holes, using the three-dimensional parabolic numerical scheme [1] is made. The details, advantages and the limitations of this approach are discussed in subsequent sections. Comparison with experimental results and the effect of variation of the main stream turbulence intensities, turbulence scales and injection mass flow rates on the adiabatic wall temperature are presented. The study also demonstrates the successful extension of the regular k-**e** model to this complex problem. Further, this approach can be extended to consider the injection jet characteristics and their interaction with the mainstream flow in detail, complex injection geometries, and curvature of the adiabatic walls. Extensive comparisons with the available experimental results due to Kadotani, Kadotani and Goldstein and with the numerical studies of Bergeles, Launder, Gosma , Rodi and Demuren are presented which validate the fully parabolic approach as a significant and inexpensive tool to predict the flow and heat transfer in the film cooling situations

THE PHYSICAL AND COMPUTATIONAL PROBLEM

Figure F1 shows the problem considered in this study. The hot gases flow over the flat plate and the angular injection of cold fluid is achieved a row holes in the plate. The various geometric parametres governing the performance of the film cooling configuration are shown in the figure along with the computational domain. The single hole geometry is a special case of the geometry shown in the figure F1 with the pitch of the holes increased to delink the possible interference of the neighboring jets. The single hole study was conducted for different blowing rates of 0.1 to 2.0 into a mainflow of velocity 16.5 m/s over the plate with the injection at angle of 30 degrees. The diameter of the injection hole was 1.092 cm in accordance with experimental studies.

The single row multihole configuration, the main area of interest in this study is done for the cases shown in the Table 1. The diameter and pitch of the holes (s/D) were kept at 1.092 cm and 3 respectively for all the cases presented. The list is not claimed to be exhaustive, but contains the cases investigated and documented so far. The notable parameters missing from the list are the pitch, the diameter of the holes, and the boundary layer thickness at the injection hole(s). The work is planned for the next set of investigation and so not included in this report.

Table 1

No.	β (deg.)	M	U_{in}(m/s)	Tu_{in}(%)	Tu_{inj}(%)
1	35	0.2	16.4	20	4
2	35	0.35	16.4	20	4
3	35	0.5	16.4	20	4
4	35	1.5	16.4	20	4
5	35	0.35	16.7	4.8	4
6	35	0.35	16.4	8.21	4
7	35	1.0	16.7	4.8	4
8	35	1.0	16.7	8.21	4
9	35	1.0	16.7	20	4
10	35	0.5	16.7	20	10
11	35	0.5	16.7	20	20
12	35	0.5	16.7	20	50
13	35	0.5	16.7	20	70
14	15	0.5	16.7	20	35
15	25	0.5	16.7	20	35
16	45	0.5	16.7	20	35

GOVERNING EQUATIONS AND TURBULENCE MODEL

The governing equations for time-independent, three-dimensional turbulent flow in terms of the time-averaged quantities in the Cartesian tensor notation are as follows:

Continuity equation:

$$\frac{\partial}{\partial x_i}\left(\rho U_i\right) = 0 \qquad (1)$$

Conservation of momentum:

$$\frac{\partial}{\partial x_j}\left(\rho U_i U_j\right) = \frac{\partial}{\partial x_j}\left(\mu\frac{\partial U_i}{\partial x_j} - \rho\,\overline{u'_i u'_j}\right) + S_i - \frac{\partial p}{\partial x_j} \qquad (2)$$

Conservation of thermal energy:

$$\frac{\partial}{\partial x_j}\left(\rho U_i T\right) = \frac{\partial}{\partial x_j}\left(\Gamma\frac{\partial T}{\partial x_j} - \rho\,\overline{u'_i T'}\right) + S \qquad (3)$$

The Reynolds stress term in equation (2) is expressed in terms of turbulent viscosity μ_t (in the conventional isotropic model) as:

$$-\rho\,\overline{u'_i u'_j} = \mu_t\left(\frac{\partial U_i}{\partial x_j} + \frac{\partial U_j}{\partial x_i}\right) - \frac{2}{3}\delta_{ij}\left(\mu_t\frac{\partial U_l}{\partial x_l} + k\right) \qquad (4)$$

Bergeles, Gosman and Launder proposed an anisotropic modification to the stress terms, which increased the cross-stream diffusion based on the experimental correlation from Quark and Quarmby. The terms involved in this augmentation are described by

$$-\rho\,\overline{uw} = \mu_{tx}\left(\frac{\partial W}{\partial x}\right)$$

$$-\rho\,\overline{vw} = \mu_{ty}\left(\frac{\partial W}{\partial y}\right)$$

$$\frac{\mu_{tx}}{\mu_{ty}} = 1 + \alpha$$

where

$\alpha = 3.5 * (1 - y / \Delta)$ if $y < \Delta$

$\alpha = 0$ if $y > \Delta$.

An effective pressure is defined by including the second term in the equation (4) with the pressure in the momentum equation (2)

$$P = p - \frac{2}{3}\left(\mu_t \frac{\partial U_l}{\partial x_l} + k\right)$$

The real viscosity of the fluid is assumed uniform and thus the source term S = 0. The momentum equation thus can be written as:

$$\frac{\partial}{\partial x_j}\left(\rho U_i U_j\right) = \frac{\partial}{\partial x_j}\left(\mu \frac{\partial U_i}{\partial x_j}\right) - \frac{\partial P}{\partial x_j} + \frac{\partial}{\partial x_j}\left(\mu_{t'}\left(\frac{\partial U_i}{\partial x_j} + \frac{\partial U_j}{\partial x_i}\right)\right). \quad (5)$$

The $\mu_{t'}$ is modified to include the anisotropic terms in the appropriate equations.

The convention adopted in this section is a Cartesian coordinate system with z as the mainstream direction, x and y in the cross-stream directions and w, u, and v are the corresponding time averaged velocities. Under the parabolic assumption, the diffusion is considered negligible compared to the convective transport in the main-stream directions. The general momentum equation can be further simplified to:

$$\frac{\partial}{\partial x_j}\left(\rho U_i U_j\right) = \frac{\partial}{\partial x_j}\left(\mu_{eff} \frac{\partial U_i}{\partial x_j}\right) - \frac{\partial P}{\partial x_i} + S_i \quad (6)$$

where,

u-momentum $S_x = \left(\frac{\partial \mu_t}{\partial y}\right)\frac{\partial V}{\partial x} - \left(\frac{\partial \mu_t}{\partial x}\right)\frac{\partial V}{\partial y}$

v-momentum $S_y = \left(\frac{\partial \mu_t}{\partial x}\right)\frac{\partial U}{\partial y} - \left(\frac{\partial \mu_t}{\partial y}\right)\frac{\partial U}{\partial x}$

w-momentum $S_z = \frac{\partial}{\partial x}\left(\alpha \mu_t \frac{\partial W}{\partial x}\right)$

and effective viscosity $\mu_{eff} = \mu_t + \mu$

in the energy equation (3) we define the turbulent flux term

$$-\rho\,\overline{u'_i T'} = \Gamma_t \frac{\partial T}{\partial x_i}$$

where

$$\Gamma_t = \frac{\mu_t}{pr_t}$$

and since $\mu_t >>> \mu$

$$\Gamma_{eff} = \frac{\mu_t}{pr_t}$$

The anisotropic diffusion model is extended to the scalar transport in the similar manner to the momentum transport. Therefore, the ratio of x direction diffusion coefficient to y direction diffusion coefficient is given by

$$\frac{\Gamma_{tx}}{\Gamma_{ty}} = 1 + \alpha$$

where α is defined as in the momentum equations.

The energy equation is then

$$\frac{\partial}{\partial x_i}\left(\rho U_i T\right) = \frac{\partial}{\partial x_i}\left(\Gamma_{eff}\frac{\partial T}{\partial x_i}\right) + \frac{\partial}{\partial x}\left(\alpha\Gamma_{eff}\frac{\partial T}{\partial x}\right). \qquad (7)$$

The last term is the anisotropic contibution and note that it is not in the tensor form (x is the x-direction in the physical and computational domain)

The boundary conditions for the problem are :

$\frac{\partial V}{\partial x} = 0,\quad u = 0,\quad \frac{\partial W}{\partial x} = 0,\quad \frac{\partial T}{\partial x} = 0$ at x = 0 and x = xl

(symmetric - boundary)

$v = 0,\ w = 0,\ u = 0$ at y = 0 (wall boundary)

$\frac{\partial U}{\partial y} = 0,\ \frac{\partial W}{\partial y} = 0,\ V = 0$ at y = yl (symmetric boundary)

in the injection zone (at y = 0)

$w = v_{inj}\cos(\beta)$

$v = v_{inj}\sin(\beta)$.

The initial conditions at the inlet are

$w = w_{in}$, $u = 0$, $v = 0$, and $T = T_{in}$ for all x and y at $z = 0$.

The **k-ε** turbulence model

This **k-ε** model is used to formulate an expression for the turbulent viscosity or equivalently the turbulent Reynolds stress in momentum equations. We need to solve the additional transport equations for the turbulent kinetic energy **k** and dissipation ε .The equations describing the model are presented here for the steady case.

$$\mu_t = \frac{C_\mu \rho k^2}{\varepsilon} \qquad (8)$$

$$\frac{\partial}{\partial x_i}\left(\rho u_i k\right) = \frac{\partial}{\partial x_i}\left(\frac{\mu_t \partial k}{\sigma_k \partial x_i}\right) + G - \rho\varepsilon \qquad (9)$$

$$\frac{\partial}{\partial x_i}\left(\rho u_i \varepsilon\right) = \frac{\partial}{\partial x_i}\left(\frac{\mu_t \partial \varepsilon}{\sigma_\varepsilon \partial x_i}\right) + (G\, C_1 - \rho\varepsilon C_2)\frac{\varepsilon}{k} \qquad (10)$$

where,

$$G = \mu_t\left(\frac{\partial U_i}{\partial x_j} + \frac{\partial U_j}{\partial x_i}\right)\frac{\partial U_i}{\partial x_j}$$

and the empirical constants of the regular k-ε model are :

$C_1 = 1.44$, $C_2 = 1.92$, $C_\mu = 0.09$

$\sigma_k = 1.0$, $\sigma_\varepsilon = 1.3$.

The boundary conditions are as follows:

$\frac{\partial k}{\partial y} = 0$, $\frac{\partial \varepsilon}{\partial y} = 0$ y = yl (symmetric boundary)

$\frac{\partial k}{\partial y} = 0$ y = 0 (wall boundary)

$\frac{\partial k}{\partial x} = 0$ $\frac{\partial \varepsilon}{\partial x} = 0$ at x = 0 and x = xl (symmetric boundary)

while, in the injection zone on the wall (y= 0)

$k=k_{inj}$ and $\varepsilon = \varepsilon_{inj}$

and the initial conditions at z = 0 are $k = k_{in}$ and $\varepsilon = \varepsilon_{in}$.

The turbulent viscosity is much greater than the molecular viscosity for most part of the flow, but near the wall both the viscosities are comparable. Here we use the wall functions to deduce the effective viscosity in the near wall region. The k-ε turbulence model has been successfully tested for many problems in two dimensions and a few three dimensional cases. The effectiveness of the model in capturing this three dimensional mixing phenomenon is being tested in this work.

The three-dimensional parabolic solution procedure developed by Patankar and Spalding(1972) is used to solve the five transport equations introduced in this section. The cross-stream pressure distribution in and around the injection zone will be non-uniform leading to large amounts of secondary cross-stream flow. But this method computes an average effective pressure gradient uniform over the cross-section, while in reality the flow near the jet will have non-inform pressure gradients. The errors introduced by this step will be serious if the parabolic assumption for the flow breaks down. As the results will show, the effects of the errors in the pressure gradient computations are limited to the zone very close to the injection port. It is this pressure computation that allows the development of the marching procedure which saves large amounts of computer effort and memory compared to a full-scale three-dimensional elliptic solution procedure.

RESULTS AND DISCUSSION

The objective of the reasearch is develop the capabilty to control, predict and study the adiabatic wall temperature under various flow situations. This adiabatic wall temperature is expressed by a dimensionless temperature called the film cooling effectiveness, defined as :

$$\eta = \frac{(T_{aw} - T_{inf})}{(T_c - T_{inf})}$$

where T_{aw} is the adiabatic wall temperature, T_{inf} is temperature of the hot main stream and T_c is the temperature of the cooler injectant fluid. The results presented in this section show the effects of the variation in some key parameters on the film cooling effectiveness.

a) The performance of the augmented turbulence model is studied through comparisons of the calculations of the single hole configuration with the available experimental and numerical data from the work performed by Bergeles, Launder and Gosman (1976, 1977, 1978). The Figures F2a and F2b show this comparison for two different blowing rates of 0.2 and 1.0. The performance of both the solution procedure is in good agreement the experimental and numerical data from a partially parabolic calculation.

b) A similar comparitive study is shown in Figure F3 for the sinle row of holes configuration (case 3) with the experimental results from Kadotani (PhD thesis U. of Minn.). The centerline and the away-from-centerline effectiveness of the fully parabolic procedure are in good agreement with the experiments. Figure F4a-c show the lateral effectiveness along with those of Kadotani's and the numerical results of three-dimensional calculations of Demuren and Rodi. The performance of the present procedure is comparable to that of the more expensive and computationally intensive procedure of Rodi and Srivatsa used by Demuren.

c) Figures F5a-c show the extension of the study of single row of holes configuration to cover different blowing rates. The results are in excellent agreement with the expected qualitative behavior for the physical situation. Figure F6 shows the typical secondary motion, set up due to the injection of the jet into the mainstream, at cross-sections 5, 10, 15 and 20 diameters downstream of the injection. It is this secondary motion that reduces the film cooling performance of the discreet hole cooling process as compared to the slot cooling.

d) The previous report demonstrated the insensitivity of the centerline cooling effectiveness to the variations in the mainstream turbulence intensity for a blowing rate of M = 0.5. Figure F7 shows a similar study for M = 1.0 (cases 7, 8 and 9). The observed insensitivity, as previously discussed, is attributed to the comparable thickness of boundary layer and penetration height of the jet which pevents the proper mixing of the two streams. A study at a even higher blowing rate should be more informative.

e) The injection characteristics of the jet are as important as the mainstream characteristics. Figure F8 shows the sensitivity of the centerline cooling effectiveness to the variations in the injection turbulence intensity. The higher mixing or turbulent diffusive transport results due to the increase in jet turbulence intensity. This initially increases the cooling effectiveness as the increased diffusion overcomes the effect of the convective inertia of the jet which tends to carry the injected fluid away from the surface just aft of the injection port. The increased diffusion also increases the mixing of the cold jet fluid with hot fluid in the boundary layer. This results in the decrease of the effectiveness beyond 2 or 3 diameters downsteream of the injection holes.

f) The angle of injection has a pronounced effect on the film cooling performance. Figure F9 shows that the cooling effectiveness decreases along the calculation domain as the angle of injection becomes larger. The shallow injection angle tends to keep the cool jet fluid within the boundary layer leading to better cooling performance compared to the larger angles of injection. As the angle of injection becomes larger the reliabilty of the fully parabolic solution procedure becomes questionable, while the very shallow angles are limited by engineering considerations.

SUMMARY OF PROGRESS TO DATE

The numerical solution procedure is successful in capturing the phenomenon of film-cooling. It can be seen that through these sensitivity studies we can establish the important parameters that affect the film cooling effectiveness.The results of such studies can aid an experimentalist to decide on design of the setup, and identify quantities that are important to be measured or deduced in the course of the experiment. The numerical method can calculate all the variables, at all locations in the domain and the results, when confirmed through experiments, will enrich the body of information obtained experimentally. Further, the detailed computational results will provide a cleaner picture of the flow and lead to a better physical insight into the physical phenomenon.

NEAR-TERM PLANS

Throughout this study many areas of possible study have been suggested. Now that the procedure has been tested satisfactorily, the following further investigations are planned.

a) effects on the cooling effectiveness downstream and cross-stream with changes in:

i) injection angles.

ii) turbulence intensity and scales of coolant.

iii) many cross correlations of these parameters.

b) study the flow pattern and its sensitivity to various parameters that have already been identified.

FUTURE PLANS

1) MORE FILM COOLING STUDIES:

More film cooling studies are planned, which include computing flow with more complex injection geometries, two rows of holes in a staggered configuration, more complex wall geometries viz. curvature effects such as in the turbine blade geometries.

2) COMPLETE THREE DIMENSIONAL COMPUTATION:

This study is being planned to predict the horse-shoe vortex near the base of cylinder in the flow. This is being done as a preliminary study to investigate the flow near the base of a turbine blade. The effects on the film cooling of the blade geometries is also being planned.

REFERENCES

Bergeles, G., Gosman, A.D. and Launder, B.E., (1976), "The Prediction of Three Dimensional Discrete Hole Cooling Process, ASME J. Heat Transfer, Vol. 98, p. 379.

Bergeles, G., Gosman, A.D. and Launder, B.E., (1978), "The Turbulent Jet in Cross Stream at Low Injection Rates: A Three-Dimensional Numerical Treatment, Num. Heat Tran., Vol. 1, pp. 217-242.

Chen, P. H. and Goldstein, R. J., (1988), "Convective Transport Phenomena on a Turbine Blade," Proc. of the 3rd Intl. Symp. on Transport Phenomena in Thermal Control, Taipei.

Chen, P. H. and Goldstein, R. J., (1989), "The Influence of Secondary Flows on Convective Transport from the Convex Surface of a Turbine Blade," Submitted for Publication.

Demuren, A.O. and Rodi, W., (1983), "Three-Dimensional Calculation of Film Cooling Jet by a Row of Holes," Notes, Num. Fluid Mech., Vol. 7, pp. 49-56.

Dunham, J., (1970), "A Review of Cascade Data on Secondary Losses in Turbines," J. of Mechanical Engineering Science, vol. 12, pp. 48-59.

Goldstein, R.J., Eckert, E. R. G, Ericksen,V. L. and Ramsey, J.W., (1970), "Film Cooling Following Injection through Inclined Circular Tubes," Israel J. of Technology, Vol.8, p. 145.

Goldstein, R. J. and Spores, R. A., (1988), "Turbulent Transport on the Endwall in the Reqion between Adjacent Blades," J. Heat Transfer, Vol. 110, No. 4A, pp. 862-869.

Goldstein, R. J., Yoo, S. Y. and Chung, M. K., (1989), "Mass Transfer from a Square Cylinder and its Endwall in Crossflow," to appear in the Intl. J. of Heat and Mass Transfer.

Hain, R. C., Wang, H. P., Chen. P. H. and Goldstein, R. J., (1988), "A Microcomputer-controlled Data Adquisition system for Naphthalene Sublimation Measurement," to be published.

Jabbari, M.Y., Goldstein, R.J., (1978), 'Adiabatic Wall Temperature and Heat Transfer Downstream of Injection Through Two Row of Holes,' Eng.of Power, Vol. 100, No.2, pp. 303-307.

Kadotani, K., Goldstein, R.J., (1979), "Effect of Mainstream Variables on Jets Issuing from a Row of Inclined Round Holes," Eng.of Power, Vol. 101, No.2, pp 298-304.

Kadotani, K. (1975) PhD Thesis, U. of Minn

Karni, J. and Goldstein, R. J., (1989), "Surface Injection Effect on Mass Transfer from a Cylinder in Crossflow: A Simulation of Film Cooling in the Leading Edge Region of a Turbine Blade," to appear in the J. of Turbomachinery.

Karni, J. and Goldstein, R. J., (1985), "Endwall Effects on Local Mass Transfer from a Cylinder in Crossflow," Proc. of the 2nd Intl. Symp on Refined Flow Modeling and Turbulence Measurements, Vol. 1 K4, pp. 1-33.

Kim J., Simon T. W. and Kestoras M., (1989), "Fluid Mechanics and Heat Transfer Measurements in Transitional Boundary Layer Conditionally Sampled on Intermittency," to be given at the National Heat transfer Conference, Philladelphia, PA.

Kim J., Kline S. J. and Johnston J. P., (1978), "Investigation of Separation and Reattachment of a Turbulent Shear Layer: Flow over a Backward Facing Step," AFOSR, Mechanics Division, Contract AF-F44620-74-C-0016, Report MD-37, p.137.

Langston, L. S., Nice, M.L. and Hooper, R.M., (1977), "Three-Dimensional Flow Within a Turbine Cascade Passage," ASME J. of Engineering for Power, vol. 99, No. 1, pp. 21-28.

Patankar, S.V. and Spalding, D.B., (1972), 'A Calculation Procedure for Heat, Mass and Momentum Transfer in Three-Dimensional Parabolic Flows," Int. J. Heat Mass Transfer, Vol. 15, p. 1787.

Patankar, S.V. (1980), Numerical Heat Transfer and Fluid Flow, Hemisphere Pub. Co .

Rodi, W., (1980), Turbulence Models and their Applications in Hydraulics, Int. Assoc. for Hydraulic Research, Delft, The Netherlands.

Sieverding, C. H., (1985), "Recent Progress in the Understanding of Basic Aspects of Secondary Flows in Turbine Blade Passages," J. of Engineering for Gas Turbines and Power, vol. 107, pp. 248-257.

Schwarz, S. G. and Goldstein, R. J., (1989), "The Two-dimensional Behavior of Film Cooling Jets on Concave Surfaces," J. of Turbomachinery, Vol, 111, pp. 124-130.

APPENDIX I

PUBLICATIONS FROM THE SPONSORED RESEARCH:

Ito, S., Eckert, E. R. G. and Goldstein, R. J., "Aerodynamic Loss in a Gas Turbine Stator with Film Cooling," J. Engrg. Power, Vol. 102, pp. 964-970, 1980.

Goldstein, R. J. and Yoshida, T. "The Influence of a Laminar Boundary Layer and Laminar Injection on Film Cooling Performance," J. Heat Transfer, Vol. 104, pp. 355-363, 1981.

Goldstein, R. J. and Taylor, J. R., "Mass Transfer in the Neighborhood of Jets Entering a Crossflow," ASME Paper 82-HT-62, Presented at the 1982 National Heat Transfer Conference, 1982; J. Heat Transfer, Vol. 104, pp. 715-721, 1982.

Goldstein, R. J. , Kornblum, Y. and Eckert, E. R. G., "Film Cooling Effectiveness on a Turbine Blade, " Presented at the 24th Israel Annual Conference on Aviation and Astronautics, February 1982; Published in the Israel J. of Technology, Vol. 20, pp. 193-200, 1982.

Yoshida, T., and Goldstein, R. J., "On the Nature of Jets Issuing from a Row of Holes into a Low Reynolds Number Mainstream Flow," 83-TOKYO-IGTC-18, Proceedings of the 1983 Tokyo Gas Turbine Congress, Vol. I, p. 135, 1983; J. Heat Transfer, Vol. 104, pp. 355-363, 1982.

Goldstein, R. J., "Heat Transfer in High-Temperature Gas Turbines: Film Cooling and Impingement Cooling," Heat Transfer in Energy Problems, Proceedings of the Japan-United States Joint Seminar, Tokyo, 1980, pp. 13-21, New York: Hemisphere Publishing Corp., 1983.

Eckert, E. R. G., "Analysis of Film Cooling and Full-Coverage Film Cooling of Gas Turbine Blades," 83-TOKYO-IGTC-15, Proceedings of the 1983 Tokyo Gas Turbine Congress, Vol. I, p. 109, 1983; ASME J. Engrg. for Power, Vol. 106, pp. 206-213, 1984.

Goldstein, R. J., "Mass Transfer System for Simulating Heat Transfer Processes, Proceedings of the 1983 ICHMT Conference, J. Engrg. for Gas Turbines and Power, p. 612, July, 1984.

Goldstein, R. J., "Film Cooling on a Gas Turbine Blade near the End Wall," 84-GT-42, 1984 International Gas Turbine Conference, Amsterdam, The Netherlands, 1984.

Goldstein, R. J. and Karni, J., "The Effect of a Wall Boundary Layer on Local Mass Transfer from a Cylinder in Crossflow," ASME Journal of Heat Transfer, Vol. 106, No. 2, pp. 260-267, May 1984.

Goldstein, R. J. and Chen, P. H. "Film Cooling on a Gas Turbine Blade Near the End Wall," Paper No. 84-GT-42, 1984, Presented at the 1984 International Gas Turbine Conference, 1984; J. Engrg. for Gas Turbines and Power, Vol. 107, pp. 117-122, 1985.

Karni, J. and Goldstein, R. J., "Endwall Effects on Local Mass Transfer from a Cylinder in Crossflow," Proc. of the 2nd Intl. Symp on Refined Flow Modeling and Turbulence Measurements, Vol. 1 K4, pp. 1-33, 1985

Wang, T., Simon, T. W. and Buddhavarapu, J., "Heat Transfer and Fluid Mechanics Measurements in Transitional Boundary Layer Flows," ASME Paper 85-GT-113, Presented at the 1983 International Gas Turbine Conference, Houston; J. of Engrg. for Gas Turbines and Power, Vol. 107, pp.1007-1015, 1985.

Goldstein, R. J., Chyu, M. K. and Hain, R. C., "Measurement of Local Mass Transfer on a Surface in a Region of the Base of a Protruding Cylinder with a Computer-Controlled Data Acquisition System," Int. J. Heat and Mass Transfer, Vol. 28, no. 6, pp. 1187-1196, 1985.

Wang. T. and Simon, T. W., "Heat Transfer and Fluid Mechanics Measurements in Transitional Boundary Layer Flows," J. Engr. Gas Turbines and Power, Vol. 107., No. 4, pp. 1007-1015., 1985.

You, S. M., Simon, T. W. and Kim, J., "Boundary Layer Heat Transfer and Fluid Mechanics Measurements on a Mildly-curved Convex Wall," Proc. of the Eighth Int. Heat Transfer Conference, Vol. 3, pp. 1089-1094, 1986.

You, S. M., Simon, T. W. and Kim, J. "Free-stream Turbulence Effects on Convex-curved Turbulent Boundary Layers," ASME Paper No. 86-WA/HT-46, 1986.

Wang, T. and Simon, T. W., "Heat Transfer and Fluid Mechanics Measurements in Transitional Boundary Layers on Convex-curved Surfaces, Paper no. 85-HT-60, 1985, Presented at the 1985 National Heat Transfer Conference, Denver Colorado; ASME J. of Turbomachinery, Vol. 109, No. 3, pp. 443-452, 1987.

Eckert, E. R. G., "Cross-Transport of Energy in Fluid Streams," Wärme und Stoffübertragung, 21, pp. 73-81, 1987.

Shadid, J. N., and Eckert, E. R. G., "The Mass Transfer Analogy to Heat Transfer in Fluids with Temperature Dependent Properties", circa, 1987.

Park, W., and Simon, T. W., "Prediction of Convex-Curved Transitional Boundary Layer Heat Transfer Behavior Using MLH Models," Proc. of the 1987 AASME-JSME Thermal Engr. Joint Conference, 1987.

Kim, J. and Simon, T. W., "Measurements of the Turbulent Transport of Heat and Momentum in Convexly Curved Boundary Layers: Effects of Curvature, Recovery and Free-stream Turbulence," ASME Paper No. 87-GT-199, Presented at the 1987 International Gas Turbine Conference, 1987; J. of Turbomachinery, Vol. 110, No. 1, pp. 80-87, 1988.

Chen, P. H. and Goldstein, R. J., :"Convective Transport Phenomena on a Turbine Blade," Proc. of the 3rd Intl. Symp. on Transport Phenomena in Thermal Control, Taipei, 1988.

Goldstein, R. J. and Spores, R. A., "Turbulent Transport on the Endwall in the Reqion between Adjacent Blades," J. Heat Transfer, Vol. 110, No. 4A, pp. 862-869, 1988

Schwarz, S. G. and Goldstein, R. J., "The Two-dimensional Behavior of Film Cooling Jets on Concave Surfaces," J. of Turbomachinery, Vol, 111, pp. 124-130, 1989.

Goldstein, R. J., Yoo, S. Y. and Chung, M. K. "Mass Transfer from a Square Cylinder and its Endwall in Crossflow," to appear in the Intl. J. of Heat and Mass Transfer, 1989.

Kim J., Simon T. W. and Kestoras M., "Fluid Mechanics and Heat Transfer Measurements in Transitional Boundary Layer Conditionally Sampled on Intermittency, to be given at the National Heat transfer Conference, Philladelphia, PA, 1989.

Karni, J. and Goldstein, R. J., "Surface Injection Effect on Mass Transfer from a Cylinder in Crossflow: A Simulation of Film Cooling in the Leading Edge Region of a Turbine Blade," to appear in the J. of Turbomachinery, 1989.

Russ, S. and Simon, T. W., "Signal Processing using the Orthogonal Probe Equations", submitted to TSI Flowlines, 1989.

Hain, R. C., Wang, H. P., Chen. P. H. and Goldstein, R. J., "A Microcomputer-controlled Data Adquisition system for Naphthalene Sublimation Measurement," to be published, 1989.

Chen, P. H. and Goldstein, R. J., "The Influence of Secondary Flows on Convective Transport from the Convex Surface of a Turbine Blade," Submitted for Publication, 1989.

APPENDIX II

PROPOSAL AND PAST PROGRESS REPORTS

Research on Heat Transfer Related to Development of High Temperature Gas Turbines: Proposal to the Air Force Office for Scientific Research: Proposed period 1 March 1986 - 28 February 1989.

Studies of Gas Turbine Heat Transfer, Airfoil Surface and End-Wall: Annual Progress Report: 1 March 1985 - 28 February 1986, April 1986.

Research on Fluid Flow and Heat Transfer Relating to Development of High Temperature Gas Turbines; Proposal and Progress Report, November 1986.

Studies of Gas Turbine Heat Transfer, Airfoil Surface and End-Wall: Annual Progress Report: 15 April 1986 - 15 March 1987, April 1987.

Review of Major Findings on AFOSR-sponsored Research, August 1987.

Studies of Gas Turbine Heat Transfer Airfoil Surface and End-Wall Cooling Effects Annual Progress and Forecast Report: 15 April 1987 - 1 December 1987 , January 1988 (a budget for the period 3/1/88- 2/28/89 was attached).

Studies of Gas Turbine Heat Transfer Airfoil Surface and End-Wall Cooling Effects Annual Progress Report: 1 March 1987 - 30 April 1988, March 1988.

Proposal to Air Force Office of Scientific Research--Research on Fluid Flow Relating to Development of High Temperature Gas Turbines, November 1988.

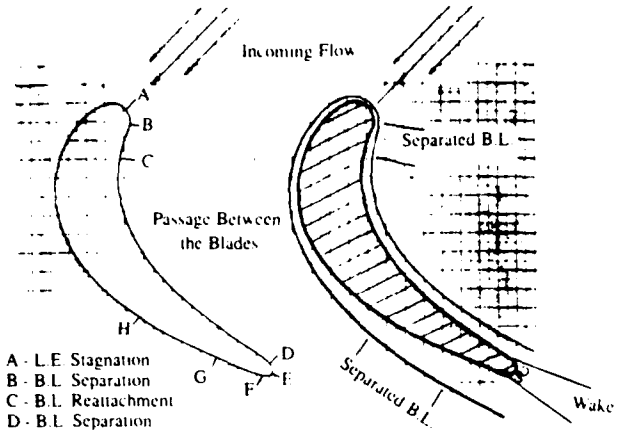

Boundary layer flow over the blade in two dimensional region

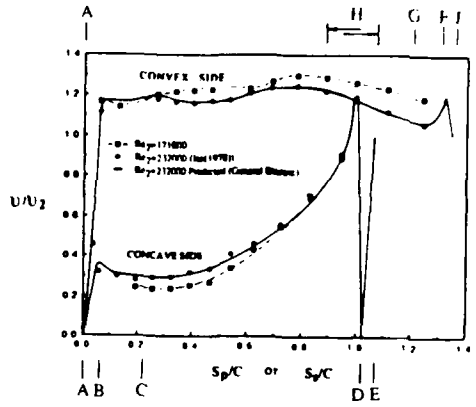

Velocity distribution along the blade surface

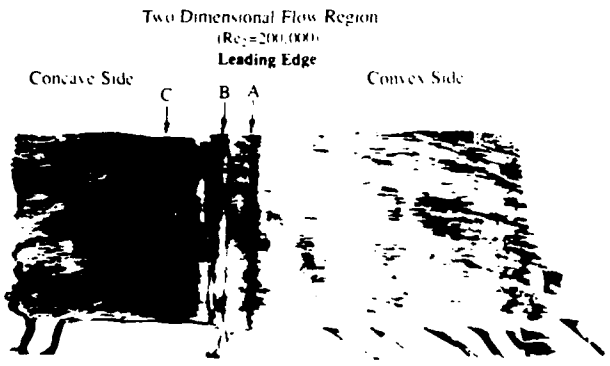

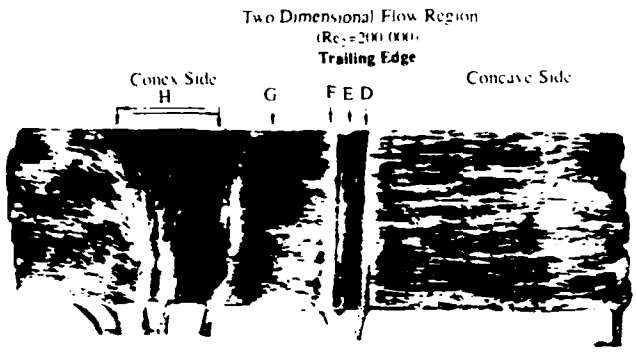

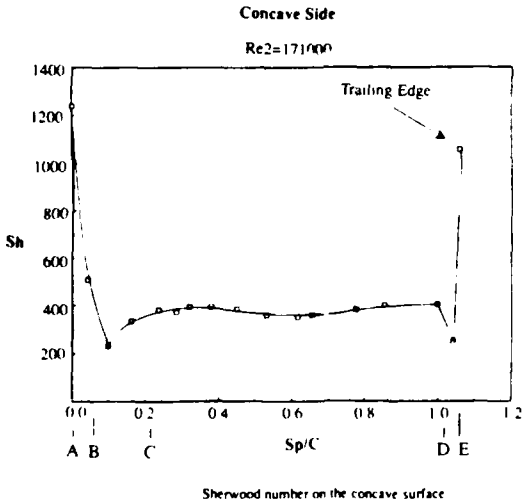

Sherwood number on the concave surface

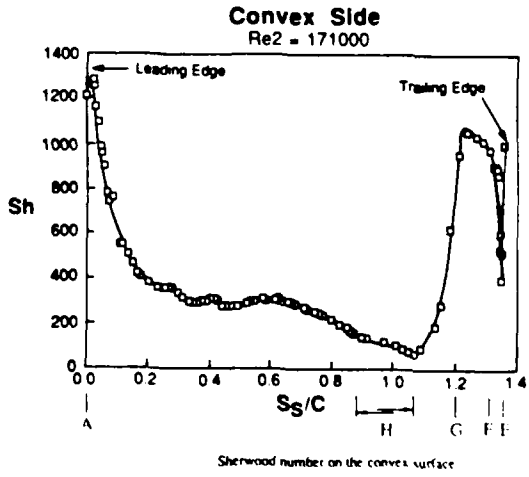

Sherwood number on the convex surface

Figure A-1. Comparison of pressure measurements, mass transfer, and visualization (two dimensional flow region)

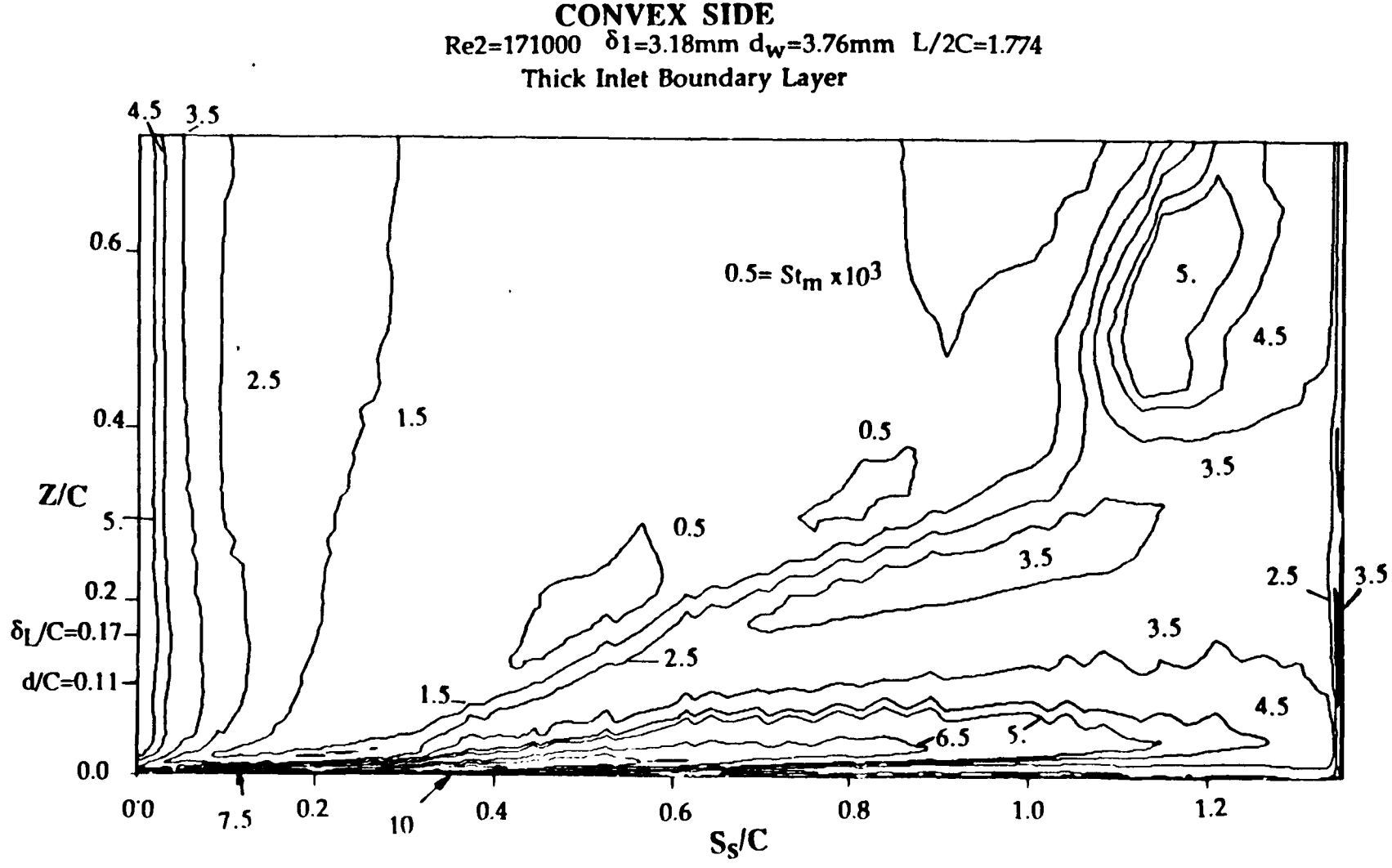

Figure A-2. Contours of mass transfer (Stanton number) near the endwall

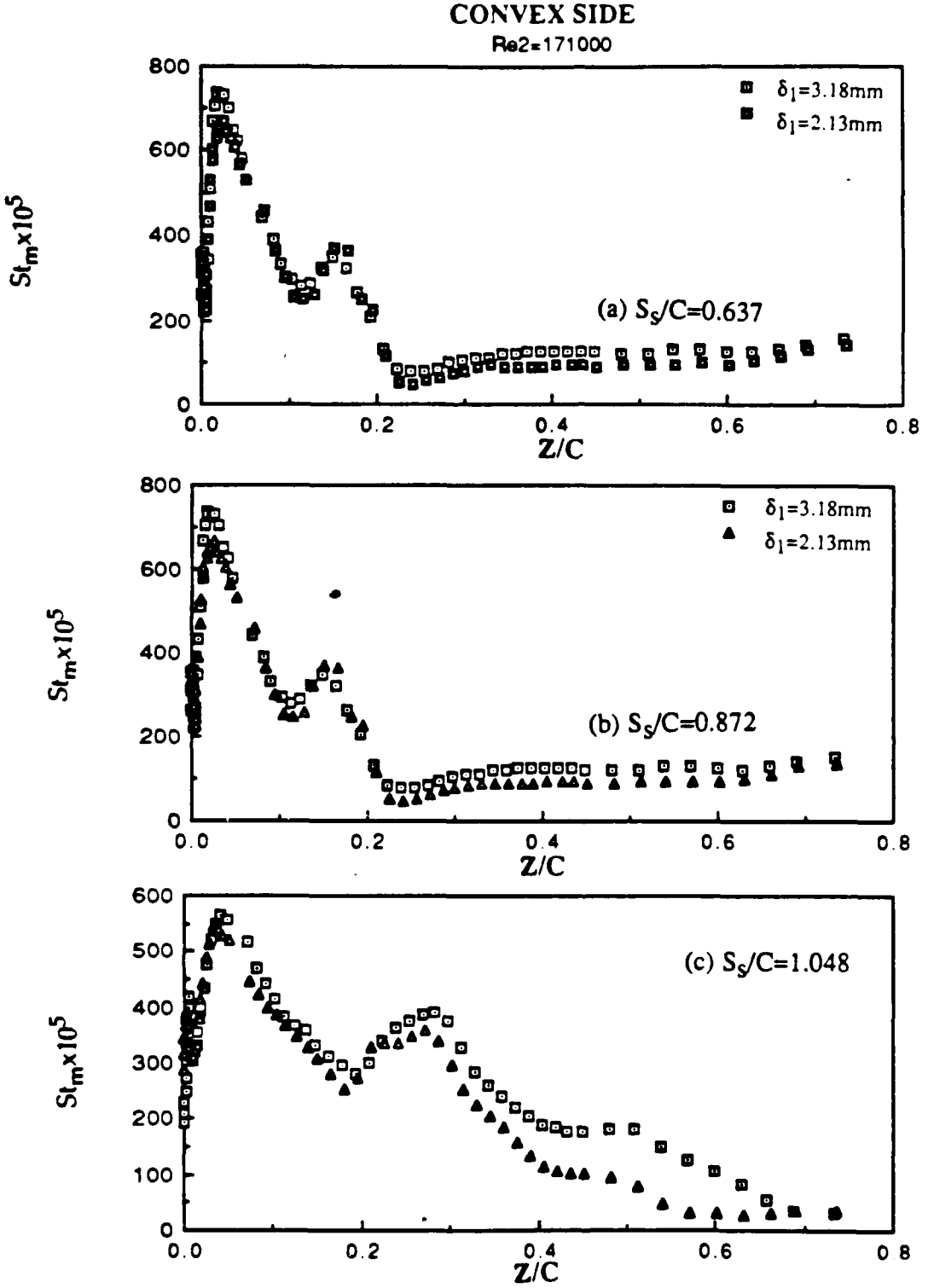

Figure A-3. Distribution of Stanton number near the endwall

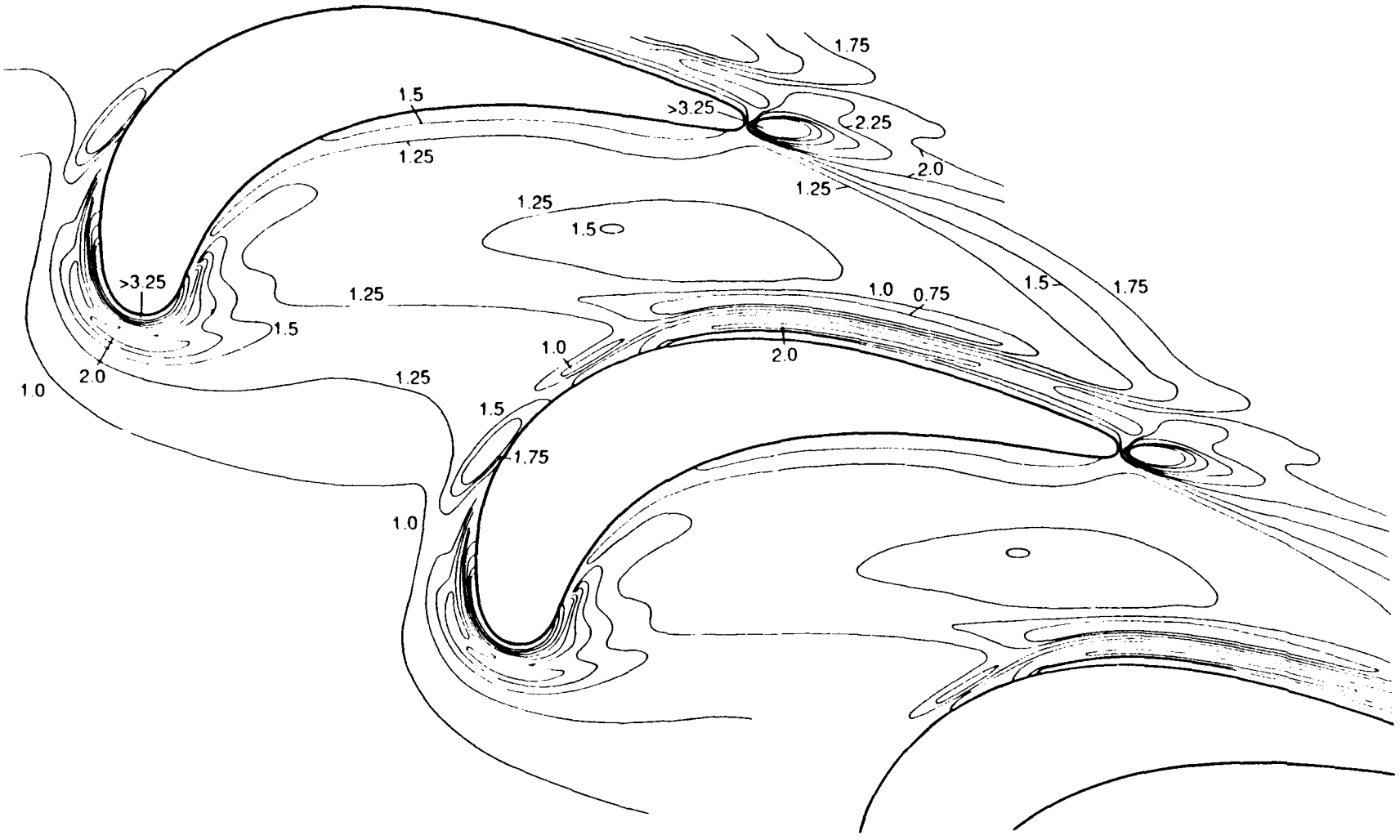

Case 1, Main Test Case

Contours of St_m/St_{mo} =

0.75, 1.0, 1.25, 1.5, 1.75, 2.0, 2.25, 2.5, 2.75, 3.0, 3.25

Figure A-4. Contours of mass transfer on the endwall of a turbine blade passage

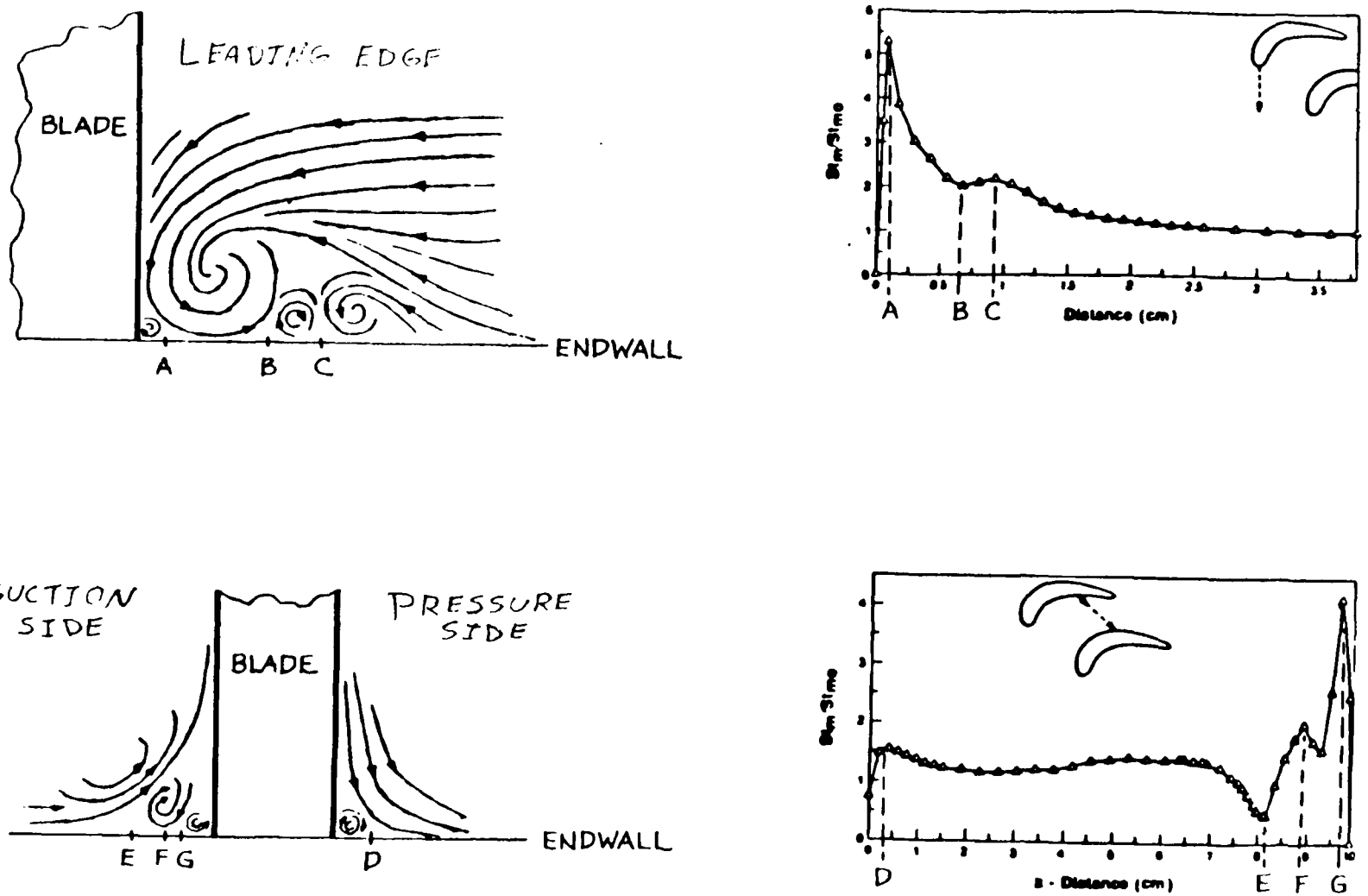

Figure A-5. Distribution of the Stanton number on the endwall and a sketch of the leading edge and corner vortices

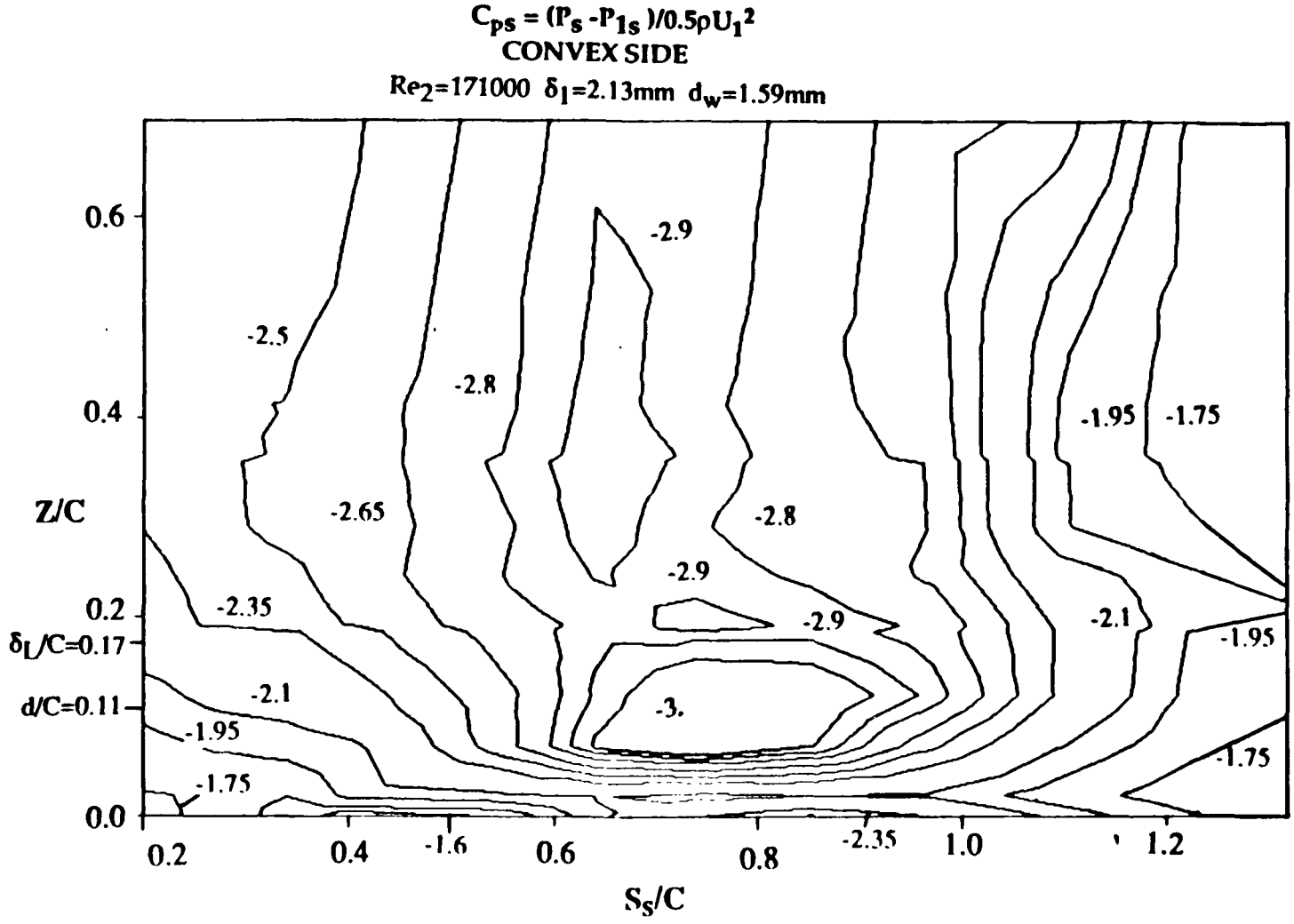

Figure A-6. Contours of the pressure coefficient

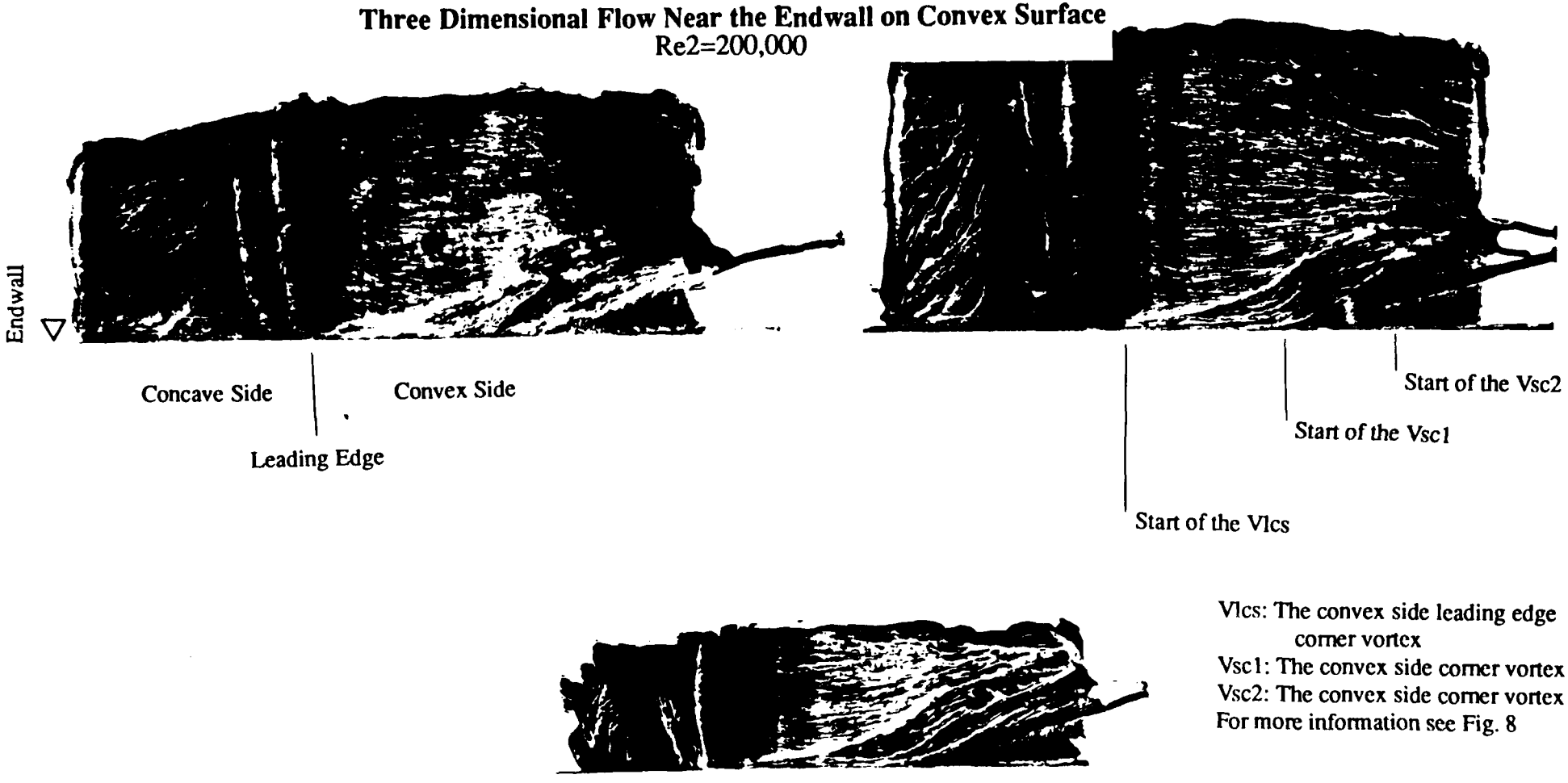

Figure A-7. Flow visualization near the endwall

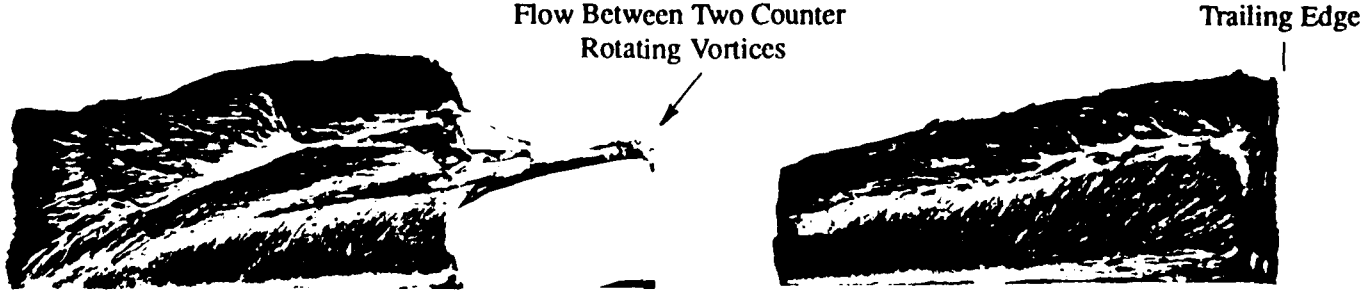

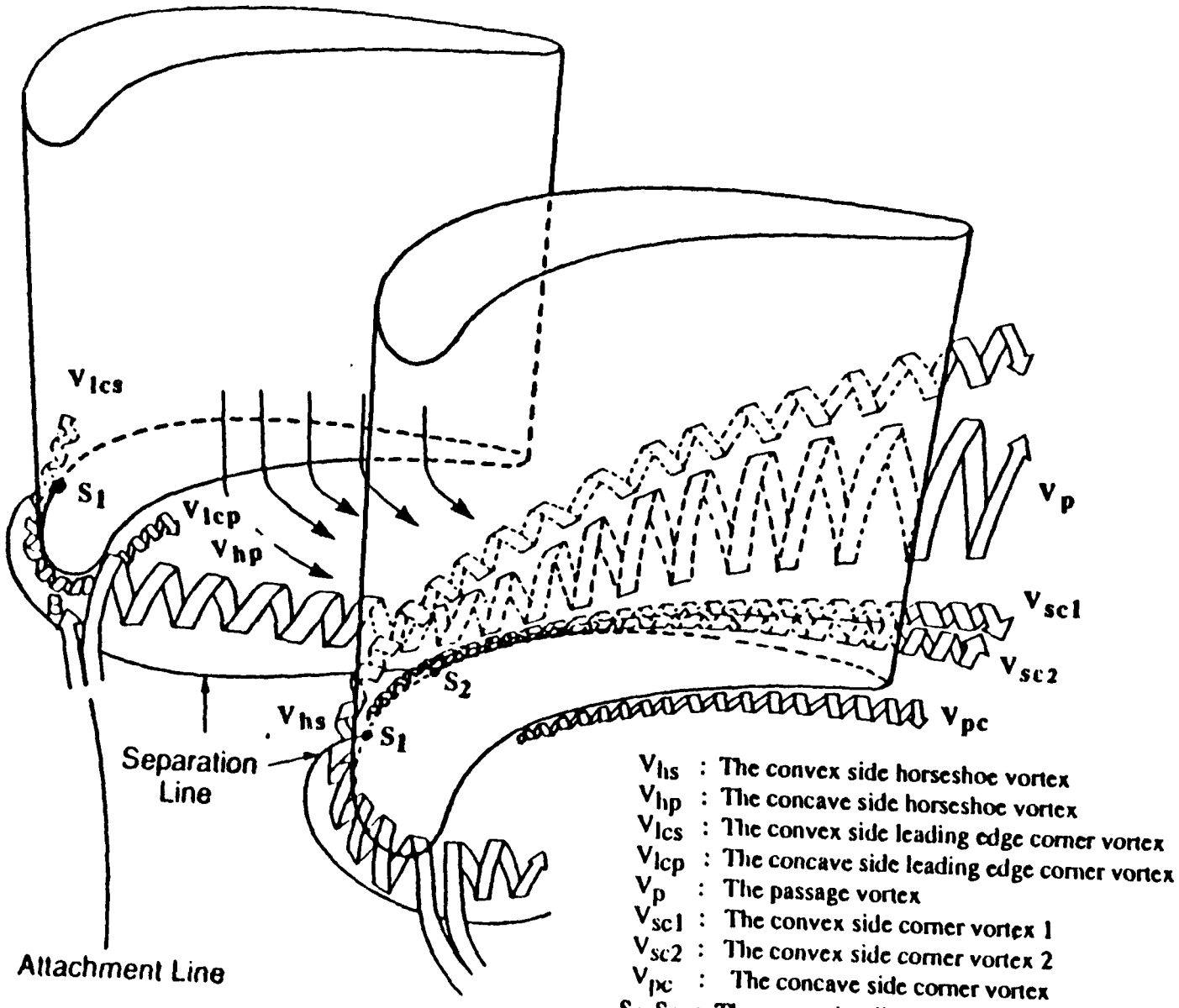

Diagrams of turbine blade vortices

Figure A-8. Sketch of vortices forming around a turbine blade

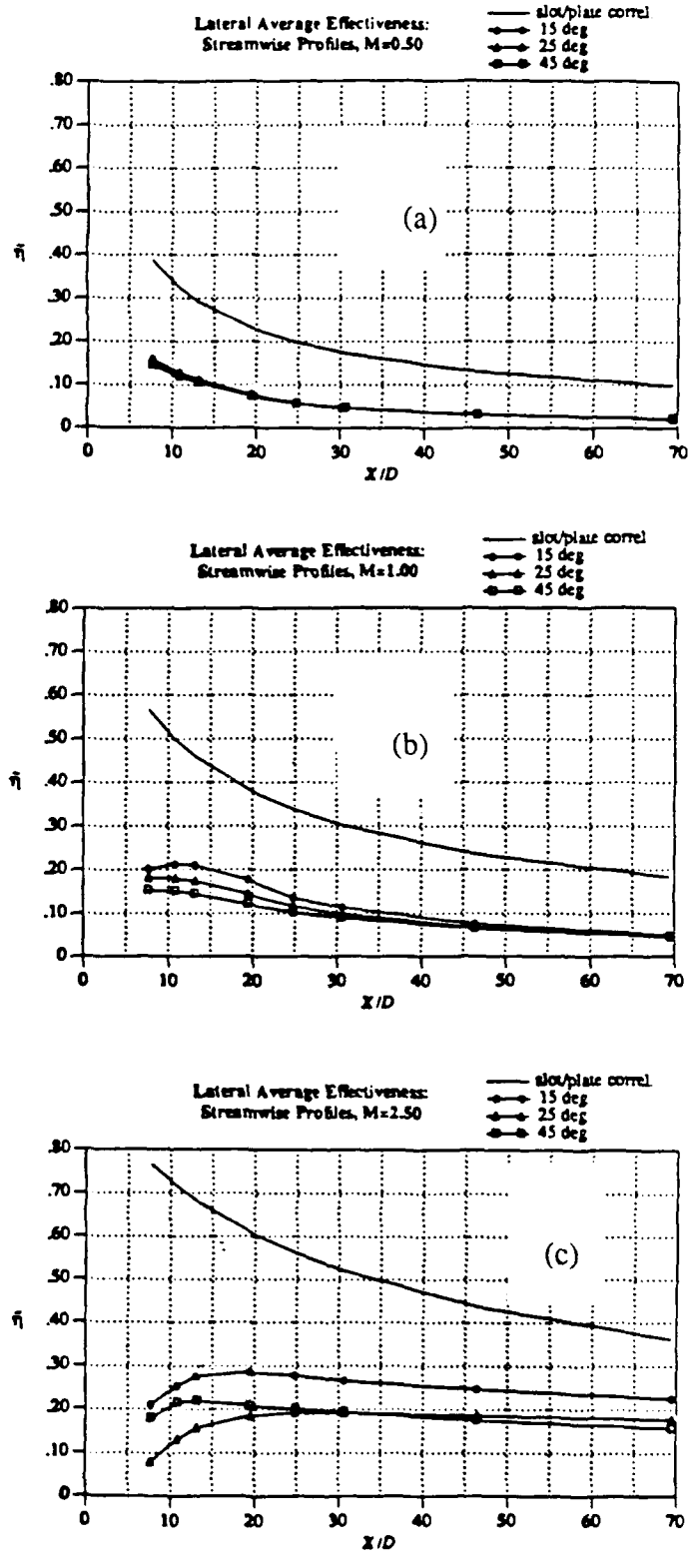

Fig. B-1 - Effect of Injection Angle on Laterally Averaged Effectiveness

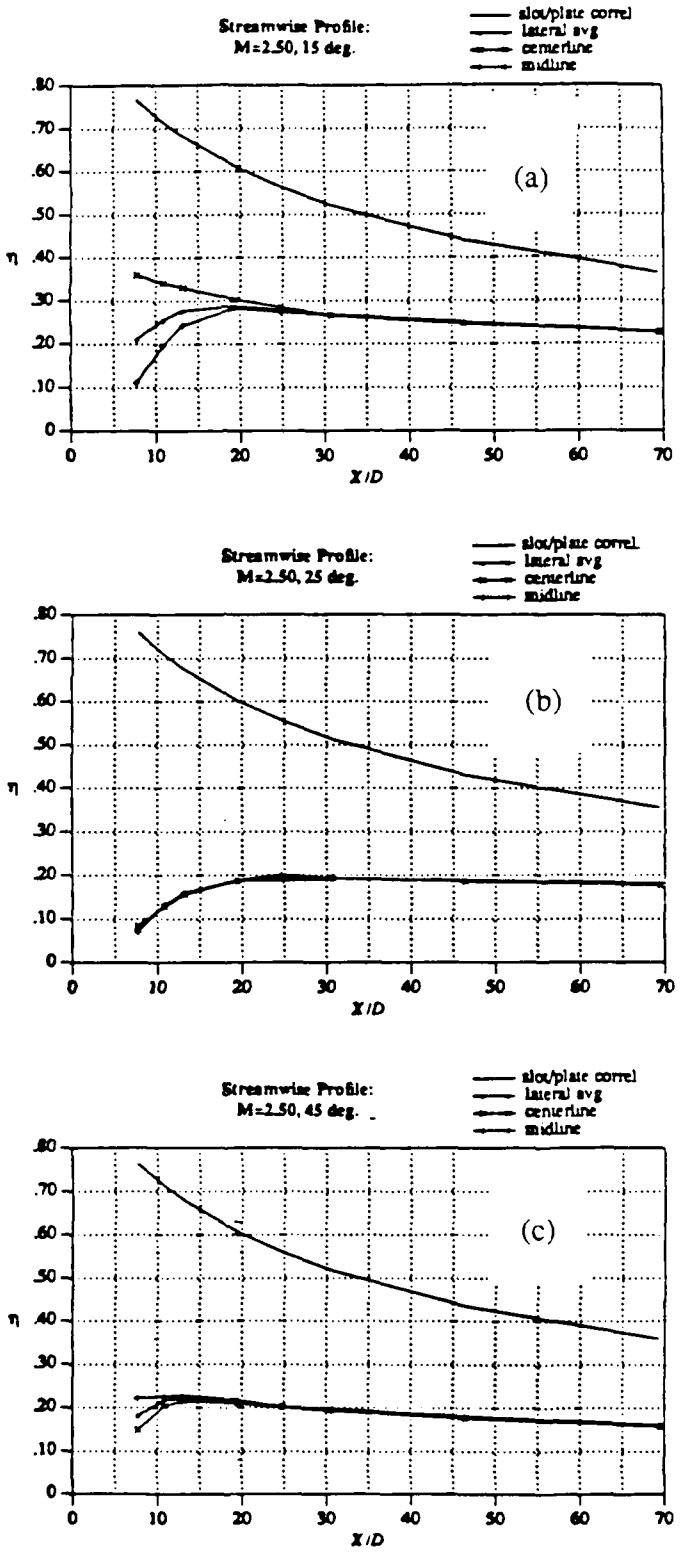

Fig. B-2 - Comparison of the Effect of Injection Angle on Effectiveness at Different Locations

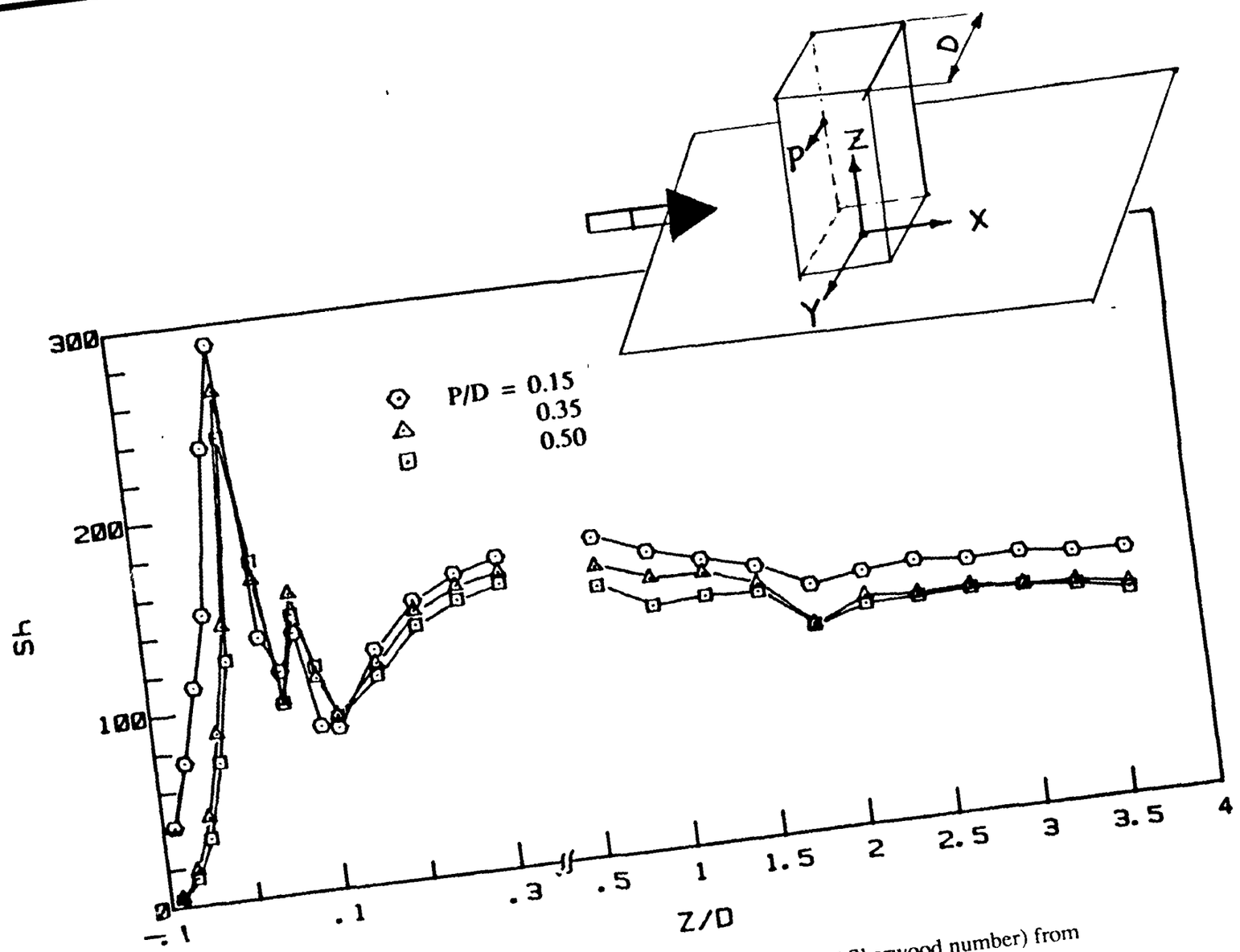

Figure C-2. Effect of vortex system on mass transfer (Sherwood number) from the front face of a square cylinder

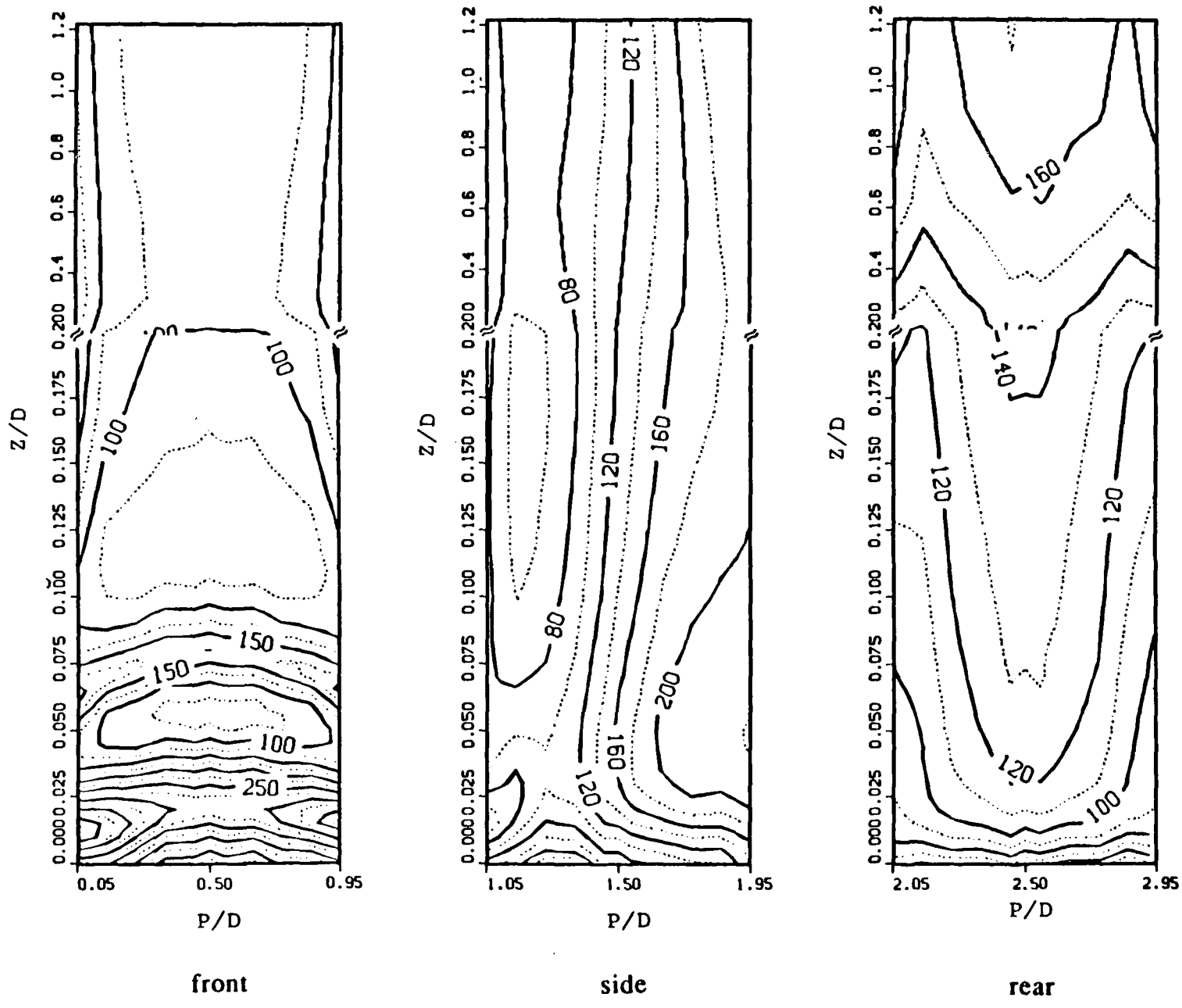

Figure C-3. Contours of Sherwood number on the sides of a square cylinder

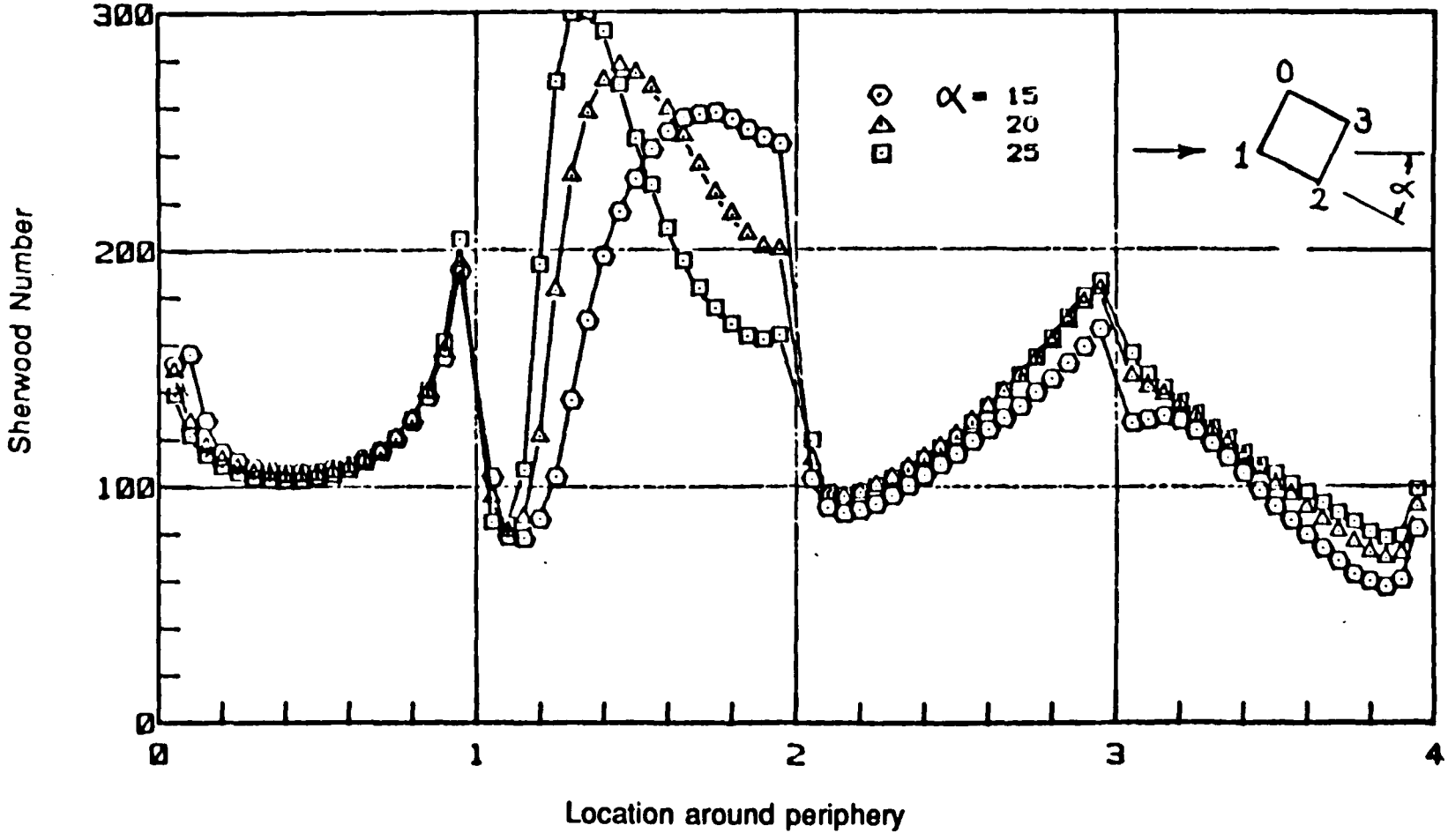

Figure C-4. Mass transfer from sides of a square cylinder under different angles of attack

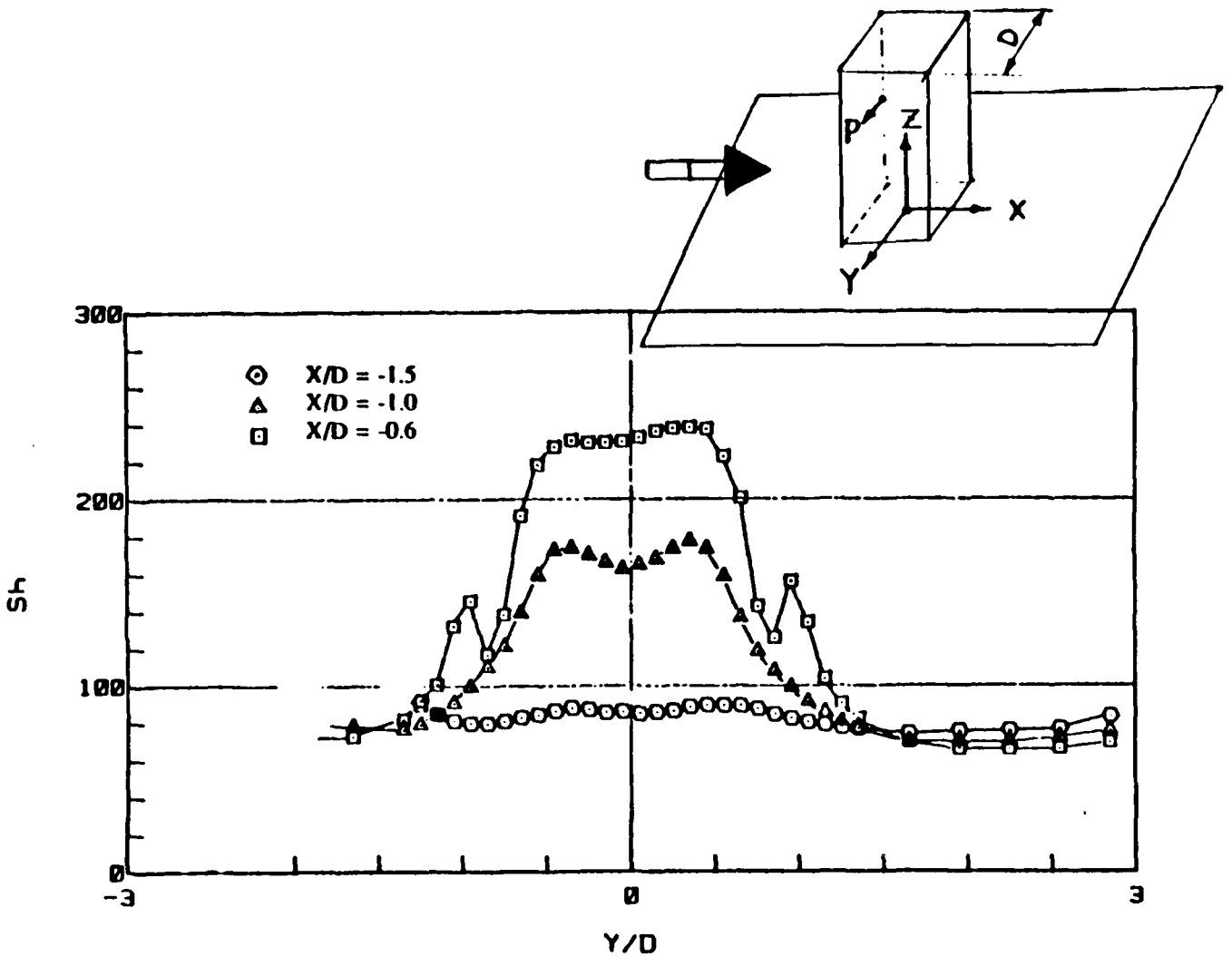

Figure C-5. Effect of vortex system on mass transfer from the endwall

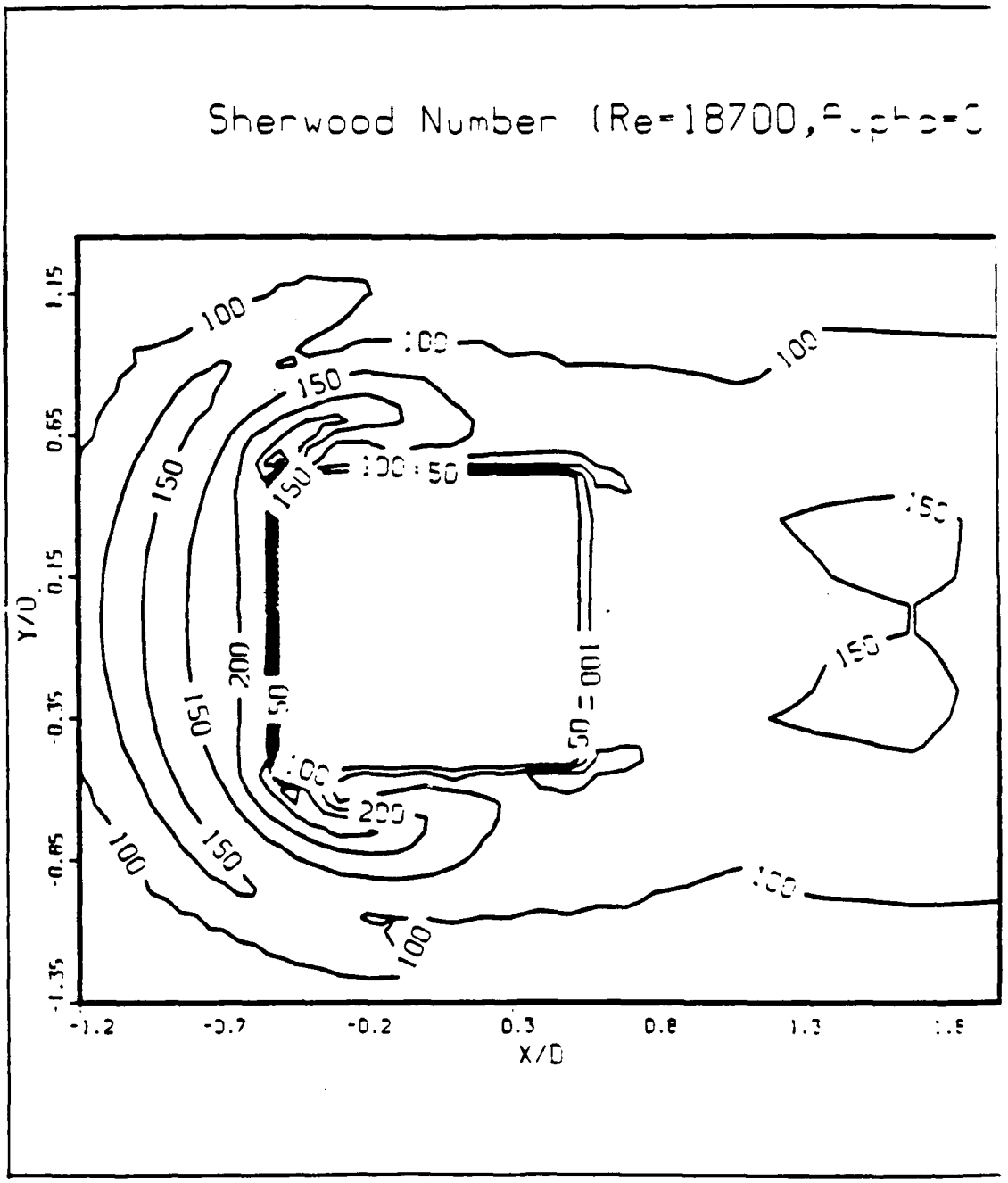

Figure C-6. Contours of mass transfer from the endwall (attack angle 0 deg.)

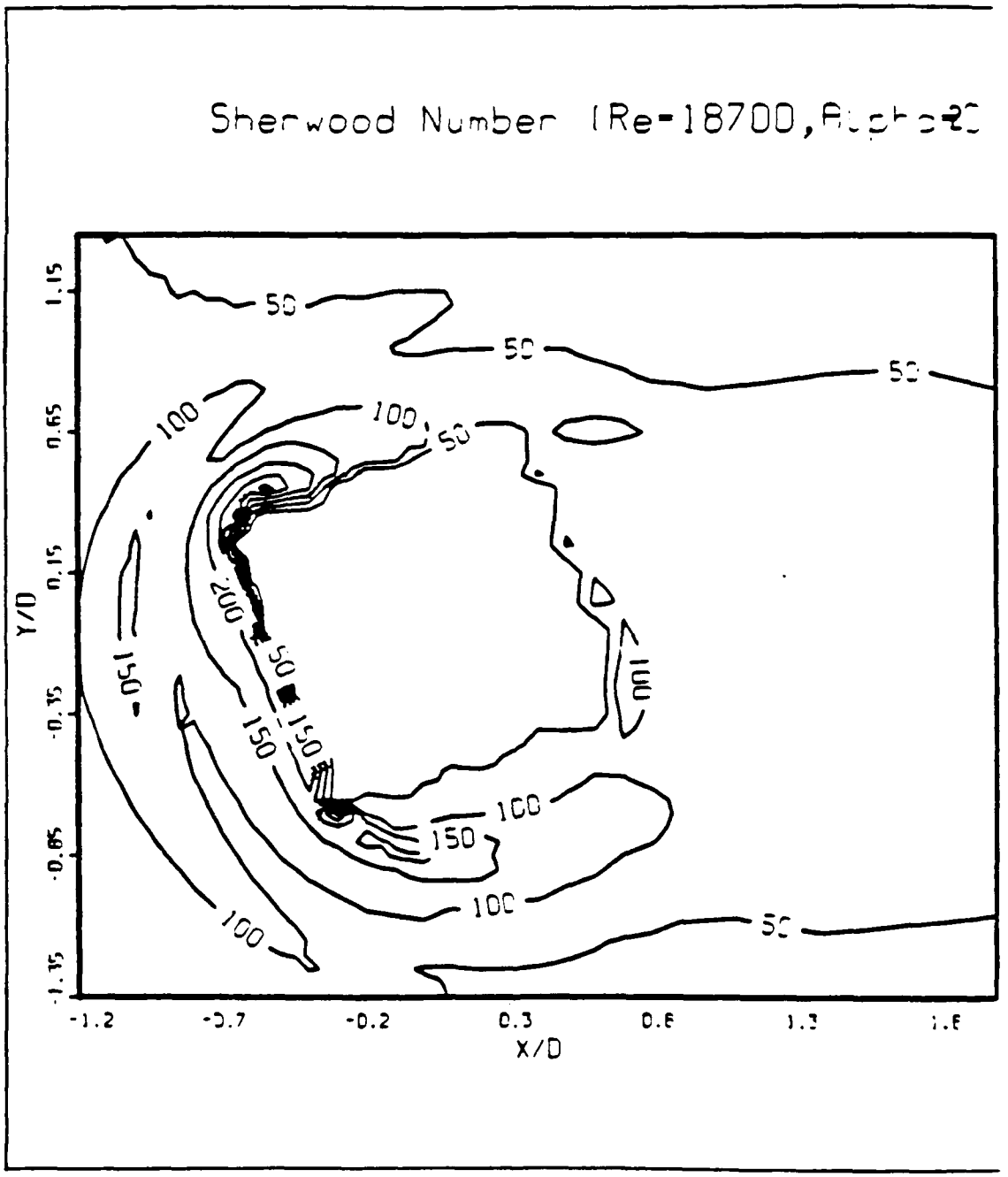

Figure C-7. Contours of mass transfer from the endwall (attack angle 20 deg.)

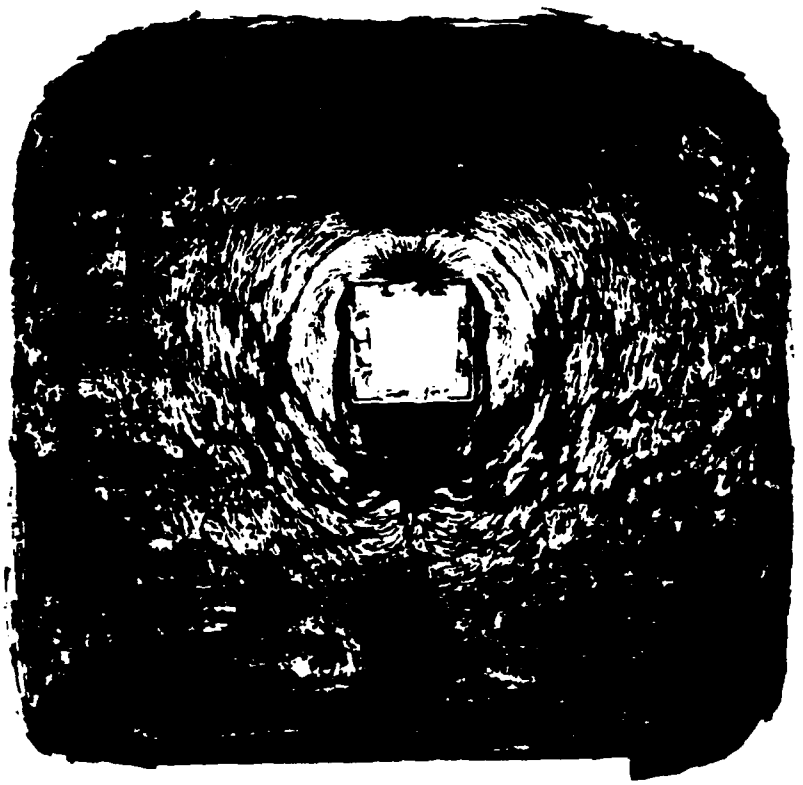

Angle of attack 0 deg

Angle of attack 30 deg

Figure C-8. Visualization of flow over the endwall

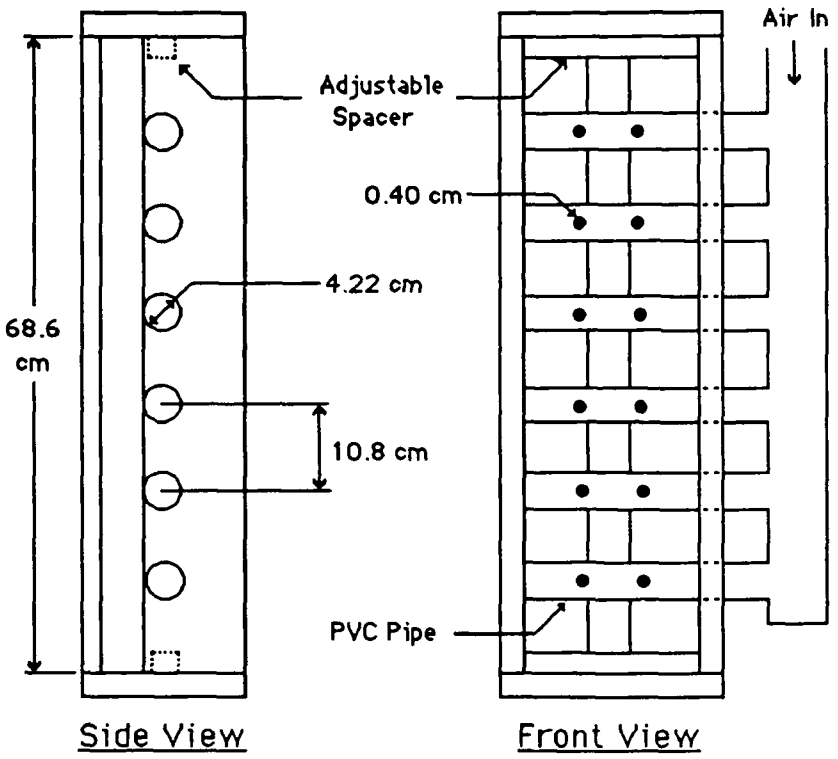

Fig. D-1 Diagram of Bi-Plane Jet Grid

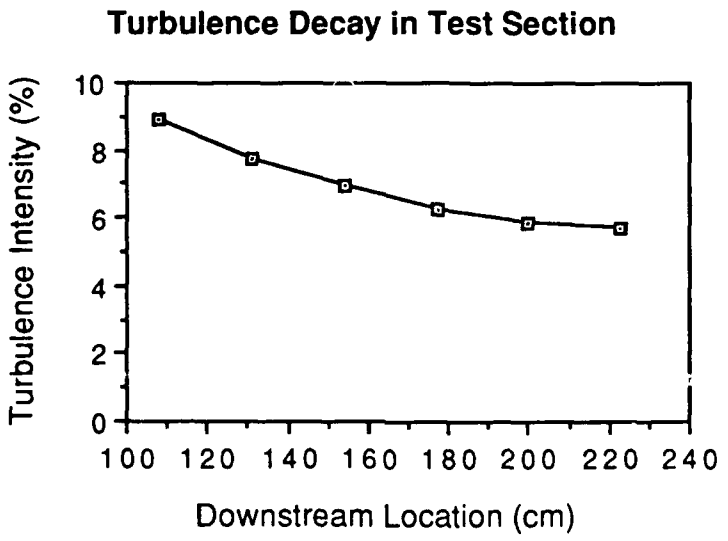

Fig. D-2 Streamwise Turbulence Intensity in Test Section

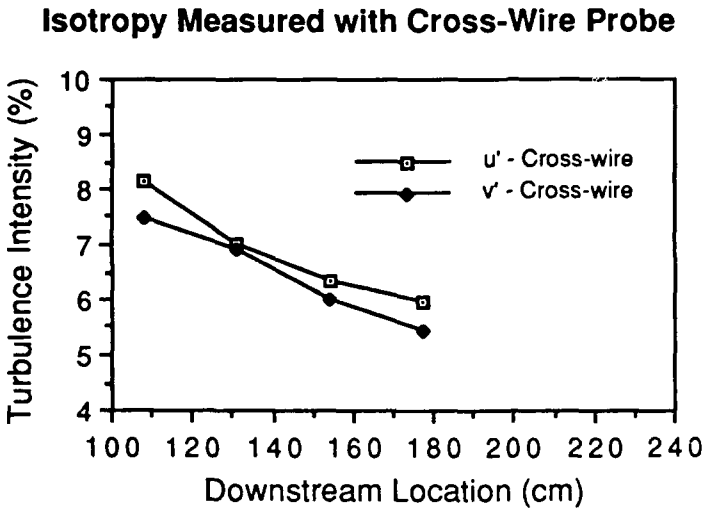

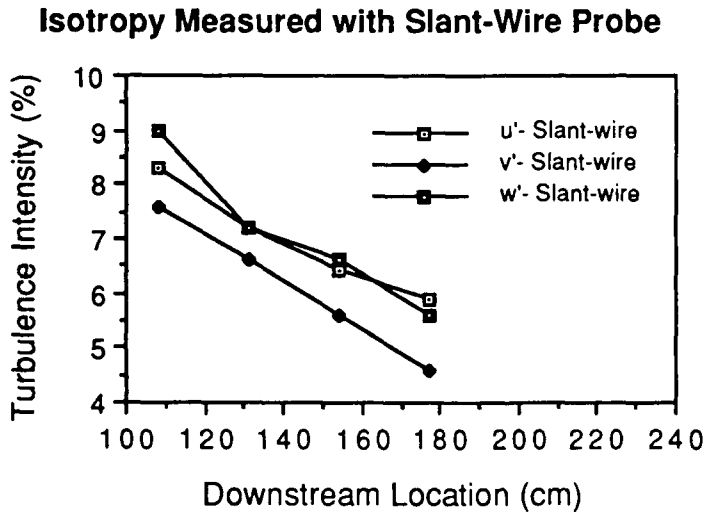

Fig. D-3 Isotropy of Grid Generated Turbulence

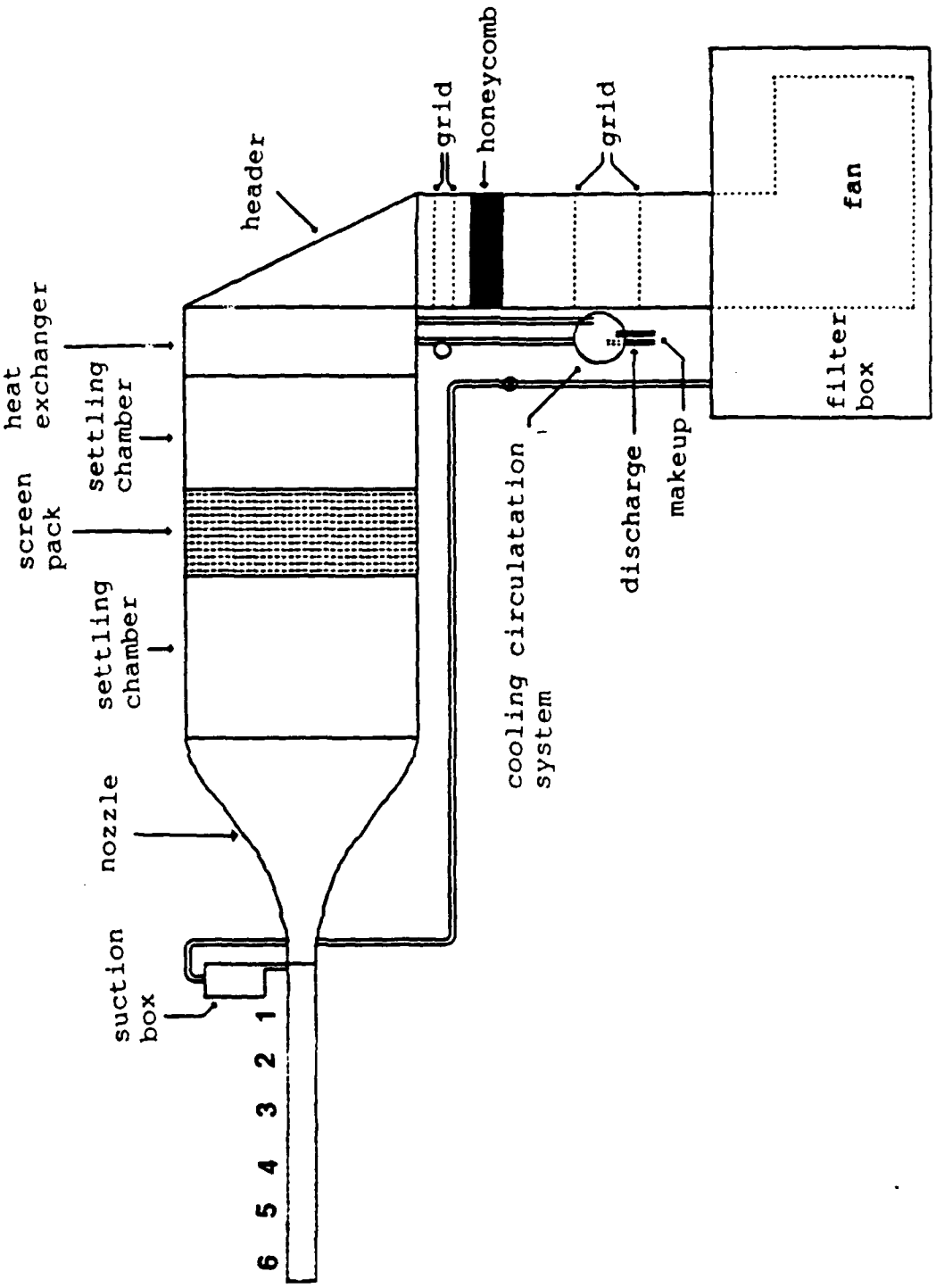

Fig. D-4. Schematic of test facility.

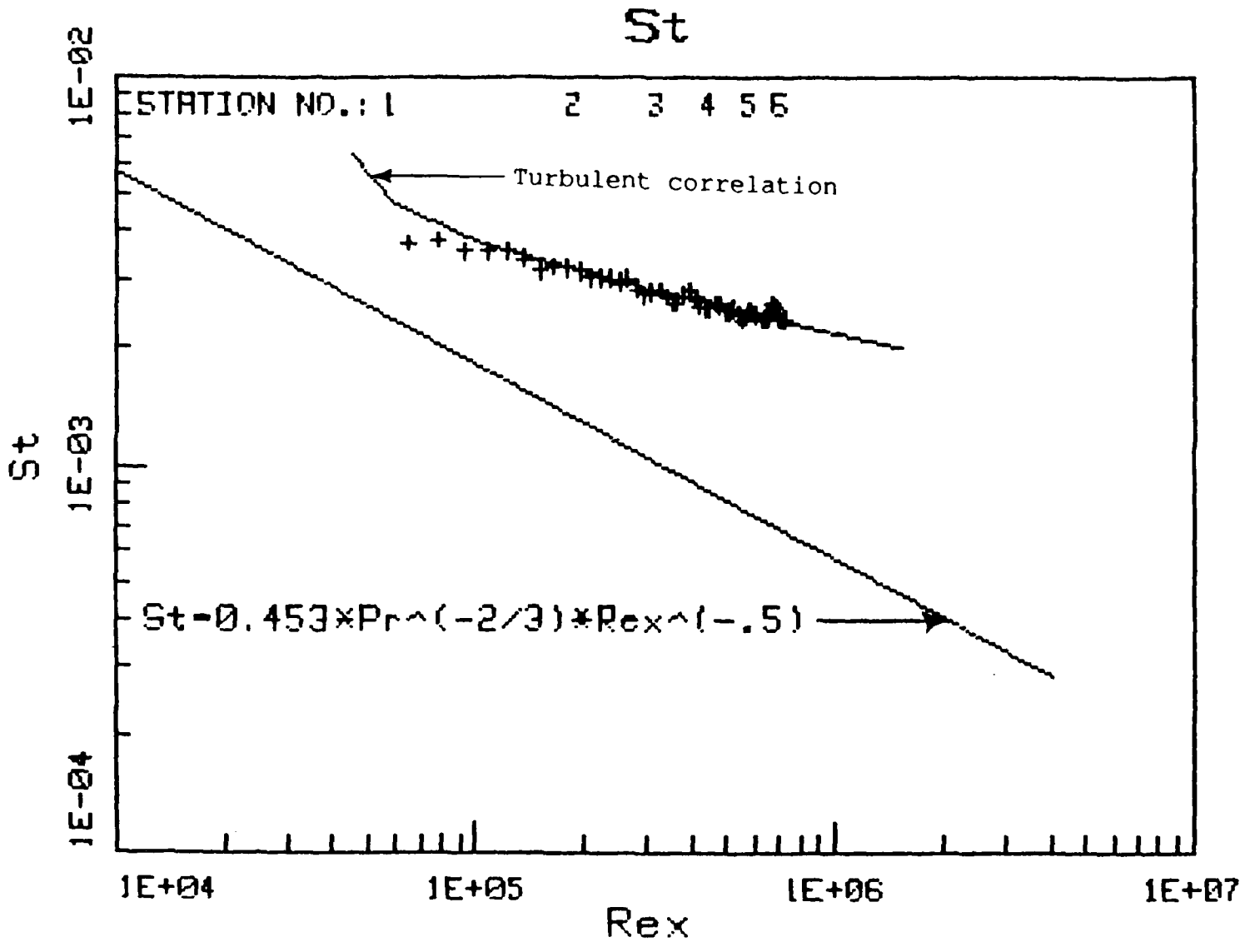

Fig. D-5. Stanton number variation along test wall

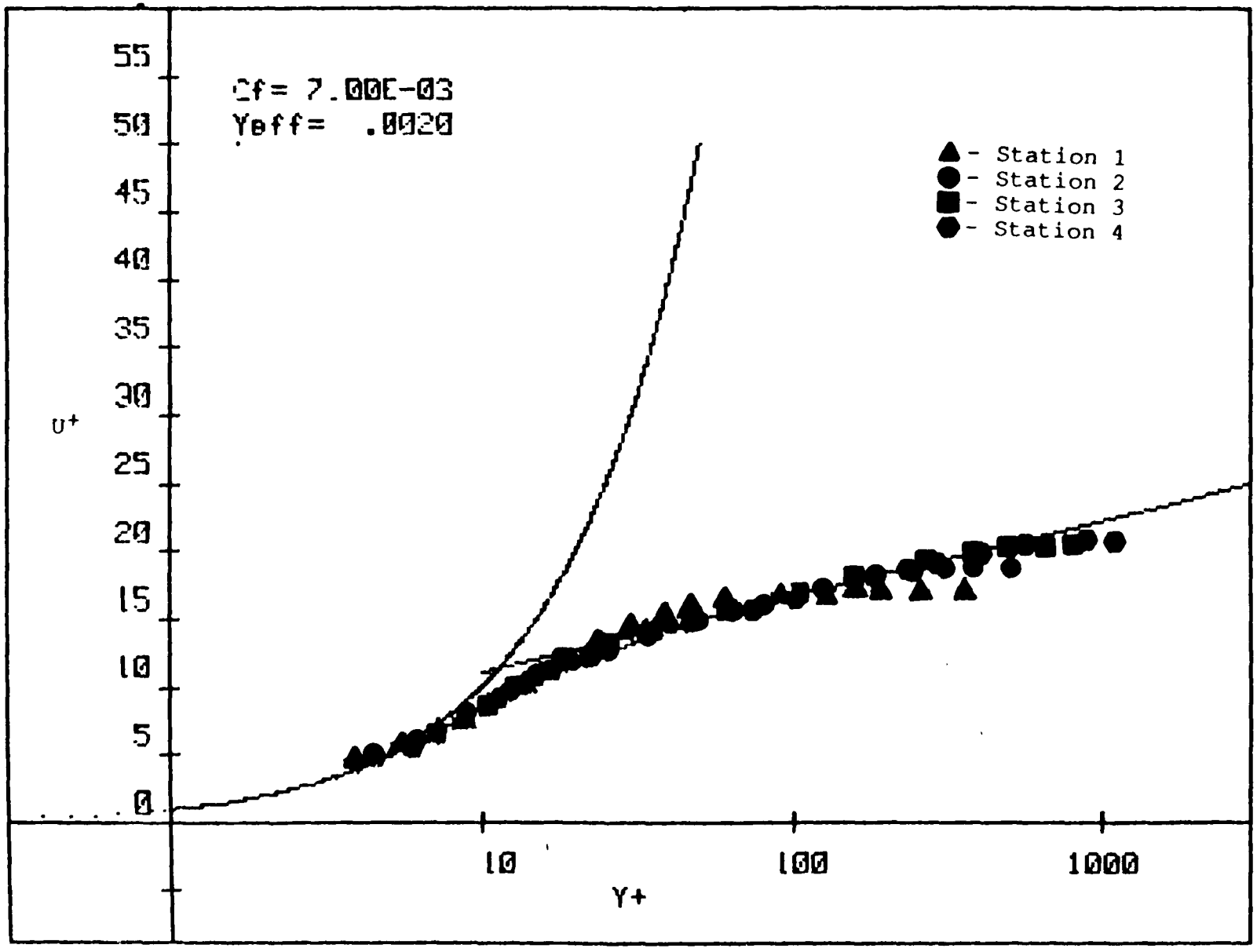

Fig. D-6. Mean velocity profiles normalized on wall coordinates (flat-wall)

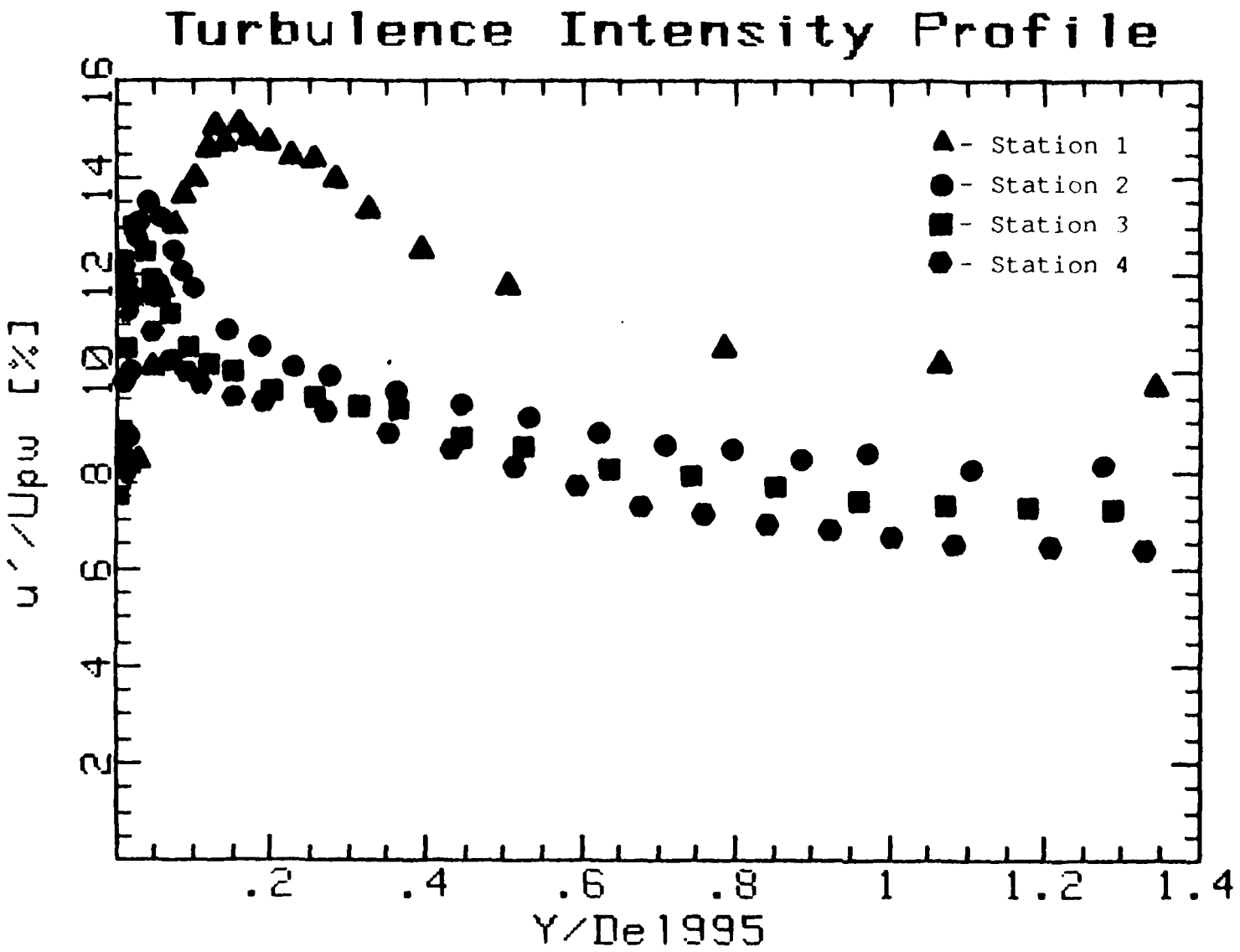

Fig. D-7. Turbulence intensity profiles along test wall.

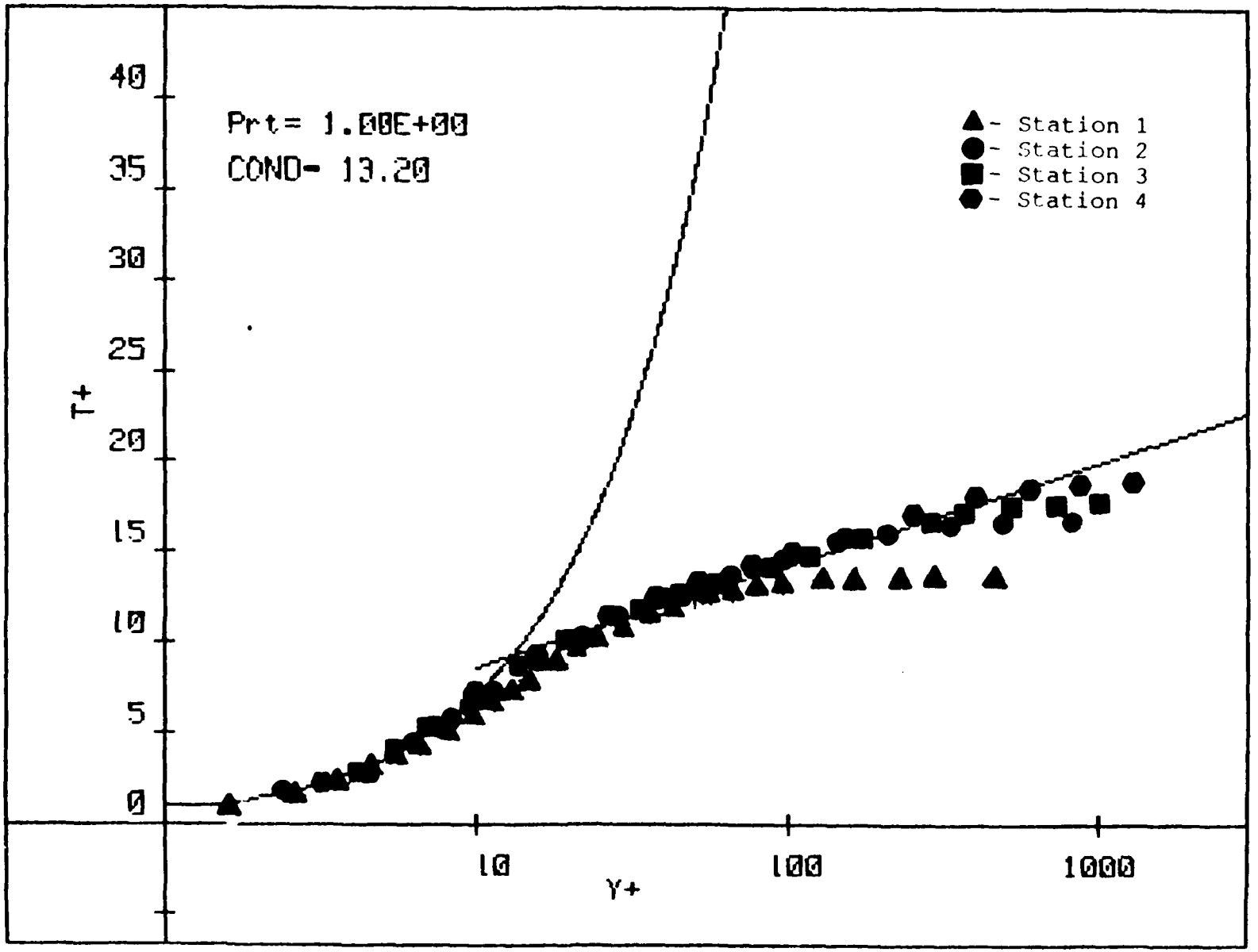

Fig. D-8. Mean temperature profiles normalized on wall coordinates (flat-wall).

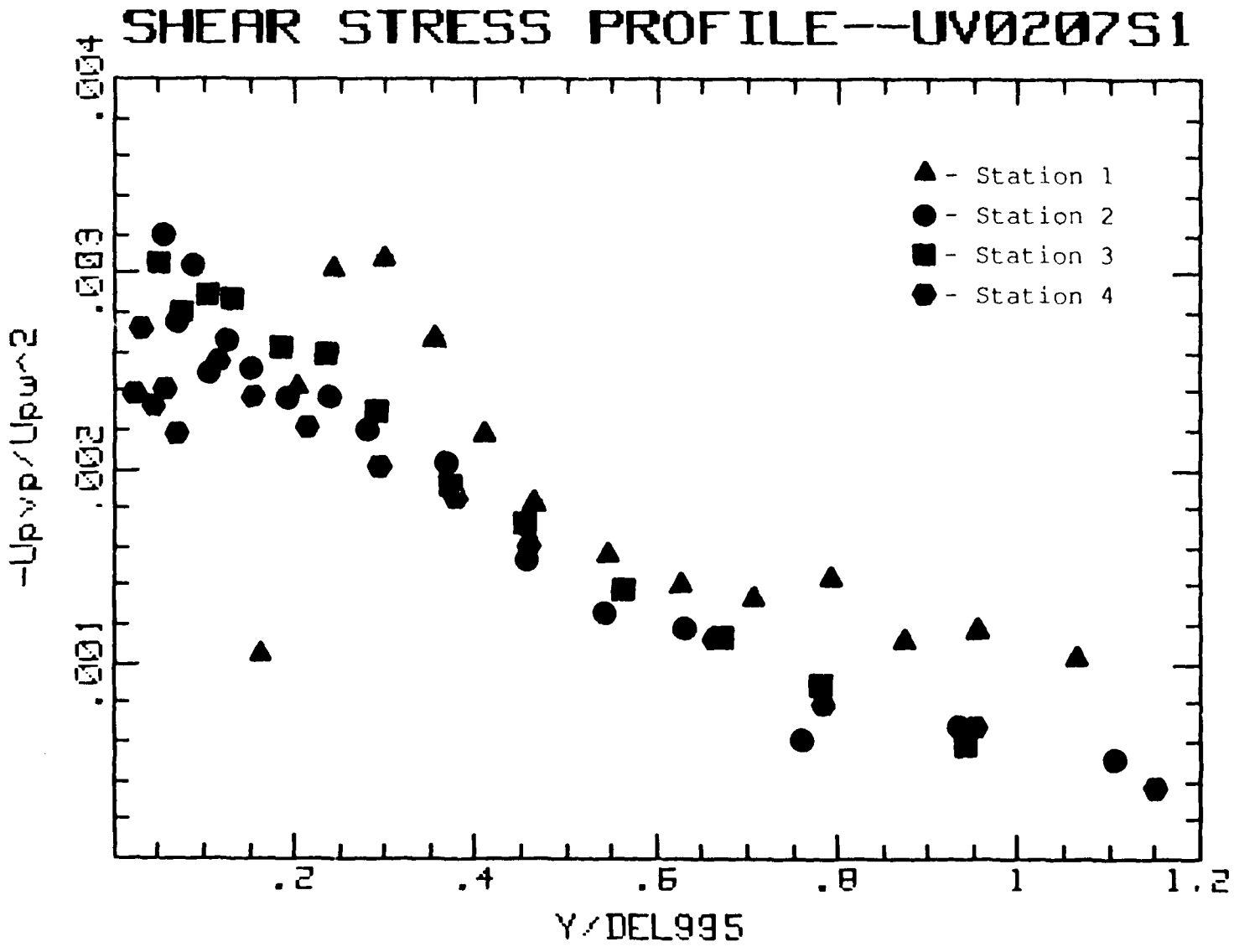

Fig. D-9. Shear stress profiles along test station.

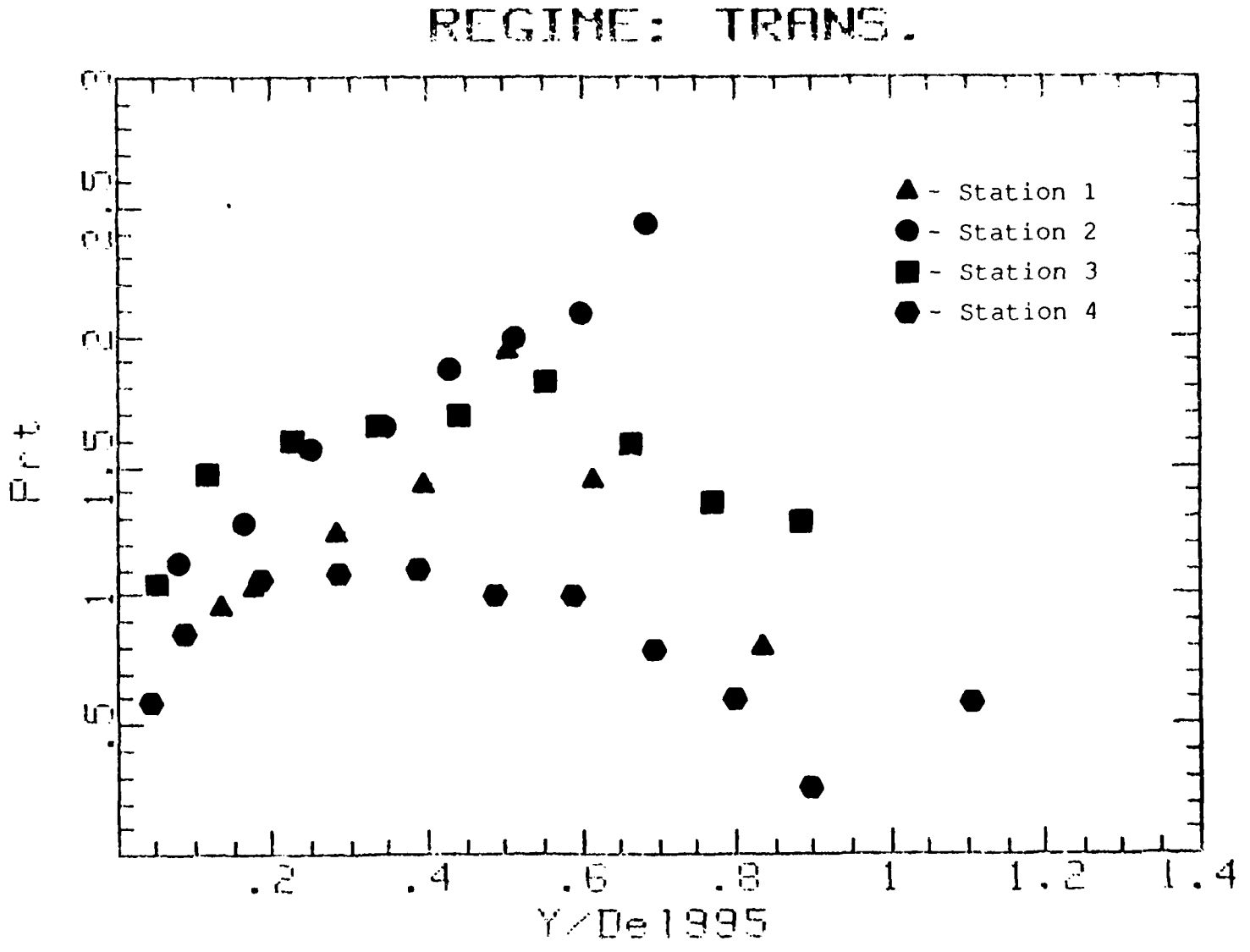

Fig. D-10. Turbulent Prandtl number profiles along test section.

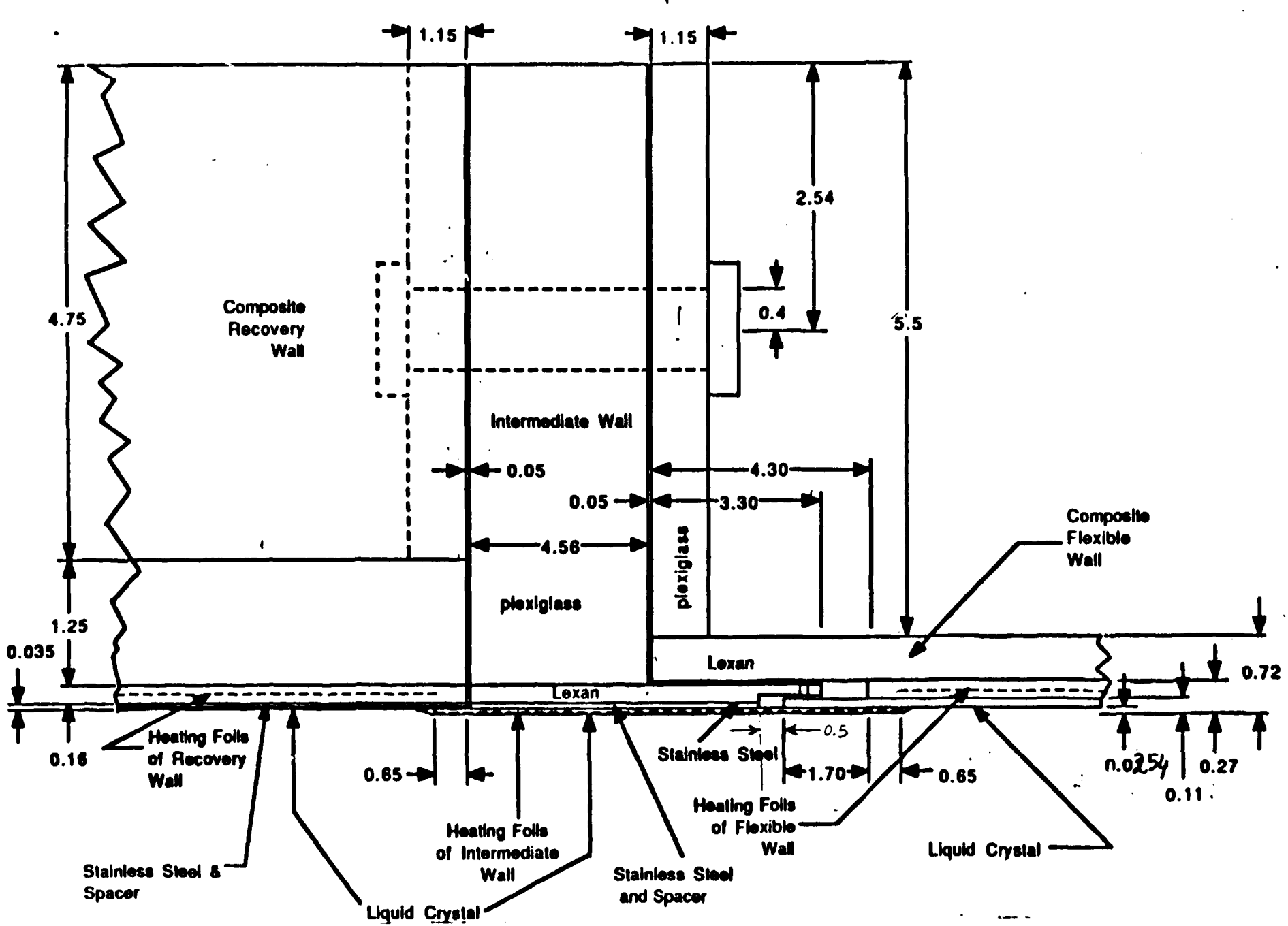

Fig. D-11. Installation of the Recovery Wall (All Dimensions in cm).

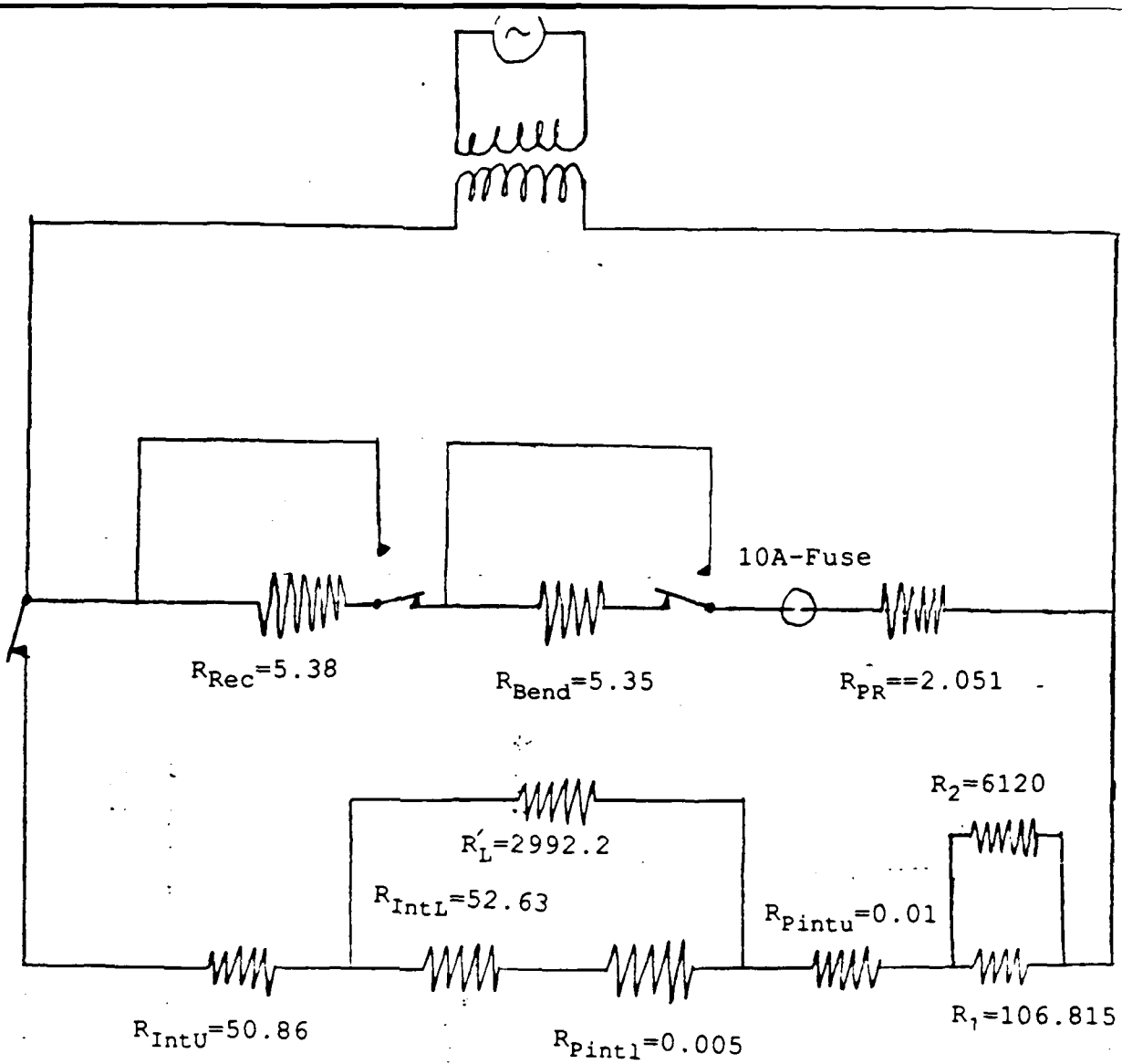

Fig. D-12. Uniform Heat-Flux Circuit (All Values in Ohms).

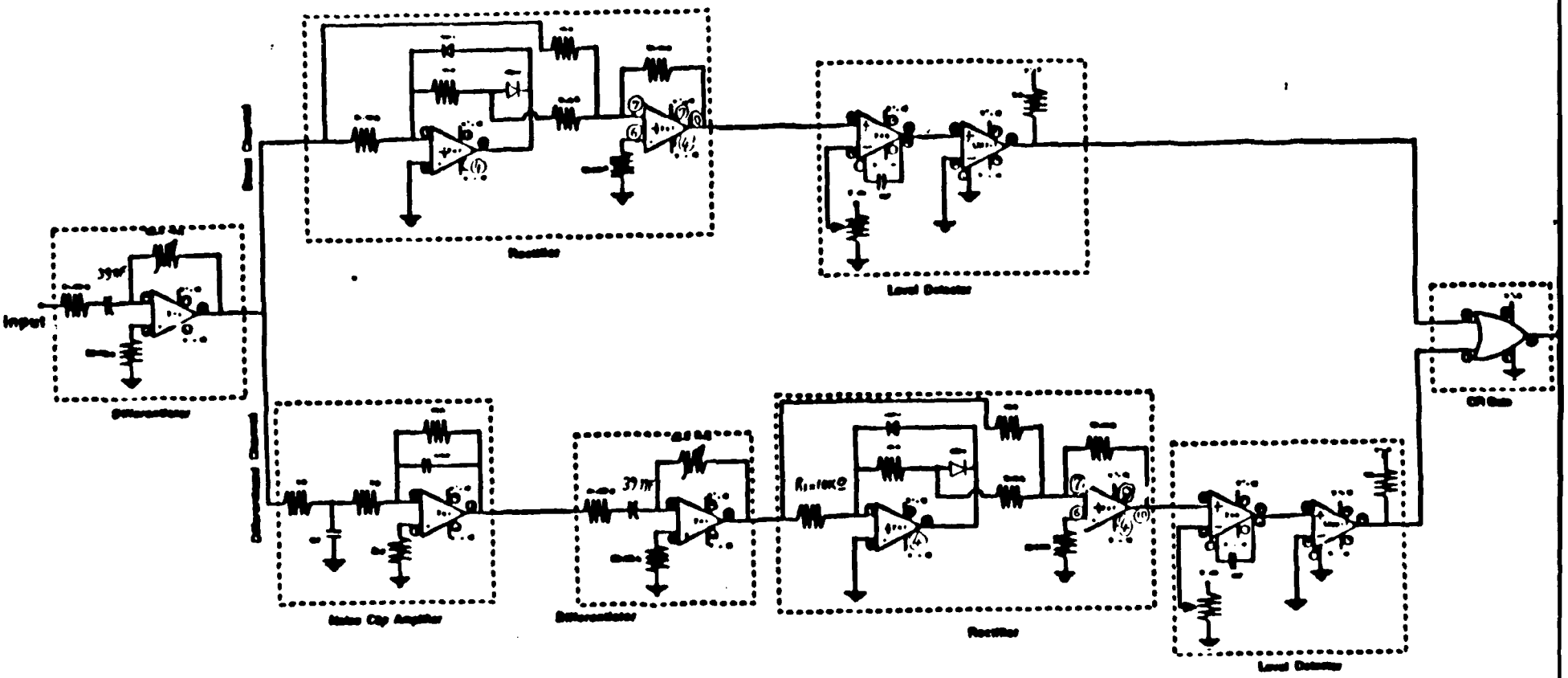

Fig D-13 . Circuit Diagram of the Intermittency-Measuring Unit.

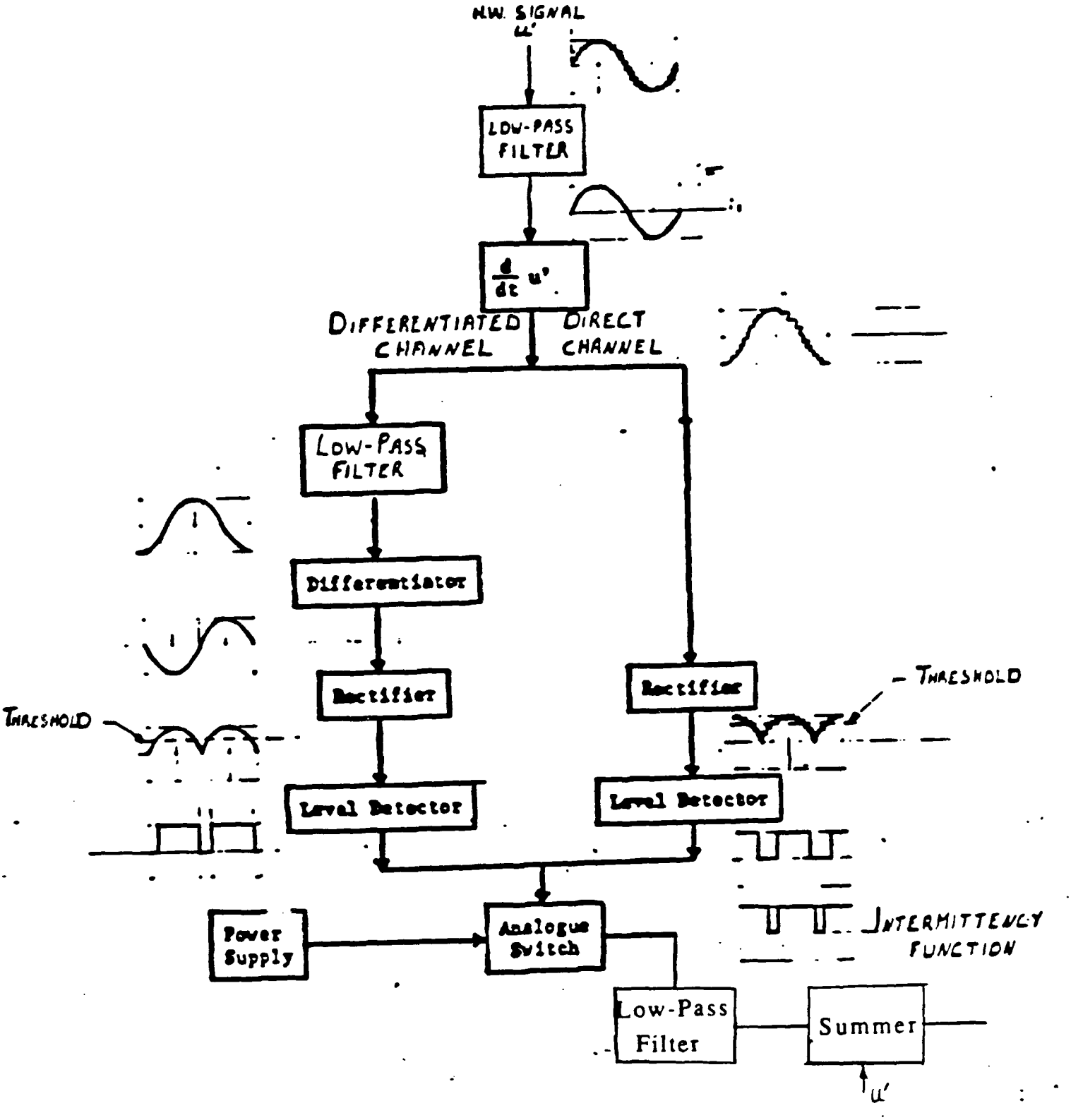

Fig D-14. Block Diagram of Intermittency Measuring Unit.

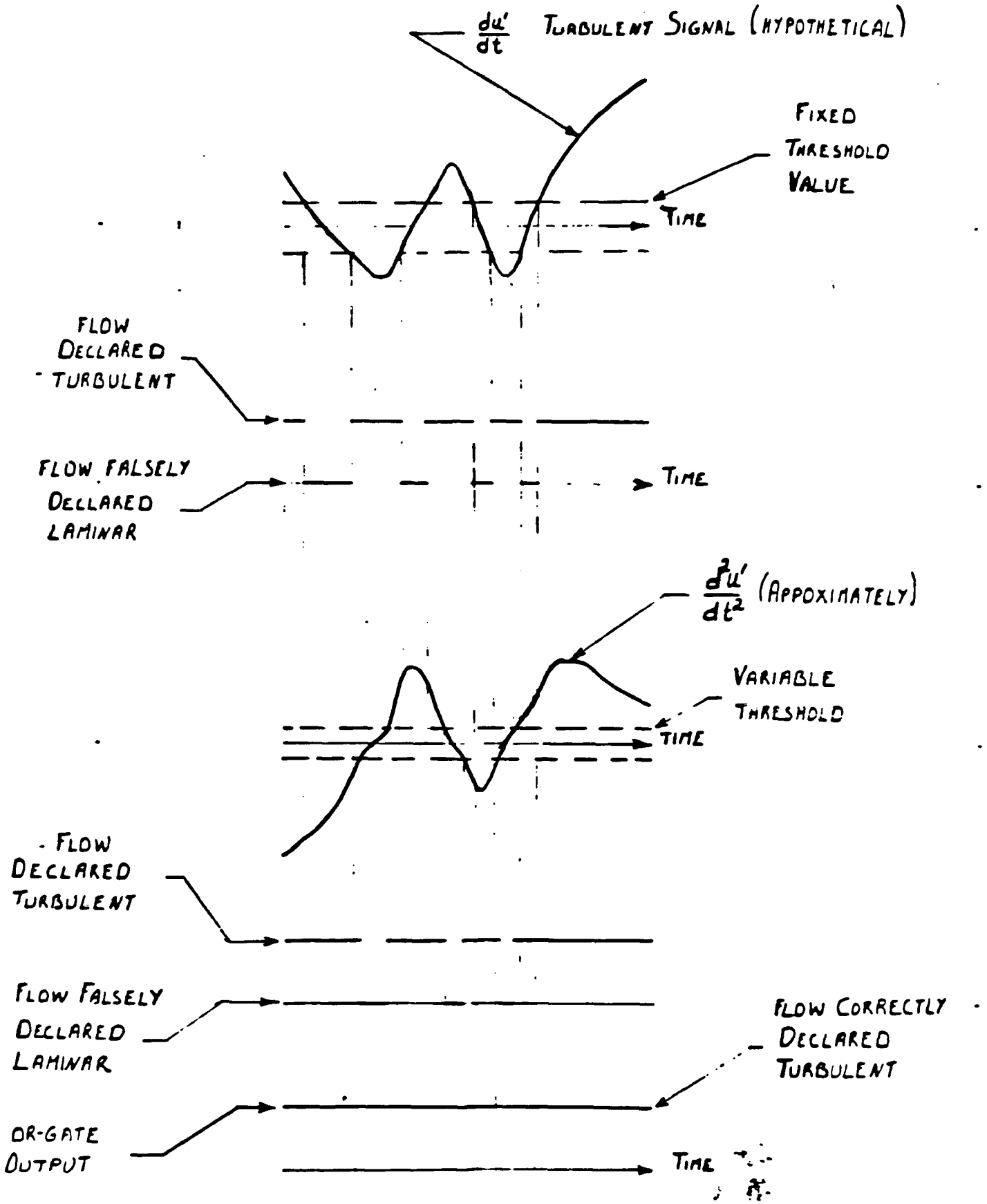

Fig D-15. Avoiding the Problem of Zero Crossing.

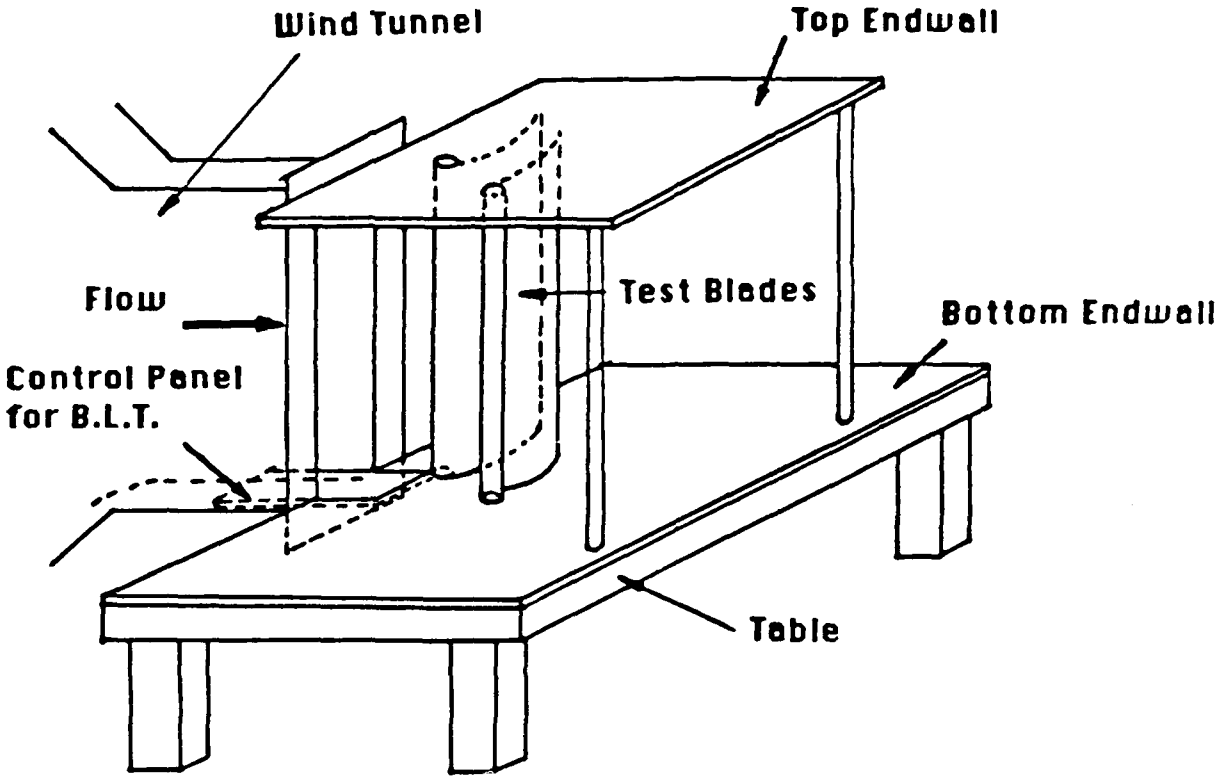

Fig. E-1a A Perspective View of the Two-half-blade Cascade Flow Simulator Without the Side Wall

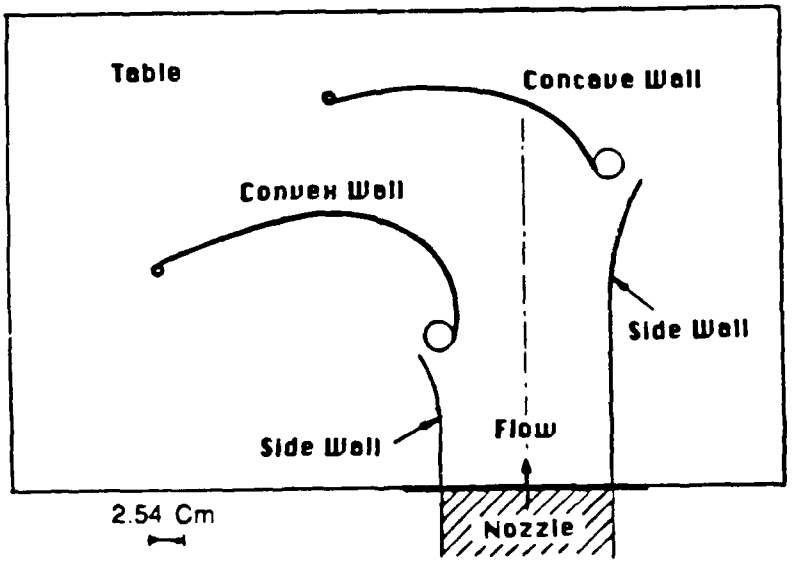

Fig. E-1b A Top View of the Simulator With the Side Wall

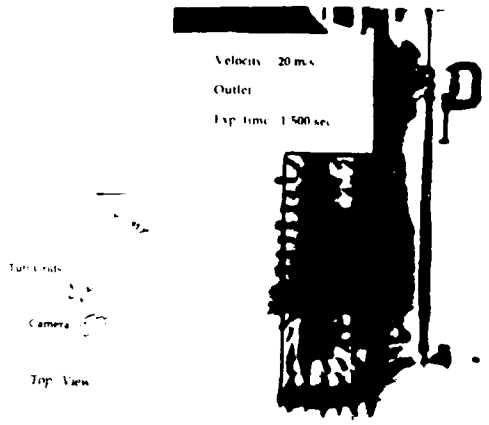

(a)

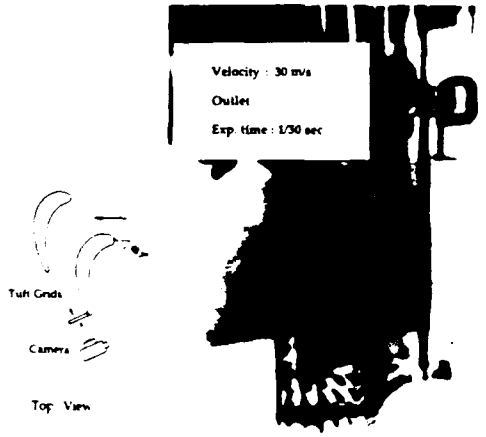

(b)

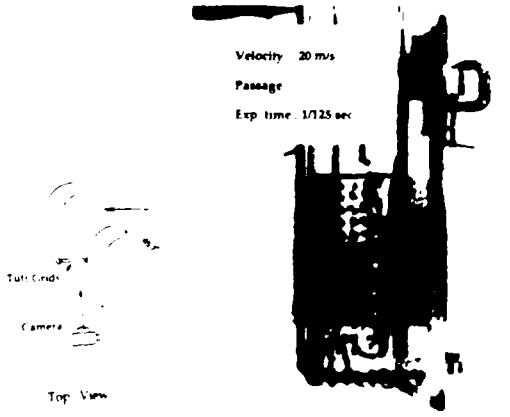

(c)

Fig. E-2 Passage Vortex in the Passage and at the Outlet as Visualized by a Tuft Grids

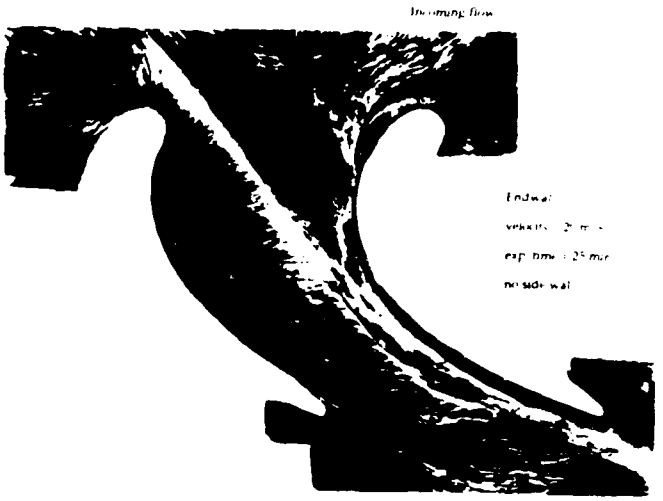

Fig. E-3a Visualization of the Flow Through the Cascade Passage

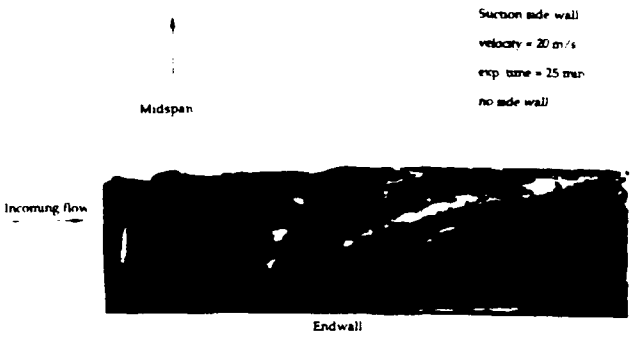

Fig. E-3b Visualization of the Three Dimensional Flow on the Suction-side Surface near the Endwall

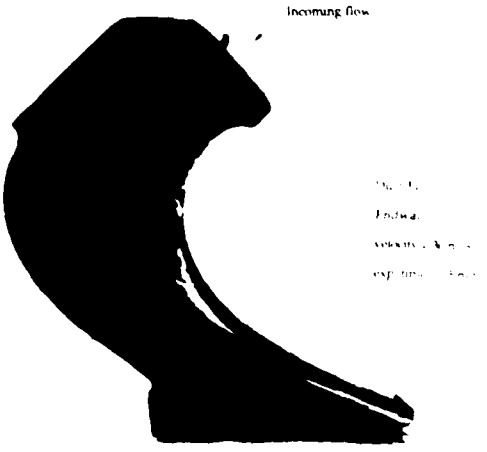

Fig. E-3c Visualization of the Flow Through the Curved Duct

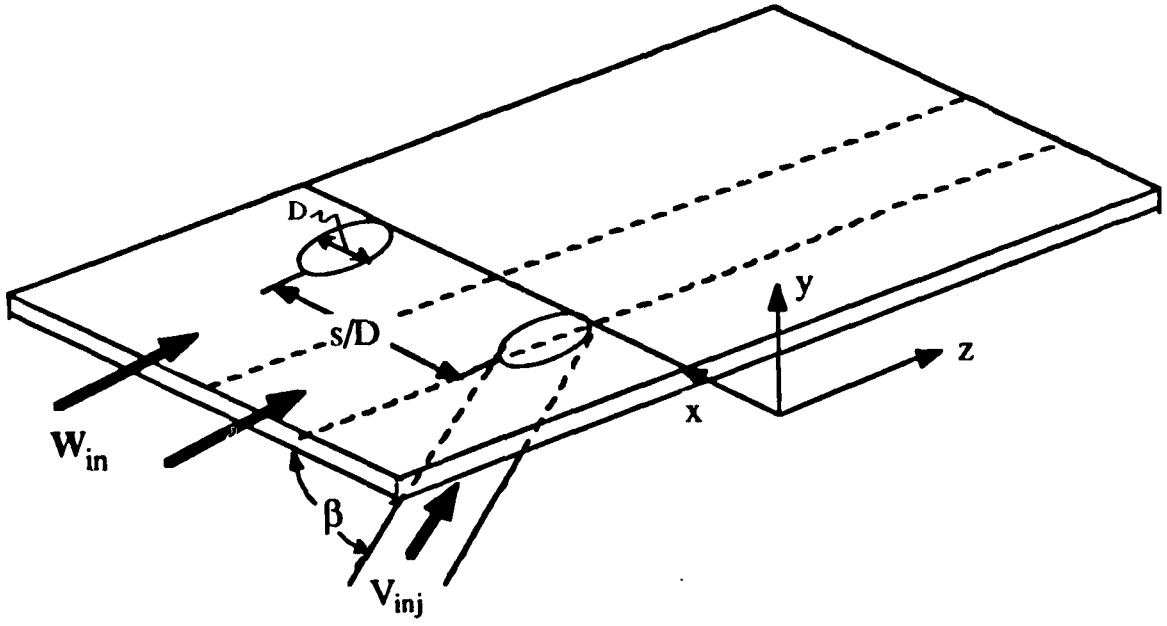

Fig. F1 The flow configuration.

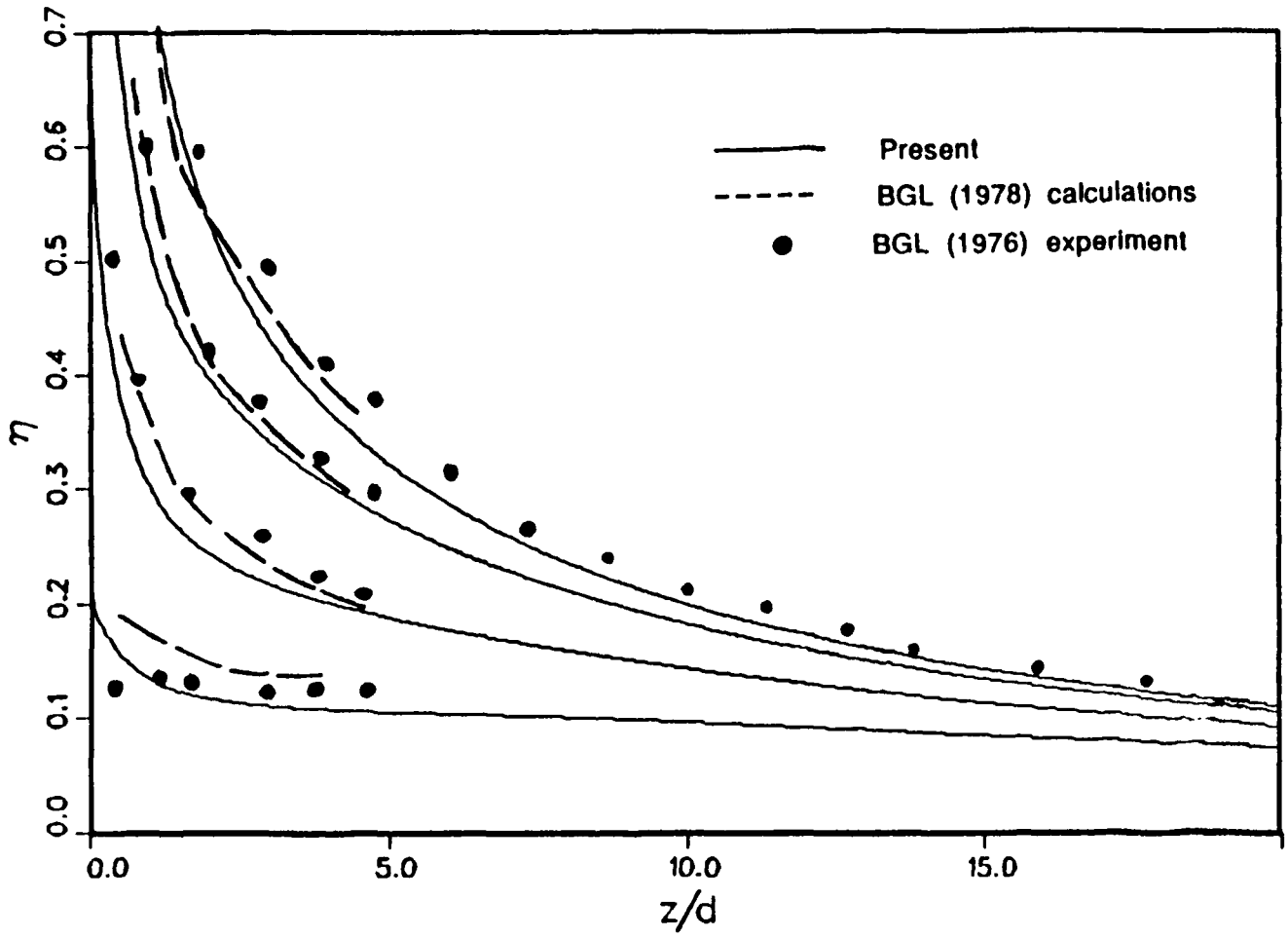

Fig. F2a Single hole cooling effectiveness at different x/D for M = 0.2.

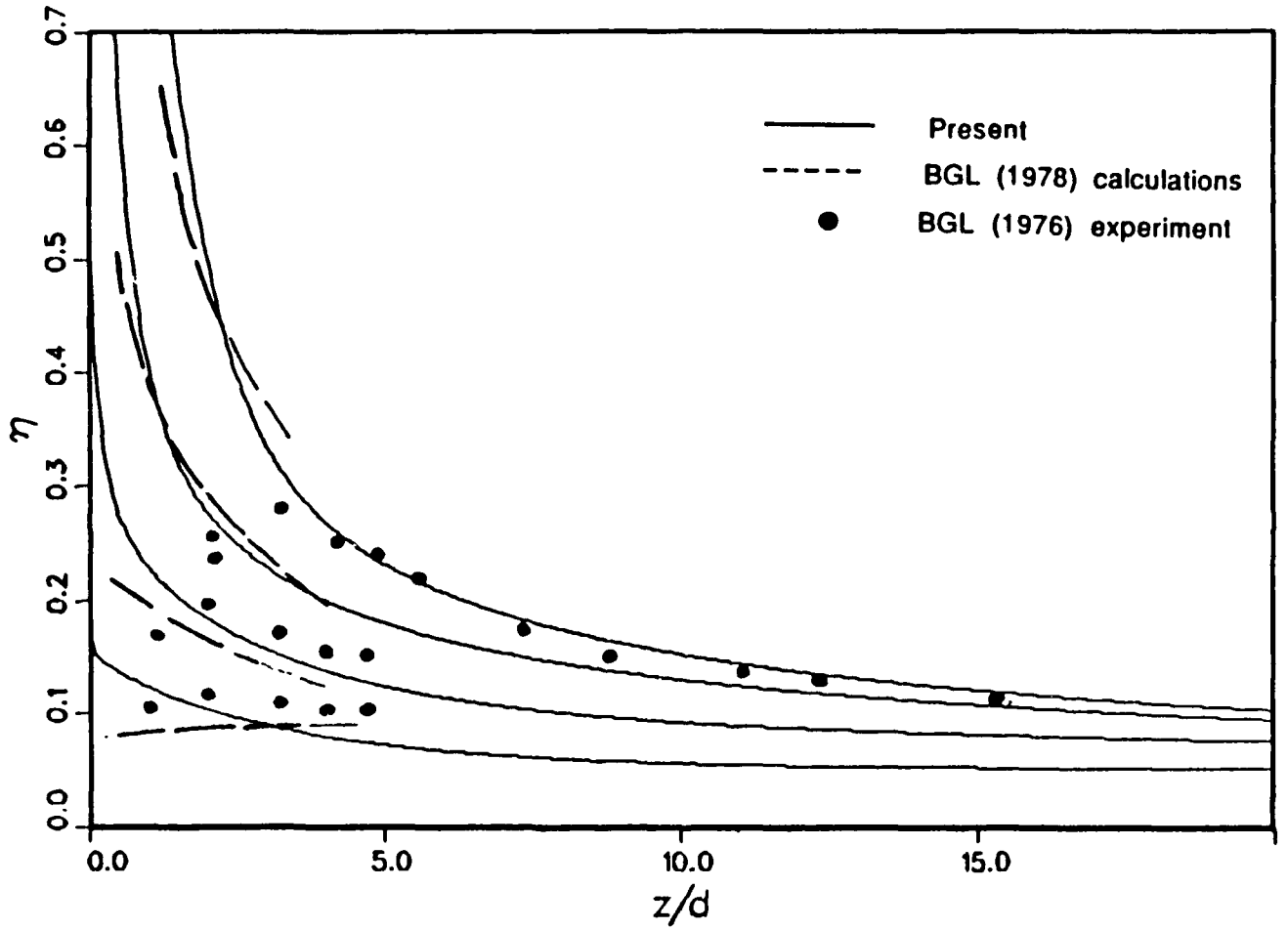

Fig. F2b Single hole cooling effectiveness at different x/D for M = 1.0.

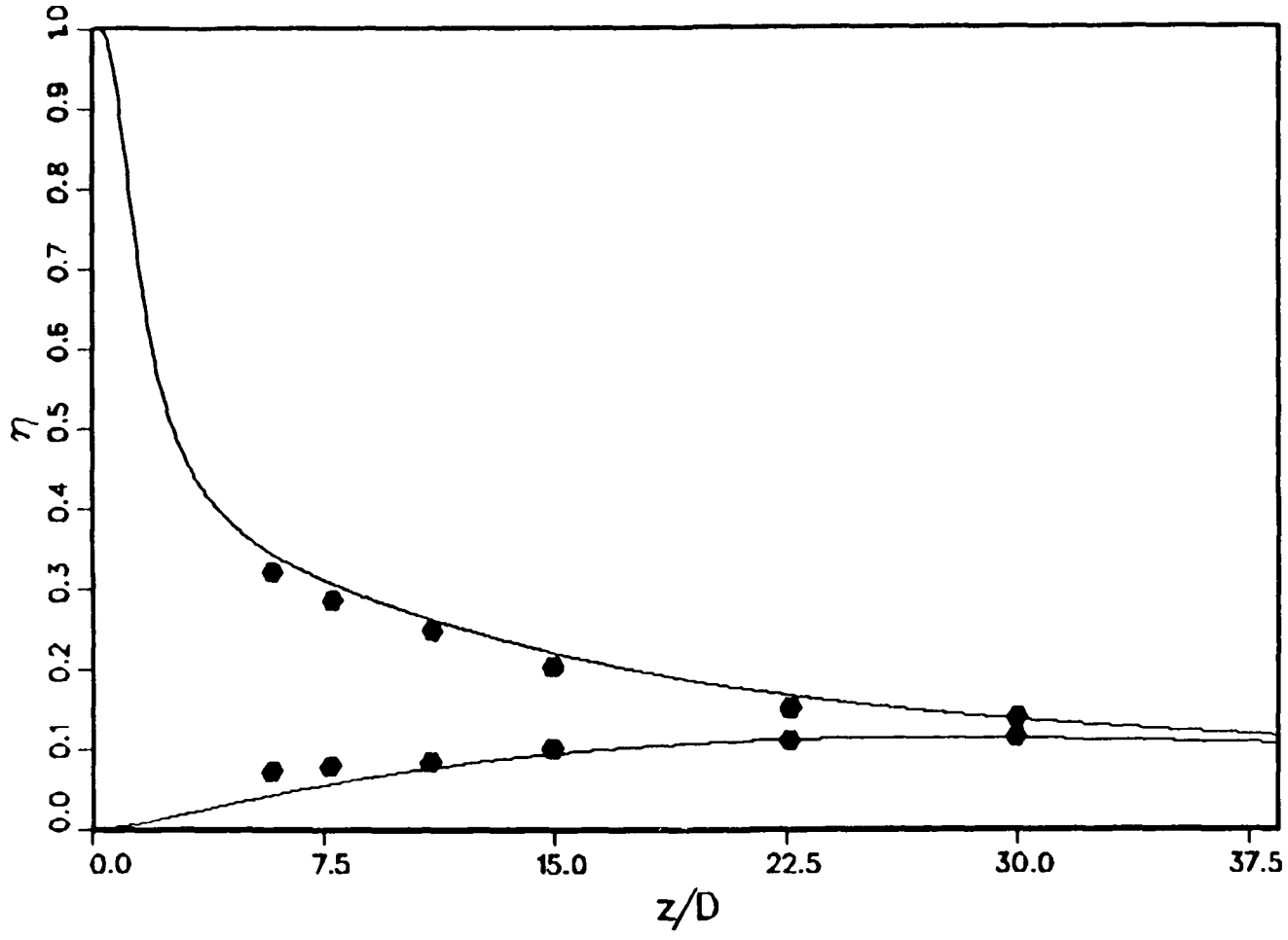

Fig. F3 **Row of holes cooling effectiveness at x/D of 0 and 1.5 for M = 0.5 (Comparison of predicted end experimental results)**

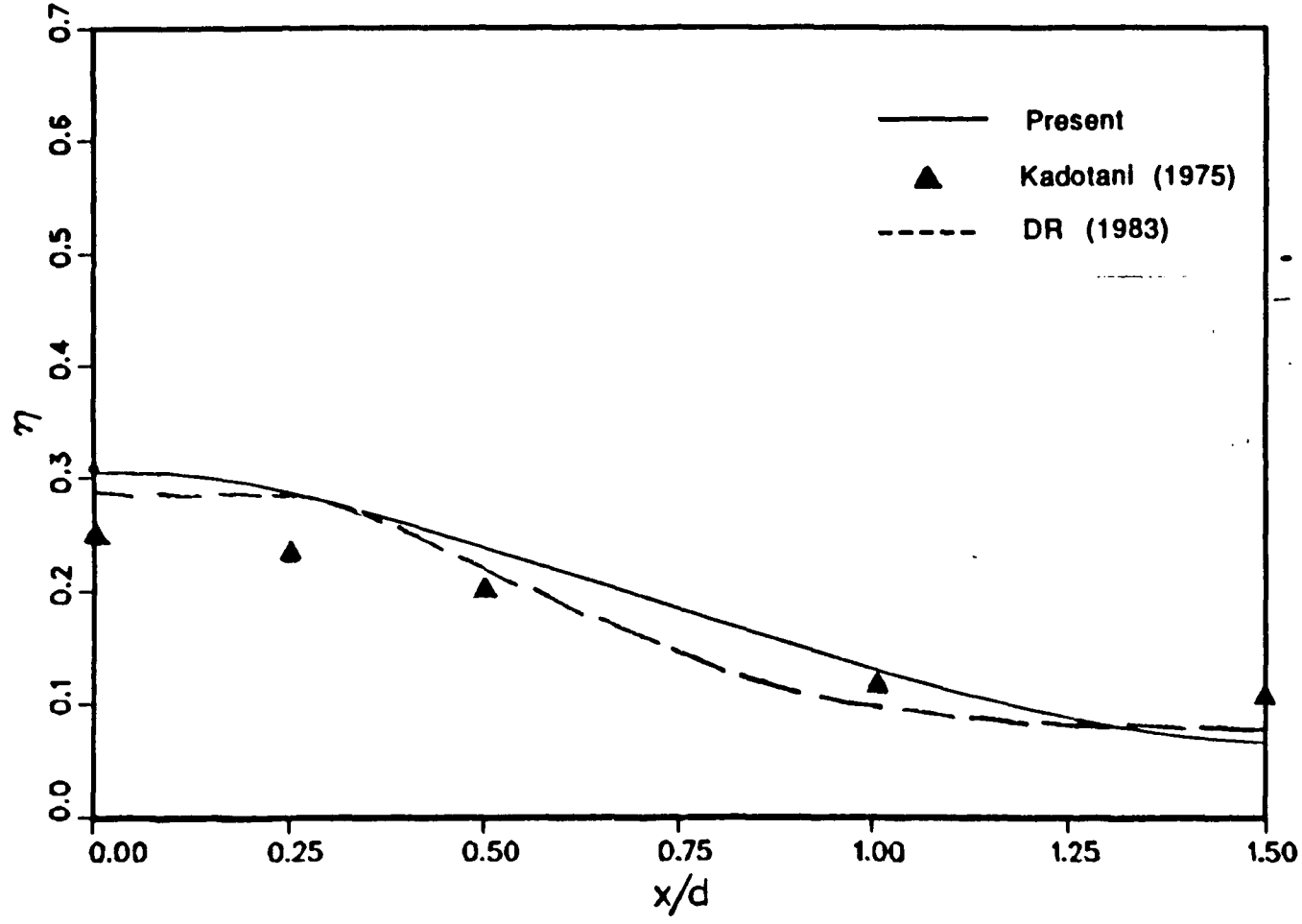

Fig. F4 Lateral cooling performance at z/D = 6.65

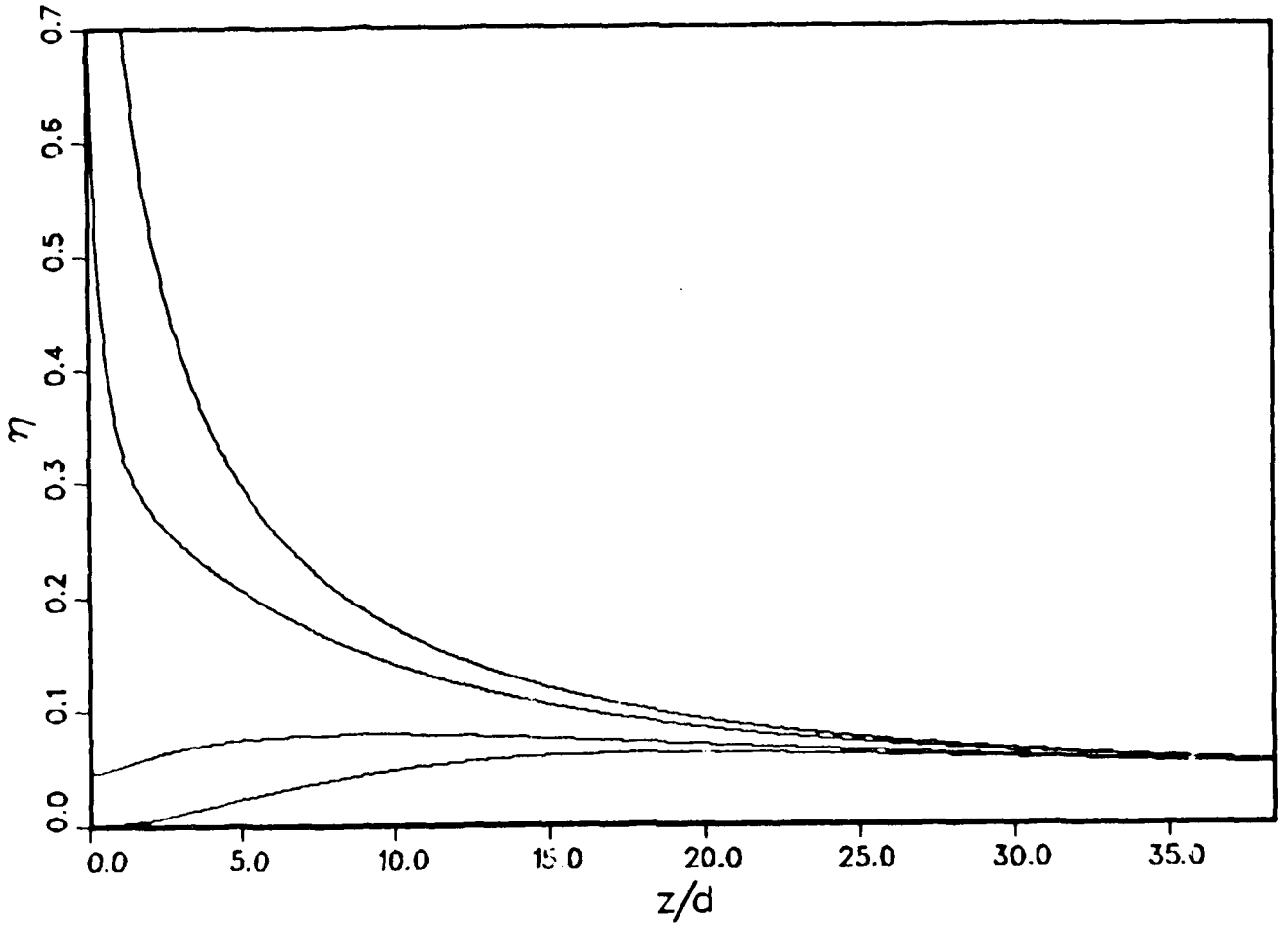

Fig. F5a Row of holes cooling effectiveness at different x/D (0, 0.5, 1 and 1.5) for M = 0.2.

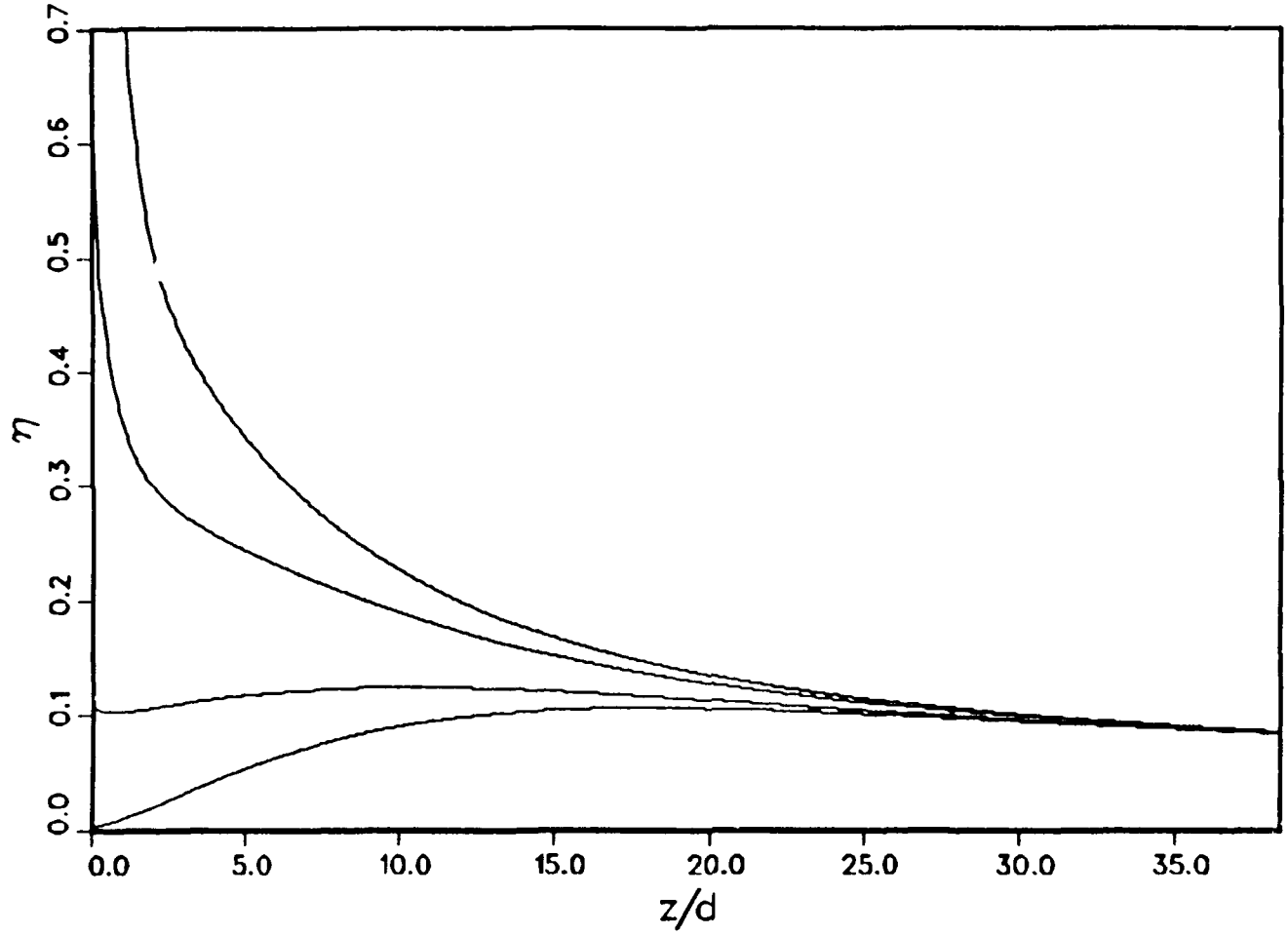

Fig. F5b Row of holes cooling effectiveness at different x/D (0, 0.5, 1 and 1.5) for M = 0.35.

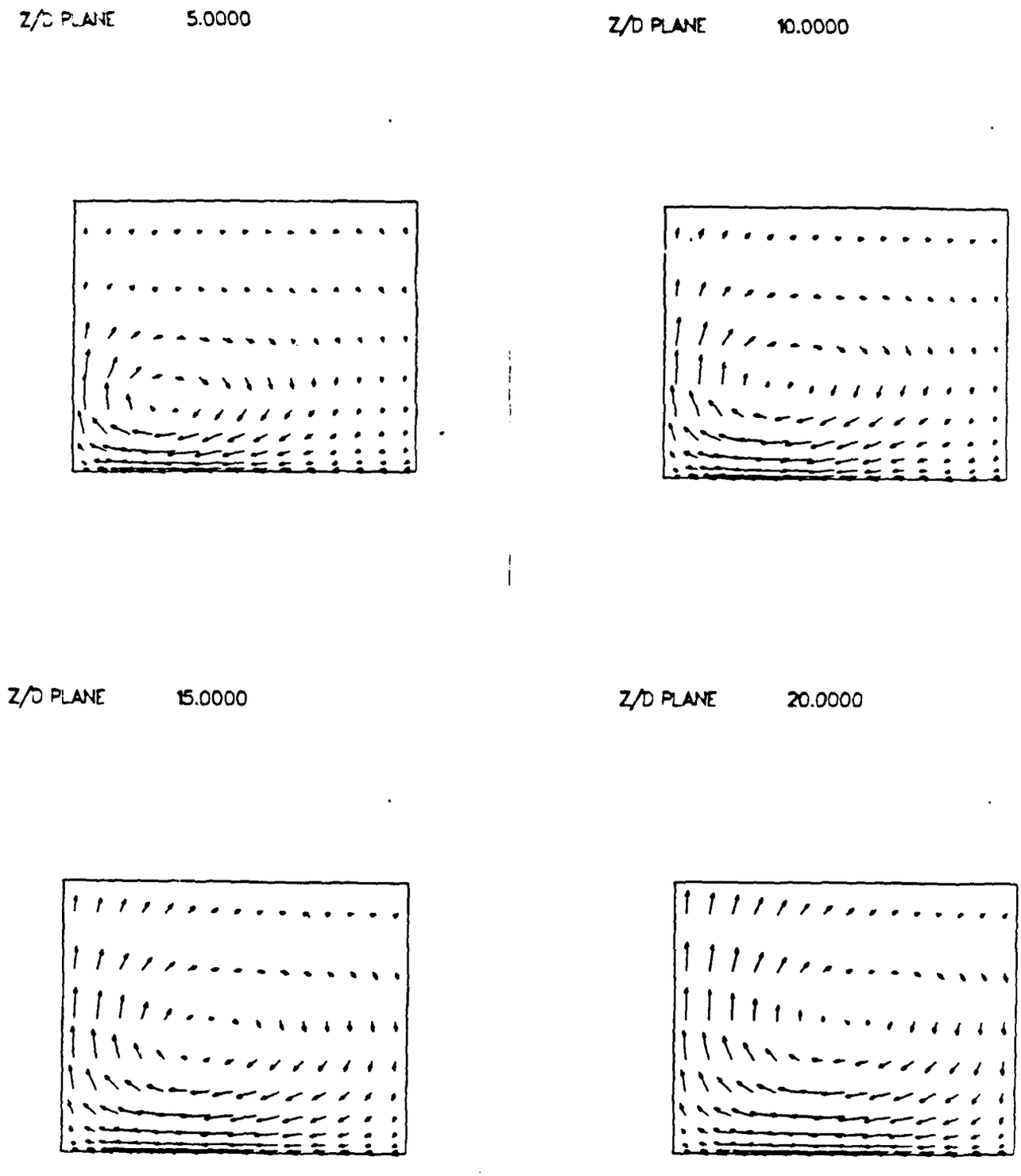

Fig. F6 Secondary flow structure for an injection rate of M = 0.5.

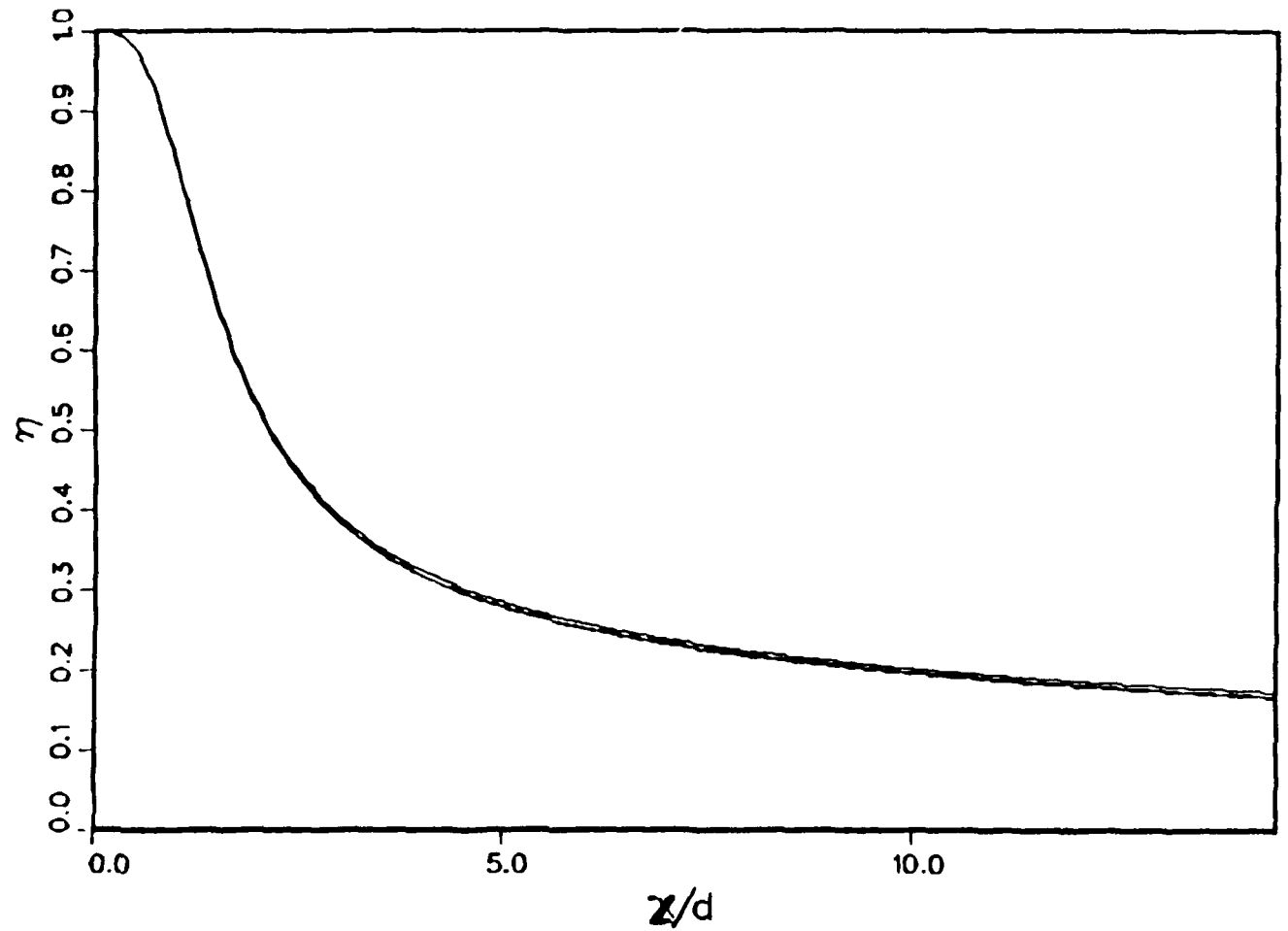

Fig. F7 Sensitivity of centerline effectiveness to variations in mainstream turbulence intensity.

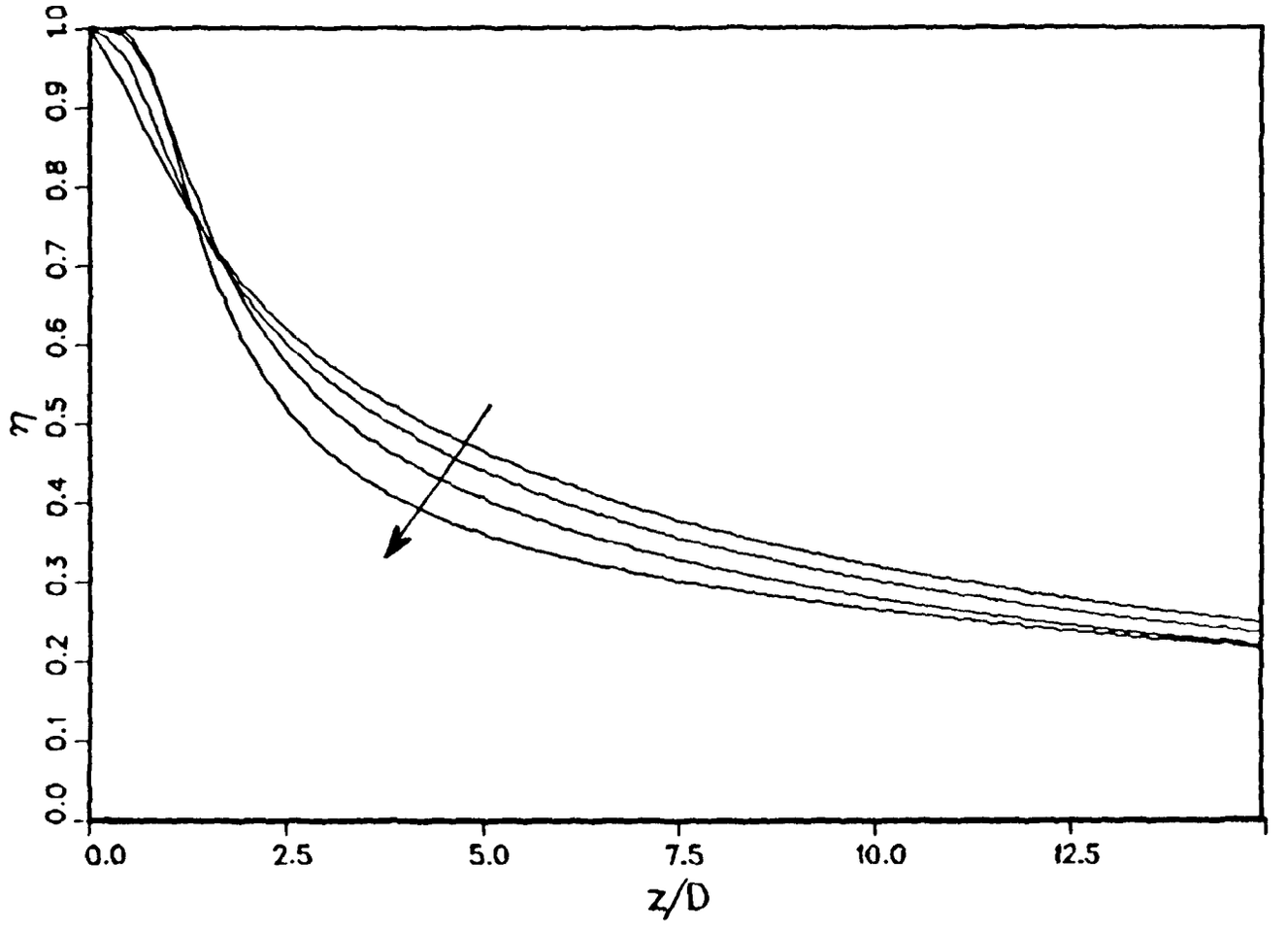

Fig. F8 Sensitivity of centerline effectiveness to variations in injection turbulence intensity.

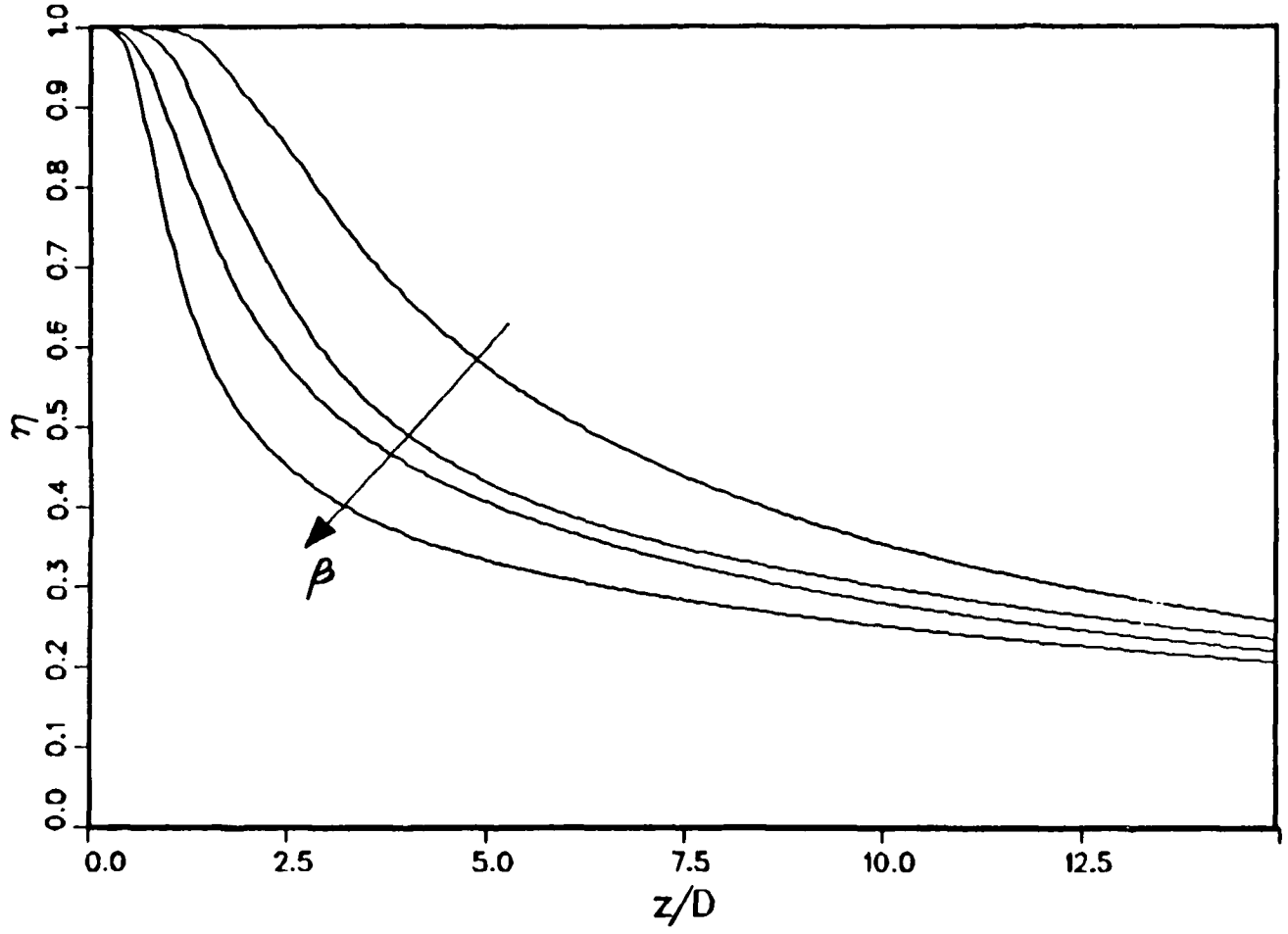

Fig. F9 Effect of the angle of injection on the centerline cooling effectiveness.